Journal of Plant Nutrition and Soil Science

WILEY-VCH

REVIEW OPEN ACCESS

Current Practices for Analyzing Soils and Sediments via Mössbauer Spectroscopy

Aaron Thompson[1] | James M. Byrne[2] | Carolin L. Dreher[3] | Andrew R. C. Grigg[4] | Prachi Joshi[3] | Drew E. Latta[5] | Anke Neumann[6] | Luiza Notini[7] | Katie E. B. O'Neill[2] | Katherine A. Rothwell[2,8]

[1]Department of Crop and Soil Sciences, University of Georgia, Athens, Georgia, USA | [2]School of Earth Sciences, University of Bristol, Bristol, UK | [3]Geomicrobiology, Department of Geosciences, University of Tübingen, Tübingen, Germany | [4]Soil Chemistry Group, Institute of Biogeochemistry and Pollutant Dynamics, Department of Environmental Systems Science, ETH Zurich, Universitätstrasse 16, Zurich, Switzerland | [5]Department of Civil & Environmental Engineering, University of Iowa, IIHR-Hydrosciences and Engineering, Iowa City, Iowa, USA | [6]PSI Center for Nuclear Engineering and Sciences, 5232 Villigen PSI, Switzerland, and School of Engineering, Newcastle University, Newcastle upon Tyne, UK | [7]Department of Civil, Construction and Environmental Engineering, University of Delaware, Newark, Delaware, USA | [8]Biological and Environmental Sciences, University of Stirling, Stirling, UK

Correspondence: Aaron Thompson (AaronT@uga.edu)

Received: 12 December 2024 | **Revised:** 27 June 2025 | **Accepted:** 29 June 2025

Academic editor: Ines Mulder

Funding: We thank the UKRI Future Leaders Fellowship (MR/V023918/1) for funding the workshop "Iron Moessbauer applied to environmental systems" that facilitated this review. A.T. was supported by US National Science Foundation Projects #2307254 and #2241390. A.N. was funded through an Alexander von Humbolt Foundation Research Fellowship for Experienced Researchers. Author D.L. was supported by the U.S. Department of Energy, Office of Science, Office of Basic Energy Sciences, Chemical Sciences, Geosciences, and Biosciences Division, through its Geosciences program at Pacific Northwest National Laboratory (PNNL). J.M.B is funded by a UKRI Future Leaders Fellowship (MR/V023918/1).

ABSTRACT

Environmental scientists are increasingly returning to Mössbauer spectroscopy (MBS) to reveal details about iron (Fe)-bearing phases in soils and sediments. MBS is particularly powerful at distinguishing between Fe(II) and Fe(III) and, given appropriate background information, can offer exceptionally precise information on Fe speciation in compositionally complex environmental samples. However, there are relatively few accessible guides for analyzing environmental samples by MBS. In this review, we seek to distill the essential understanding of MBS for earth scientists and provide guidance on analysis, spectral fitting, and interpretation for new practitioners and a consolidation of approaches for experienced users. As a rule, Fe phases in soils and sediments are more disordered and complex than synthetic or geogenic Fe minerals. We cover the most successful ways MBS can be applied to soils, including the determination of Fe(II)/Fe(III) ratios, characterization of Fe (oxyhydr)oxide crystallinity, and the use of ^{57}Fe isotope spikes, as well as highlighting how to avoid common pitfalls and arrive at Fe phase identification and quantification by leveraging complimentary data and environment context. We outline procedures for sample preparation, analysis, and spectral fitting using decision trees based on the analytical goals and sample conditions. The fitting and interpretation of magnetically ordered ferrous phases at low temperature is lacking in the literature and so we offer an expanded discussion of approaches to these challenging spectra. We provide a discussion and fitting guidance for the most common Fe phases in soils and sediments organized around environmental contexts: young soils (and sediments derived from them) dominated by aluminosilicates, highly weathered soils rich in Fe oxides, organic-rich soils, soils in sulfur-rich environments, and soils exposed to anoxia. For each context, we describe expected Fe phases and their characteristic spectral features while emphasizing the importance of complementary

All authors made equal contributions to the manuscript. Thompson led the effort and is listed first, all other authors are listed in alphabetical order.

analyses for reliable interpretation. Finally, we identify two critical needs in the field: improved theoretical frameworks for fitting low-temperature ferrous octets and Fe–sulfur phases and a need for standardization of parameter reporting and data sharing within the environmental MBS community. This review aims to both facilitate broader adoption of MBS in the environmental sciences and advance the technique's application to complex natural samples.

1 | Introduction

Mössbauer spectroscopy (MBS) is a powerful technique that can be used to determine the oxidation state of iron (Fe) and structure of Fe-bearing solid materials. Shortly after Rudolf Mössbauer discovered and proved the Mössbauer Effect in 1958 (Mössbauer 1962), MBS was rapidly deployed by physicists and chemists to understand the fundamentals of solid-state Fe. Within a decade, scientists began the foundational MBS work on environmental minerals (Bowen et al. 1969) and throughout the 1970s, 80s, and 90s, seminal work was carried out using MBS on soils and sediments (Bigham et al. 1978; Murad and Schwertmann 1980; Murad and Schwertmann 1982; Murad and Schwertmann 1984; Murad and Schwertmann 1988; Wagner et al. 1988; Wagner et al. 1990). Since the early 2000s, earth and environmental scientists are increasingly leveraging MBS to understand environmental processes in soils and sediments where Fe is ubiquitous and impacts ecosystem biogeochemistry.

Fe is the fourth most abundant element by weight in Earth's crust, and after (alumino)silicate phases, Fe minerals are the dominant minerals in soils and sediments. Present as large structural phases as well as ubiquitous nanoscale coatings on other minerals, Fe solid phases can influence soil colors and can significantly contribute to a soil's surface area (Cornell and Schwertmann 1996). These solid Fe phases have large capacities to sorb other metals, nonmetals, and organic compounds, making Fe a key element governing the fate of nutrients and contaminants alike. But Fe is also a potent electron acceptor and donor, readily transitioning between an oxidized state (Fe(III), or ferric) that is largely insoluble and a reduced state (Fe(II), or ferrous) that is largely soluble at circumneutral pH. This redox activity is unique among the major rock-forming elements. These redox transitions are regulated strongly by biological systems yet can also occur abiotically. Fe redox dynamics occur in response to changes in soil oxygen and are immediately evident through Fe(III) concentrations and depletions in wetlands, tidal sediments, at water-table boundaries, or in hydric soils, but they also occur readily within organic-rich microaggregates in surface soils.

Understanding Fe's diverse forms and functions requires analytical techniques that can probe nondestructively both its oxidation state and mineral structure. MBS excels when sensitivity, specificity, and detailed information is needed on Fe in complex environmental matrices (Rancourt 1998). The technique is isotope specific and can quantify the relative Fe solid phase species in soils or sediments without influence from other elements in mineral phases. The technique is nondestructive, enabling analysis without alteration of the sample's chemical or physical state. MBS is among the best approaches to determine Fe oxidation state, and it is the ideal technique to examine so-called poorly crystalline minerals, which are highly reactive Fe phases with small particle sizes (<30 nm) and high-degrees of substitution (most appropriately and accurately termed short-range-ordered (SRO) phases). MBS is especially powerful when the results are combined with other analytical techniques such as X-ray diffraction, electron microscopy, chemical speciation, and/or synchrotron-based X-ray absorption spectroscopies (XASs).

However, applying MBS to environmental samples presents unique challenges that we address in this review. First, environmental samples often contain a mixture of Fe phases with a range of crystallinities, requiring measurements at multiple temperatures and careful spectral interpretation. Second, while MBS can uniquely distinguish Fe(II) and Fe(III), this becomes extremely difficult in soils containing large amounts of sulfur, where low-spin ferrous–sulfur phases have similar MBS parameters to ferric phases. Third, the interpretation of magnetically ordered ferrous phases (presenting as octets in low temperature MB spectra) in reducing environments remains particularly challenging and poorly described in the literature (see Sections 3.4 and 4.5.2). We also confront the practical challenges of sample preparation and measurement conditions for environmental samples, where maintaining the original Fe speciation can be crucial. Finally, we address the need for standardization in parameter reporting and data sharing within the environmental MBS community.

The aim of this review article is to provide a starting point to new practitioners considering MBS in their research. We focus on practical aspects of applying MBS to soils and sediments rather than the physics of MBS. Considering the large body of information already available on MBS, we have chosen not to repeat all the fundamental physics background but instead provide a practical guide. Nevertheless, many of the concepts and terms may be entirely new to the reader and so we first provide a brief essential theoretical background, some of the most common nomenclature, and key aspects of MBS encountered in analyzing environmental samples (Section 2). Next, we describe methods of sample preparation and decisions for the collection of spectra that are most likely to be germane to environmental scientists (Section 3). We follow this with a description of the Fe phases expected in five broad categories of soil and sedimentary environments (Section 4), with a particular emphasis on magnetically ordered ferrous phases. And finally, we close (Section 5) with a perspective on the future direction of deploying MBS in soil and sediment samples.

TABLE 1 | Hyperfine parameters used when fitting Mössbauer spectra. Additional parameters for describing octets are given in Section 3.3.

Term	Symbol(s)	Description	Unit
Center shift or isomer shift	CS, IS, δ	Offset of the center of spectral component (i.e., doublet or sextet) with respect to the center of the x-axis (0 mm/s)	mm/s
Quadrupole splitting	QS, ΔE_Q	Distance between the two peaks that make up a doublet	mm/s
Quadrupole shift	ε	Distance between the center of peaks 1 and 6 and peaks 2 and 5 in a sextet. Related to quadrupole splitting by 2ε = QS. In some literature, ε has mistakenly been denoted as QS.	mm/s
Hyperfine magnetic field	B_{hf}, H	Width of magnetic field in magnetically ordered samples. Older references typically report units of kOe which is ×10 the value in T.	T
Linewidth	w, HWHM, Γ	Half width at half maximum. Theoretical minimum of 0.097 mm/s. Measured during calibration with α-Fe(0).	mm/s
Sigma	σ	Corresponds to Gaussian width of components (for Voigt model) of either δ, QS, ε, or H.	mm/s, or T

2 | Fundamental Aspects of Environmental ^{57}Fe MBS

2.1 | Essential Theoretical Background and Definitions

Before presenting the essential theoretical background, we draw attention to several excellent references that provide comprehensive theoretical background on MBS. From the perspective of environmental samples, there are some notable contributions that summarize and incorporate the decades of seminal MBS work on soils and sediments in the late 20th century, including an excellent textbook by Murad and Cashion (2004). Similarly, Dyar et al. (2006) offer a useful baseline of many earth materials including a table describing some of the key parameters (see Table 1). Gütlich et al. (2012) offer a succinct discussion of the fundamental physics and some broad applications to Earth and space science, while Rancourt (1998) considers fundamental aspects of MBS applied to clay minerals. Yoshida and Langouche (2013) offer a more simplified summary, targeting practitioners in industry or entry-level students, and the third chapter of this tutorial book by Vandenberghe and De Grave (2013) is an excellent starting reference point for investigating minerals that vary in crystallinity. Byrne and Kappler (2019) focused on providing a starting point for geomicrobiology. Most recently, Grandjean and Long (2021) have proposed a set of best practices for collection and interpretation of Mössbauer spectra for broad applications, though it is not focused on typical challenges experienced in soils and sediments.

MBS is isotope specific, and ^{57}Fe MBS detects only the ^{57}Fe isotope. ^{57}Fe MBS detects the resonant absorption of gamma rays by ^{57}Fe nuclei in the sample. The gamma rays are generated by a radioactive ^{57}Co source (half-life 270 d), which decays to an excited ^{57}Fe nucleus, which then decays to its ground state and emits the 14.4 keV gamma ray that is absorbed by ^{57}Fe nuclei in the sample. The Mössbauer spectrometer accelerates and decelerates the ^{57}Co source to generate slight differences in the gamma ray energy (by the principle of Doppler energy shifting) that allow MBS to resolve minute differences—on the order of one part in 10^{12}, termed hyperfine—in nuclear energy levels, making MBS the most precise physical measurement ever achieved (Rancourt 1998). The resulting spectrum reflects the electronic and magnetic environment of the ^{57}Fe nuclei, providing detailed information about oxidation state, coordination environment, and magnetic properties of the Fe phases. This is due to the differences in the configuration of electrons around ferrous and ferric Fe nuclei, and whether they are low-spin (LS) or high-spin states (HS).

Three types of interactions (denoted "hyperfine" interactions) are detected by MBS as the sample's ^{57}Fe nuclei are excited by the gamma ray. These interactions give rise to distinct spectral features, or parameters, in MBS (Figure 1 and Table 1). The first is the measured *center shift* (CS), equivalent to the sum of a small temperature-dependent second-order doppler shift and the *isomer shift* (Rancourt 1998), which responds to differences in electron density at the nucleus and the nuclear volume, reflecting Fe's chemical environment and oxidation state. The second is the *quadrupole splitting* (QS), which occurs when an asymmetric electric field gradient (EFG) at the nucleus interacts with the nuclear quadrupole moment, creating two distinct energy levels from what was previously a single excited state. The third is the *magnetic hyperfine splitting* (B_{hf}, or H), where the magnetic field at the nucleus interacts with the nuclear magnetic moment, splitting both ground and excited states into multiple energy levels. While the CS appears as a simple shift of the entire spectrum relative to zero velocity, the QS creates a characteristic doublet pattern, and magnetic splitting produces a sextet pattern with six absorption peaks, or in specific situations, an octet pattern (Figure 1). Sextets perturbed by an EFG exhibit a type of quadrupole splitting, but this is mainly referred to as the *quadrupole shift* (ε)—and sometimes erroneously also labeled QS.

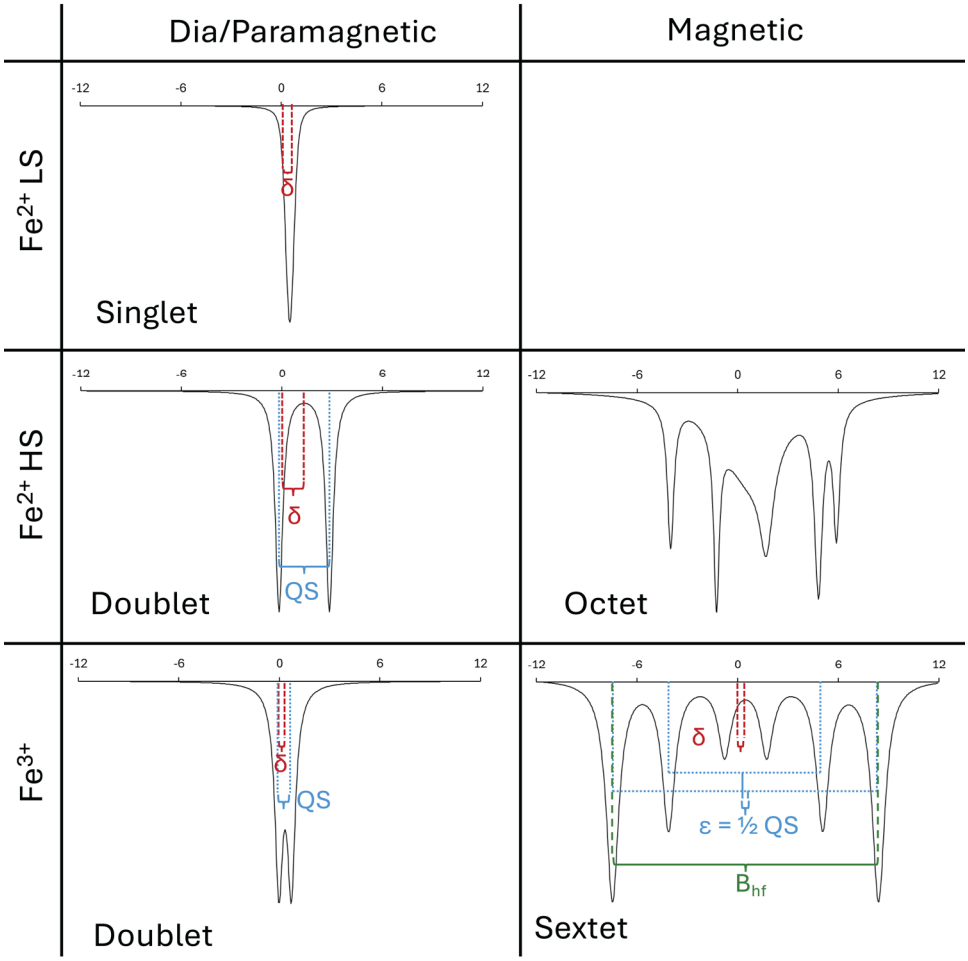

FIGURE 1 | Mössbauer spectra are characterized by sites which present as either singlets, doublets, sextets, or octets. The specific type of spectrum is dependent upon the magnetic properties of the Fe atoms within a sample, that is, whether they exhibit diamagnetic, paramagnetic, or magnetic ordering, and also spin, which can be low spin (LS) or high spin (HS). As magnetic properties are temperature dependent, some samples will present as different types when measured at different temperatures. For example, ferrihydrite is paramagnetic above ~77 K and appears as a doublet; however, at close to liquid helium temperature, it presents as a magnetically ordered sextet. Environmental samples often contain one or more of these types of sites which can be deconvoluted through fitting.

All atoms and ions are either diamagnetic or paramagnetic. *Diamagnetic Fe phases* contain low-spin ferrous Fe with no unpaired electrons. They present as *singlets* (single peaks) or *doublets* (double peaks, in the case of pyrite) (Morice et al. 1969) at all temperatures in Mössbauer spectra offset from zero according to their CS or isomer shift (δ); pyrite (FeS_2) and other Fe(II)–S_x phases are the most common example in soils. The rest of the Fe-bearing phases in soils are *paramagnetic* and can be in either a paramagnetic state or magnetic state based on the measurement temperature. Phases in a *paramagnetic state* have a net zero magnetic moment because all their individual magnetic moments are randomly orientated and thus appear as a *doublet* (two peaks separated by an energy difference QS) in MBS. All phases with sufficient concentrations of paramagnetic Fe will eventually magnetically order at a sufficiently low temperature, even if that is nearly absolute zero (0 K) (Murad and Cashion 2004). Some Fe minerals are already magnetically ordered at room temperature and need to be heated before they become paramagnetic, pure hematite is an example of such a phase. Many Fe phases in soils require cooling below room temperature to magnetically order. Magnetically ordered Fe(III) phases appear as sextets in MBS, with six distinct peaks characterized by their hyperfine field (B_{hf} or H). These magnetically ordered ferric phases can be classified into three categories based on their magnetic properties. *Ferromagnetic Fe phases*, such as elemental iron (Fe(0))—often used to calibrate a Mössbauer spectrometer—have all magnetic moments pointed in the same direction. In *antiferromagnetic minerals*, sublattices of equal magnetic moments are aligned opposite to one another, resulting in a net zero magnetization; canted antiferromagnetism is a variant where slight misalignment of sublattices results in weak magnetization, as observed in hematite. *Ferrimagnetic minerals* possess multiple sublattices with antiparallel alignment but unequal magnetic moments, leading to a net magnetic moment; examples include magnetite and maghemite. Alternatively, high-spin ferrous (Fe(II)) phases can produce *octets* when they magnetically order because they exhibit both large QS and large magnetic splitting. This strong interaction between electrical field gradient and magnetic field at the nucleus leads to complicated spectra (Figure 1) and their detailed interpretation is provided in Section 3.3.

2.2 | Temperature-Dependency of Magnetic Ordering and Spectral Parameters

Most pure (paramagnetic) Fe phases undergo transitions between magnetic states as the collection temperature changes from room temperature (298 K) to liquid helium temperature (4.2 K). These transitions manifest in Mössbauer spectra as changes from paramagnetic doublets to magnetically ordered patterns (sextets for Fe(III) or octets for high-spin Fe(II)). We refer to this transition temperature in general as the magnetic ordering temperature, but in many cases, more specific terminology can be used. For instance, the *Curie temperature* (T_C) is used to describe the transition from paramagnetic to magnetically ordered state in ferromagnetic or ferrimagnetic phases, one example being the mineral goethite. Similarly, the *Néel temperature* (T_N) signifies the magnetic ordering temperature for antiferromagnetic phases, such as hematite. When a phase remains paramagnetic below its nominal magnetic ordering temperature because of its small particle size (diameters typically less than 30 nm) or because of crystal disorder, it is called *superparamagnetic*, and the temperature at which it magnetically orders is called the *blocking temperature* (T_B), when 50% of the spectra is in the magnetically ordered state and 50% is present as a superparamagnetic doublet (Concas et al. 2017). Other specific temperature transitions are defined for specific minerals. In the mixed valent mineral, magnetite, the Verwey transition (T_V) ranges between 80 and 125 K (Jackson and Moskowitz 2021) and leads to a structural phase transition, with the spectrum exhibiting two sextets above T_V and up to five sextets below. Additionally, hematite undergoes the *Morin transition* at approximately 260 K, reflecting a significant shift in magnetic ordering. Understanding these temperature-dependent transitions is crucial for phase identification as many Fe phases appear identical at room temperature but exhibit distinct magnetic ordering behavior at lower temperatures. Moreover, in natural samples, these transition temperatures are often shifted significantly by variations in crystallinity including variations due to particle size and ion substitutions.

In addition to magnetic ordering temperature, all hyperfine parameters are temperature dependent, with CS and B_{hf} generally increasing as temperature decreases until magnetic saturation occurs. And finally, a central requirement for detection by MBS is that the ^{57}Fe nucleus must not move (or recoil) when absorbing the gamma ray (Murad and Cashion 2004). At higher temperatures, only a fraction of the ^{57}Fe nuclei in the sample do not recoil (termed the recoilless fraction, *f*-value or *f*-factor) and this fraction increases uniquely for each Fe phase or site as temperature decreases (Murad and Cashion 2004). Only when each Fe site can be assumed to have equal recoilless fractions will their spectral area match their atom abundance. In practice, one can reasonably assume equal recoilless fractions for all Fe phases at cryogenic temperatures, and often even at room temperature for dry samples (Lalonde et al. 1998; Rancourt 1998). However, this should be considered by comparing Fe in very different types of phases. When required, examples of how to check the *f*-factor and correct for it are available (Diamant et al. 1982).

2.3 | Spectral Broadening and Crystallinity Effects: Key Factors for Environmental Samples

2.3.1 | Broadened Spectral Features

Spectral broadening is one of the key features distinguishing synthetic Fe phases from environmental phases and understanding it is important for interpreting spectra from soils and sediments. Three types of broadening are relevant.

The first type of broadening (static or inhomogeneous broadening) affects all environmental samples and arises from variations in the chemical and structural environments of individual Fe atoms (Rancourt 1998). Each Fe atom experiences slightly different conditions due to variation in the amount or distribution of foreign ion substitution, differences in particle size, crystal defects, and how close the Fe atom is to the surface of the mineral. This variation creates a distribution of hyperfine parameters that manifests as broadened spectral lines.

The second type of broadening is dynamic or homogeneous broadening. This occurs when the measurement timescale of the excited ^{57}Fe nucleus is within an order of magnitude or two of the timescale of the electronic transitions (Murad and Cashion 2004). The hyperfine parameters discussed above can be reliably fitted when Fe phases are either fully magnetically ordered (i.e., the nucleus experiences a static magnetic field) or fully paramagnetic (the nucleus experiences a net zero magnetic field because the electronic state is rapidly switching). However, as the magnetic ordering temperature is approached, intermediate conditions create a probability distribution of magnetic and paramagnetic states. This leads to complicated spectra that show a gradual transition between the paramagnetic and magnetic states. This is particularly relevant for superparamagnetic phases near their blocking temperature. And of course, in most natural samples, homogeneous broadening will be superimposed on inhomogeneous broadening, leading to a distribution of spectra parameters as the sample is cooled (Chen and Thompson 2021).

The last type of broadening is slow paramagnetic relaxation, which is a type of dynamic broadening in paramagnetic materials (Murad and Cashion 2004). It is exceedingly rare in whole soils and primarily relevant for samples with *dilute* (<1% total Fe), *uniformly* distributed Fe, such as trace Fe substitutions in isolated clay minerals or organic matrices where Fe atoms are well separated. Slow paramagnetic relaxation typically manifests below 13 K as a sextet-like feature with anomalously high hyperfine field strengths (typically >55 T) (Kodama et al. 1988; Murad 1998; Schwertmann and Murad 1988).

2.3.2 | The Effect of Crystallinity on MB Spectra

While pure, bulk-crystalline Fe-bearing minerals have characteristic magnetic transition temperatures and MBS parameters, soil-derived Fe minerals are inherently disordered and therefore have significantly modified spectra. Understanding how disorder is expressed in the Mössbauer spectra is central to interpreting

Fe phases in soils and sediments. Most pedogenic Fe phases have substantially lower crystallinity—defined collectively as having more ion substitution, decreased particle sizes, or other defects—than their geogenic or synthetic counterparts. For the most part, MBS can very precisely identify the net differences in crystallinity between samples, but rarely can it pinpoint the root cause. Fe phases exhibit low crystallinity primarily due to three factors: (1) particle size effects, (2) isomorphic substitution, and (3) aggregation/clustering effects (Berquó et al. 2007; Berquó et al. 2009).

When the dimensions of Fe-bearing particles decrease below ≈30 nm, they only exhibit ordering over short distances (they are SRO) and superparamagnetic behavior will likely influence the spectra. For instance, while bulk hematite and goethite are magnetically ordered at 295 K, this ordering (blocking) temperature will be suppressed below room temperature for small particles of hematite (<8 nm) and goethite (<20 nm) (Janot et al. 1973), even without any substitution. For goethite, hematite, and magnetite nanoparticles, even small changes in the size or nanoparticle shape can alter blocking temperature (Bødker et al. 2000; Murad and Schwertmann 1983b; Roca et al. 2007), with most changes occurring below approximately 20 nm size (Janot et al. 1973).

Similarly, isomorphic (metal-for-Fe) substitution is ubiquitous and often quite substantial in soil minerals. For instance, Al can substitute for Fe up to 33% in goethite (Schulze and Schwertmann 1984), up to 18% in lepidocrocite (Liao et al. 2020), and is present in solid solution up to 5% in natural jarosite (Grigg, Notini, et al. 2024b), and Si is commonly found in soil Fe minerals. Such substitutions can suppress B_{hf} (Murad and Schwertmann 1983a; Murad and Schwertmann 1983b), alter the quadrupole interactions (QS or ε) (De Grave et al. 1982; De Grave et al. 1996)), and lower the magnetic ordering temperature in common soil minerals (Grigg et al. 2024c; Murad and Schwertmann 1983b). Isomorphic substitution may also change the distribution of hyperfine parameters (Murad and Schwertmann 1988).

Finally, Fe (oxyhydr)oxide nanoparticles are commonly present in soils as aggregates, as coatings on other minerals grains, or in close associations with organic matter. The degree of aggregation or clustering of Fe nanoparticles can alter the Mössbauer spectra. For instance, Berquó et al. (2009) showed that as ferrihydrite (Fh) nanoparticles aggregate they participate in interparticle magnetic exchange interactions that increase their blocking temperatures compared with fully disaggregated particles. This effect can partially counteract the suppression of ordering temperatures caused by small particle sizes.

As expected, most SRO Fe phases are influenced by all three of these factors simultaneously. The primary particles are often much smaller than 20 nm, are highly substituted (usually with Al and Si), and exhibit some degree of aggregation. The recent emphasis on coprecipitation of organic matter with Fe (oxyhydr)oxide phases produces just such a scenario as the organic compounds prevent crystal growth (decreasing primary particle size), yet promote aggregation, while very likely facilitating ion substitution (Chen and Thompson 2018; Eusterhues et al. 2008; Mikutta et al. 2008; Schwertmann et al. 2005). These types of combined effects make it untenable to extract precise particle sizes or degrees of Al substitution from the measured Mössbauer spectra for Fe phases in soil, although a novice practitioner might well try this based on previous success for pure mineral phases (Murad and Cashion 2004). In fact, ion substitution alone has measurable effects on both particle size and aggregation, making the separation of these effects challenging even in well controlled experiments (Murad and Schwertmann 1983b). For these reasons, often the most prudent approach for natural samples is simply to carefully characterize differences in crystallinity, which is a combined expression of all these factors (Winkler et al. 2018). Soil Fe phases with lower crystallinity will have lower magnetic ordering temperatures. As crystallinity decreases, the differences between the individual mineral phase identities becomes much harder to assign and perhaps much less meaningful (Thompson et al. 2006), while the SRO nature of the Fe phases becomes increasingly important.

2.4 | Applications of MBS in Soils and Sediments

2.4.1 | Common Effective Applications

There are several common types of research questions which MBS is exceptionally well suited to address. These applications take advantage of the isotope specificity of MBS to allow a detailed, nondestructive analysis of Fe speciation, even within a complex matrix such as a soil. Here we consider common successful applications of ^{57}Fe MBS.

Oxidation state of Fe [Fe(II) vs. Fe(III)]: MBS is among the best approaches to determine precisely the valence of Fe in a solid sample through nondestructive means, regardless of sample matrix complexity (Joshi et al. 2024; Koeksoy et al. 2018). The determination of oxidation state is most accurate if all the Fe is paramagnetic and equal *f*-factors can be assumed at the measurement temperature. In general, Fe(III) minerals have low CS and QS values compared with high CS and QS for Fe(II) (orange- and teal-colored ranges in Figure 2A, respectively). However, if low-spin ferrous compounds (purple area in Figure 2A) such as pyrite are present, their low CS is very similar to Fe(III) minerals. Thus, users should assess the likelihood that low-spin Fe(II) may be present and if so, make measurements across a range of temperatures (Section 3.3.1) or include additional analytical techniques to mitigate this issue.

Crystallinity of Fe oxyhydroxide phases: MBS is an ideal technique to determine the distribution of magnetically ordered domain sizes (e.g., crystallinity) among (oxyhydr)oxide phases in the sample. A hallmark of soil environments is the vast array of distinct microsites and unique conditions within aggregates and variable-sized pores, which promote a range of crystallinity among mineral precipitates (Mikutta et al. 2024). Even in synthetic preparations of minerals there is the potential for significant variation in crystallinity. Changes in crystallinity are reflected in the size of magnetically ordered domains in the sample, the distributions of which MBS can characterize in detail, particularly based on analysis of the blocking temperature (Chen et al. 2020; Grigg et al. 2024a) (see Sections 2.2 and 3.3.1). It is important to recognize that several factors, including isomorphic substitution, crystal size, and aggregation, can all influence the blocking temperature and hyperfine parameters. While some studies have

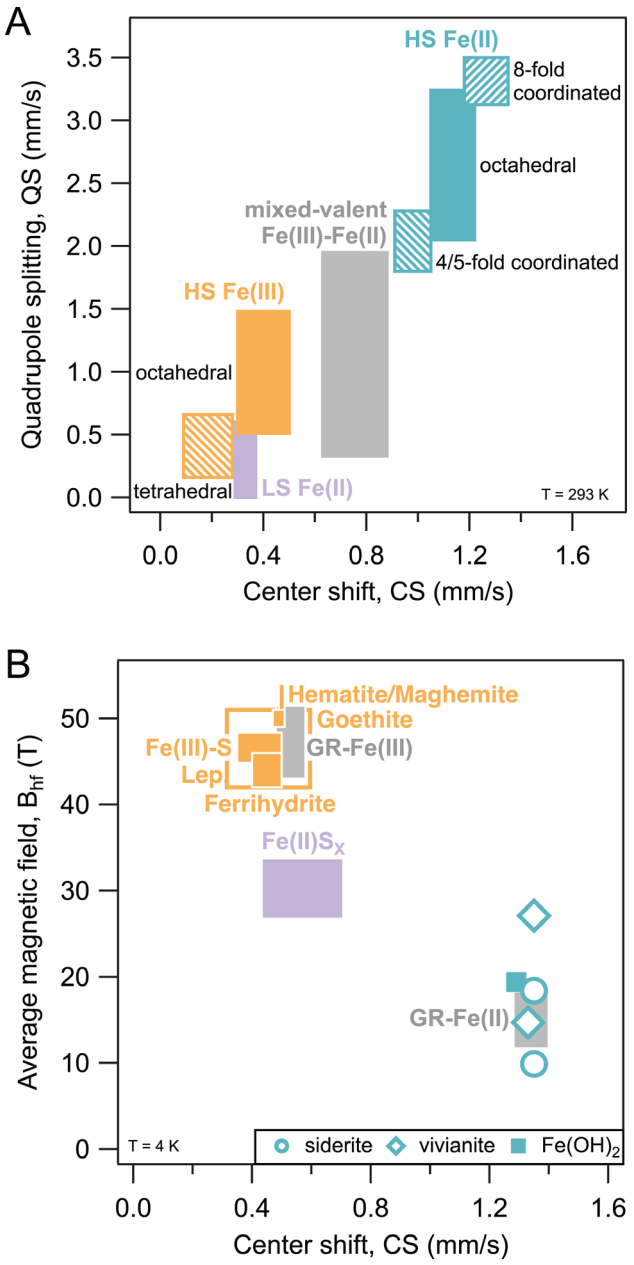

FIGURE 2 | Typical ranges of Mössbauer parameters of (A) Fe(II) and Fe(III) doublets in spectra collected at room temperature (figure adapted from Dyar et al. 2006; Murad and Cashion 2004) with data on FeS from (Schröder et al. 2020), and (B) Fe(III) sextets and Fe(II) octets in spectra collected at 4 K (key: HS = high-spin; LS = low-spin; Fe(III)–S = Fe sulfate minerals; Fe(II)S_x = nonstoichiometric mackinawite, greigite; GR–Fe(III)/GR–Fe(II) = Fe(III)/Fe(II) in Green Rusts; Lep. = lepidocrocite; synthetic reference materials with distinct values are listed in the graph legend), based on references (Bronner et al. 2023; Cashion and Murad 2012; Cornell and Schwertmann 2003; Grigg, Notini, et al. 2024b; Häggström et al. 1969; Hohmann et al. 2010; Larese-Casanova et al. 2010; MacKenzie and Bowden 1983; Murad and Schwertmann 1980; Neiser et al. 2015; Ôno and Ito 1964; Ruecker et al. 2016; Schröder et al. 2020; Tennakoon et al. 1974; ThomasArrigo et al. 2017; Ziganshin et al. 2015) as well as personal data from the authors (see Table S4).

isolated the effect of individual factors in laboratory-synthesized samples, this approach is not reliable for unknown samples or soils and sediments. To compare mixed and unknown phases in soils, a crystallinity index based on the ratio of sextet area at two temperatures can be useful for describing differences in crystallinity of Fe minerals between soils (Coward et al. 2018; Winkler et al. 2018).

^{57}Fe spiked samples: Fortuitous use of the specificity of MBS for the ^{57}Fe isotope, which is only 2.1% of natural abundance Fe (Taylor et al. 1992), has allowed researchers to follow the transformations of Fe phases added to complex samples. Fe isotope spikes can be added as ^{57}Fe(II)$_{aq}$ in soluble form (Amin and Arajs 1987; Chen et al. 2020; Latta et al. 2012; Williams and Scherer 2004), as ^{57}Fe(III)$_{aq}$ if low pH or if organic ligands are used (Rea et al. 1994), or as a synthetic ^{57}Fe mineral (Grigg et al. 2024c; Kubeneck et al. 2024; Notini et al. 2023; Schulz et al. 2024).

Initial work with ^{57}Fe spikes was carried out to quantify the electron transfer (via MBS) and atom exchange (via Inductively Coupled Plasma Mass Spectroscopy, ICP-MS) between soluble and solid phase Fe (Grigg et al. 2024c; Handler et al. 2009; Kubeneck et al. 2024; Larese-Casanova et al. 2010; Notini et al. 2023; Schulz et al. 2024; Tishchenko et al. 2015; Williams and Scherer 2004). Adsorption of Fe(II)$_{aq}$ can trigger near complete turnover of a mineral's Fe atoms in pure, optimized conditions. Many factors typical of natural systems (e.g., competitive adsorbates, ion substitution in the minerals, surface passivation by newly formed Fe phases) can attenuate the extent of Fe(II)-catalyzed recrystallization and limit its extent (Notini et al. 2019; Tishchenko et al. 2015).

This attenuated atom exchange has made it possible to follow active Fe cycling in soils and sediments by adding ^{57}Fe spikes. For instance, additions of ^{57}Fe(II)$_{aq}$ to soil slurries can effectively "stain" the soil Fe phases most reactive toward electron transfer and atom exchange, which is most prevalent with low-crystallinity (i.e., SRO) Fe(III)–phase (Chen et al. 2023; Chen et al. 2018; Mikutta et al. 2009; Tishchenko et al. 2015). Subsequent biogeochemical transformations of these more reactive phases will then strongly bias the MBS signal to the reactive Fe phases relative to the underlying, bulk Fe mineral components. An even more powerful exploration of in situ Fe cycling can be made by oxidizing the ^{57}Fe(II) mixed with the soil as the resulting MBS spectra will then largely reflect the recently precipitated Fe(III) phases (Chen et al. 2020). In both cases, it is however important to run parallel nonlabeled experiments with additions of naturally abundant Fe(II) and subtract the resulting Mössbauer spectra to account for any potential changes in the native Fe (see Supporting Information section of Chen et al. (2018) for details and an R script to process the data). Notini et al. (2023) have flipped this approach and instead synthesized ^{57}Fe phases and added them to soils and sediments to track the behavior of discrete mineral phases. Using this approach in mesocosms (Schulz et al. 2023) and field experiments (Grigg et al. 2024a; Kubeneck et al. 2024; Schulz et al. 2023), the authors have shown unique mineral behavior that occurs in the presence of the soil matrix that contrasts the transformation processes observed in experiments with fully mixed mineral suspensions. Synthetic minerals can be tailored to reflect natural minerals that occur in soil. For example, ^{57}Fe–organic matter coprecipitates have been synthesized and

added to soil incubations to explore the effect of organic matter on mineral transformation (ThomasArrigo et al. 2024; Voggenreiter et al. 2025).

Phase identification: MBS is generally not a standalone technique for mineral characterization. However, there are many examples in which MBS has been used to constrain potential mineral phases or fine-tune phase composition assignments when other sample information is available. There are certain phases that have very distinctive spectra, and their presence or absence can often be uniquely diagnosed using MBS. For example, MBS can often be used in a diagnostic sense for hematite ($Fe(III)_2O_3$), magnetite ($Fe(II)Fe(III)_2O_4$) and ilmenite ($Fe(II)TiO_3$). Similarly, MBS is singularly suited to distinguish between phyllosilicate clay minerals and even small amounts of disordered Fe(III)(oxyhydr)oxides, which is essential for understanding mechanisms of clay mineral reactivity (Zhou et al. 2022). MBS is also well suited for identification and quantification of Fe (oxyhydr)oxide minerals at near single-digit percent levels as a fraction of total Fe, often at levels well below detection limits of XRD. Phase identification of Fe (oxyhydr)oxide minerals is enhanced by their relatively well-defined sextets at low temperatures with unique hyperfine parameters (see Figure 2B).

Despite the many studies in which MBS has been used to identify and quantify mineral phases, there are several limitations to this approach. The true power of MBS for soils and sediments comes with both an understanding of the environment and contextual or complimentary analyses that constrain the presence or absence of certain Fe phases. Section 4 of this review is designed to demonstrate how an understanding of the sample environment can aid interpretation and guide the spectral fitting process.

2.4.2 | Limitations and Challenging Applications

There are some samples or research questions for which MBS is a poor choice or must be complemented by other analyses (e.g., X-ray diffraction, synchrotron-based X-ray absorption, FTIR) to provide meaningful data. Here, we outline the common limitations and challenges in deploying MBS for natural samples.

Low Fe mass and long runtimes: MBS is a bulk technique and requires a minimum Fe mass in the sample (often termed "absorber thickness" in the MBS literature). A minimum mass of 50 μg of ^{57}Fe is generally required for measurement, although 100 – 200 μg ^{57}Fe is more typical. For natural abundance Fe, this equates to a minimum of 2.5 mg and an ideal of 10 mg of Fe. The practicalities of preparing the sample usually make it challenging to run samples less than 1% natural abundance Fe by mass. This is less challenging in matrices that do not absorb gamma rays well (such as organic matter), and harder when Al concentrations are high. For typical soils with >5% Fe by mass, measurement times are upward of 16 h at each temperature and usually three measurement temperatures are required. For lower abundance samples or samples with high Al/Fe ratios, measurement times extend into weeks, even under ideal conditions, and lower gamma source strength commonly extends necessary collection time. Because of these limitations, judicious sample choice is often necessary, and, in some cases, it may be impractical to collect clean spectra within available instrument time.

Nonunique spectral parameters: Most Fe phases do not have singularly unique Mössbauer spectral parameters, leading to difficulties distinguishing some phases from one another without information from other analytical techniques. This is especially true if only room temperature (295 K) measurements are made (Section 3.3.1), where often most of the Fe phases in soils are in a paramagnetic or superparamagnetic state, producing a doublet. Even at low temperature, the doublets of many phases have overlapping hyperfine parameters—although the Fe(II) and Fe(III) oxidation states can usually be separated—including Fe in aluminosilicates (Dyar et al. 2006; Stanfield et al. 2024) and organic complexes (Goodman et al. 1991), as well as the sextets of some nonsilicate Fe(II) minerals such as white and green rusts, vivianite, and siderite (Figure 2B). Although sextets are often more easily separated than doublets, overlapping spectra are fitted with increased uncertainty (Amarasiriwardena et al. 1986). If contextual information or additional analytical techniques can constrain the candidates, MBS fitting can likely provide relative phase abundance, composition, or mineral characteristics.

Complex spectra and phase mixtures: A fundamental characteristic separating natural samples from pure Fe minerals is the degree of natural variation and the range of potential Fe site populations. MBS is exceedingly sensitive to changes in Fe speciation, with even minor changes in crystallinity evoking shifts in hyperfine parameters. This is a key advantage for systems with constrained Fe site speciation but severely limits MBS for soils of unknown origin. As Fe phase crystallinity decreases, the ordering temperature and B_{hf} values decrease and no longer match reference values. Most often, this requires the spectroscopist to relax fitting precision relative to reference compounds. For instance, pure ferrihydrite is most accurately fit with two sextets (Byrne and Kappler 2019), but typically one sextet is used to fit ferrihydrite in soils. Similarly, magnetite should be modelled with at least two sextets (more at low temperature, see Section 4.5.1), while akageneite would ideally be fit with three or four overlapping sites (Barrero et al. 2006). In soils and sediments, these phases would likely be sharing spectral space with several other Fe species and a simplified fitting approach becomes more appropriate. Most often, we are interested in the abundance of different Fe species in a sample, which necessitates spectral fitting routines that can account for all the Fe in the sample, even if the identification of those phases remains ambiguous. This creates nonuniqueness and fitting trade-off challenges that will increase uncertainty in the relative area of the target phases. Furthermore, phase quantification is complicated by potentially unequal recoilless fractions (*f*-factor) across different Fe species, with Fe(II) often exhibiting lower *f*-factors than Fe(III) and organically bound or adsorbed Fe exhibiting lower *f*-factors than Fe in mineral phases. Fortunately, these differences are generally eliminated in dry samples and at low temperatures (<77 K) (De Grave and Van Alboom 1991; Rancourt 1989). Finally, certain Fe phases produce spectra that are challenging to fit with general fitting models (e.g., octets) requiring nonideal approximations or specialized fitting approaches. Throughout this review, we highlight these challenges and suggest strategies to address them.

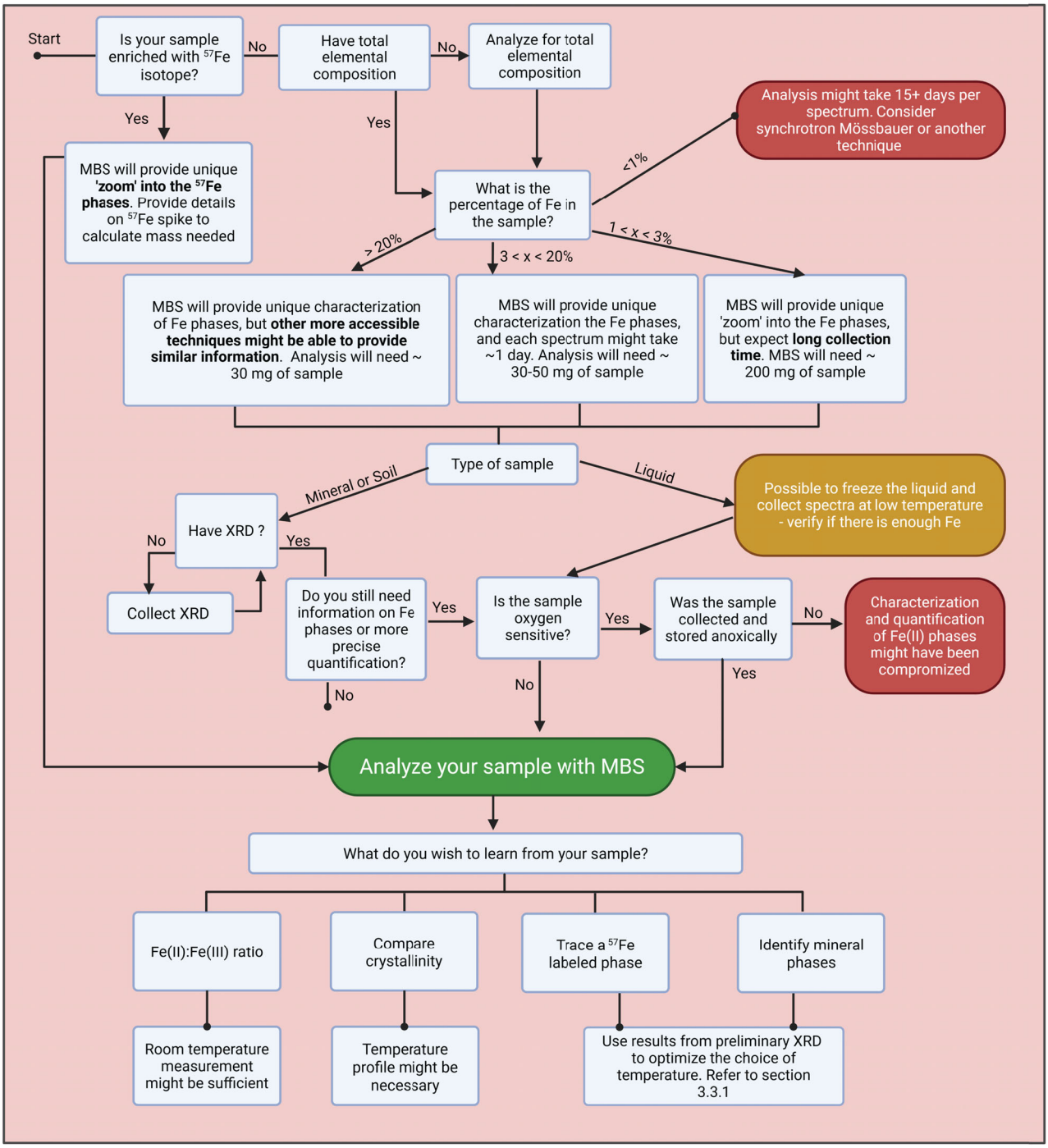

FIGURE 3 | Decision tree to guide users on whether their samples are suitable for being analyzed with Mössbauer spectroscopy, estimation of sample mass needed, and general guidance on potential approaches to analyzing the sample. Created in BioRender. Notini de Andrade (2025); https://BioRender.com/z20f870.

3 | Sample Preparation and Analysis Methods

3.1 | Analysis Method Selection and Sample Preparation

Prior to measuring a sample with MBS it is important to consider the potential phases in a sample to decide upon the appropriate sample preparation pathway and the most appropriate choice of measurement temperature(s). Figure 3 provides a useful decision tree listing some key questions including "what do you wish to learn from your sample?" Answering such questions will help in planning the experiment and maximizing the benefits of the measurement.

3.2 | Sample Preparation Methods

Mössbauer spectrometers are mostly operated in transmission mode, so the gamma rays need to move through the sample. Common approaches for preparing a sample are outlined below

and images of examples are given in Figure S1. Nearly always the sample needs to be evenly dispersed over a few cm^2, but with little to no sample alteration required; MBS is considered nondestructive.

1. *Dry powders:* The simplest way to run a sample is to load dry material in a thin layer (a few millimeters). This layer can in principle be sandwiched between two pieces of Kapton tape inside a nylon disk or between two pieces of gamma-ray transparent material. Most critical here is to achieve a uniform thickness of the entire sample. If the sample is moist, you may consider running it without drying (frozen) to preserve the Fe's valence if this is critical or you have samples with an abundance of minerals (e.g., SRO or Fe(II) phases or clay minerals) that can be altered during the drying process (Stucki et al. 2014). It is also possible to prepare samples using dry powders loaded into a pellet press, potentially with KBr or cellulose as a matrix. These pellets have the advantage of being of uniform thickness.
2. *Samples collected on filters:* Assuming the sample will be measured below 273 K (freezing point of water), this routine method can be used to measure hydrated samples such as a sediment slurry, or a sample from a microcosm.
3. *Wet pastes:* This is the method of choice for samples that may create/require high pressure during filtering (e.g., clay minerals) or that may (partially) oxidize during contact with plastic as required for collecting samples on filters. The solid should be separated from the fluid via centrifugation and transferred onto/into a holder that will be sealed with Kapton tape. For very wet, clay-rich samples, direct enclosure in the Kapton tape could interfere with the tape's adhesive properties. Wet pastes require measurement temperatures below freezing.
4. *Oxygen sensitive samples:* When samples are collected in an anoxic environment or contain potentially anoxic microsites, care must be taken if preservation of the original Fe valence is important. Once the sample is in an oxygen-free space (such as a glovebox), the simplest approach is often to prepare the absorber (as described above, wet or dry) and encase the absorber in heat sealed plastic (or carbon-based mylar, no aluminum) to limit O_2 diffusion (Kupper et al. 2023). The encased adsorber can be run directly on the spectrometer. To ensure O_2-free transport to the instrument, the absorber can be frozen, sealed in a jar, or vacuumed in a bag, and stored with an oxygen scavenger. In general, drying the sample risks oxidation, even under an anoxic atmosphere (Stucki et al. 2014) or when using a freeze-drier, and should be avoided for sensitive samples unless absolutely necessary.

3.3 | Data Analysis and Interpretation

Once MBS spectra are collected, they must be interpreted, most often through a process of fitting proposed Fe site populations (unique or discrete Fe atom locations in the sample). The basic workflow is highlighted in Box 1.

Workflow for Analyzing and Fitting Mössbauer Spectra

1. Run the sample
   a. Collect sample spectra at one or more temperatures.
   b. Collect α-Fe(0) standard on same instrument at 295 K.
2. Calibrate and fold the spectrum using measured α-Fe(0) standard.
3. Choose software and appropriate lineshape model for fitting.
4. Fitting/interpreting the spectra
   a. Apply a measured α-Fe(0) linewidth to the Lorentzian HWHM.
   b. Visually decide if the spectrum contains doublets, sextets, or perhaps octet features.
   c. Add spectral sites one at a time with parameters close to reference values (see below).
   d. Float parameters one at a time or interactively to fit the spectra.
   e. Evaluate the fitted parameters against references and reality. Consider improvements of χ^2 value equally with a visually appropriate fit. Overfitting is common and can lead to meaningless results. Less is more.
5. Include all parameter values and the raw datafiles in any report or publication.

3.3.1 | Measurement Temperature

Selecting the appropriate measurement temperature is critical for optimizing the analysis of Mössbauer spectra. If the primary goal is to quantify the Fe(II)/Fe(III) ratio, room temperature measurements (295 K) may suffice, provided there are no low-spin ferrous compounds in the sample. However, for identifying specific Fe phases, it is essential to collect spectra at temperatures where the expected phases exhibit distinct and well-documented spectral features. Commonly used temperatures include 295 K (room temperature), 77 K (liquid nitrogen), 13 K, and 5 or 4.2 K (liquid helium).

For samples containing a mixture of Fe phases, choosing the appropriate measurement temperature can help distinguish the phases more effectively. At certain temperatures, different phases produce spectra with more distinct features, such as a sextet and a doublet instead of two overlapping doublets, making them easier to identify and quantify. However, some temperatures may yield complex spectral features that are difficult to fit (e.g., magnetite splitting into five sextets or Fe(II)-bearing minerals forming octets). If such complexities are irrelevant to the research question, selecting temperatures that produce simpler spectra should be preferred.

Information on magnetic ordering temperature (T_B, T_N, T_C) allows us to propose a simplified guideline for predicting the expected Mössbauer spectral shape (sextet, doublet, octet, or singlet) of various Fe phases as a function of temperature (Figure 4). While the expected spectral shape can aid users in selecting ideal

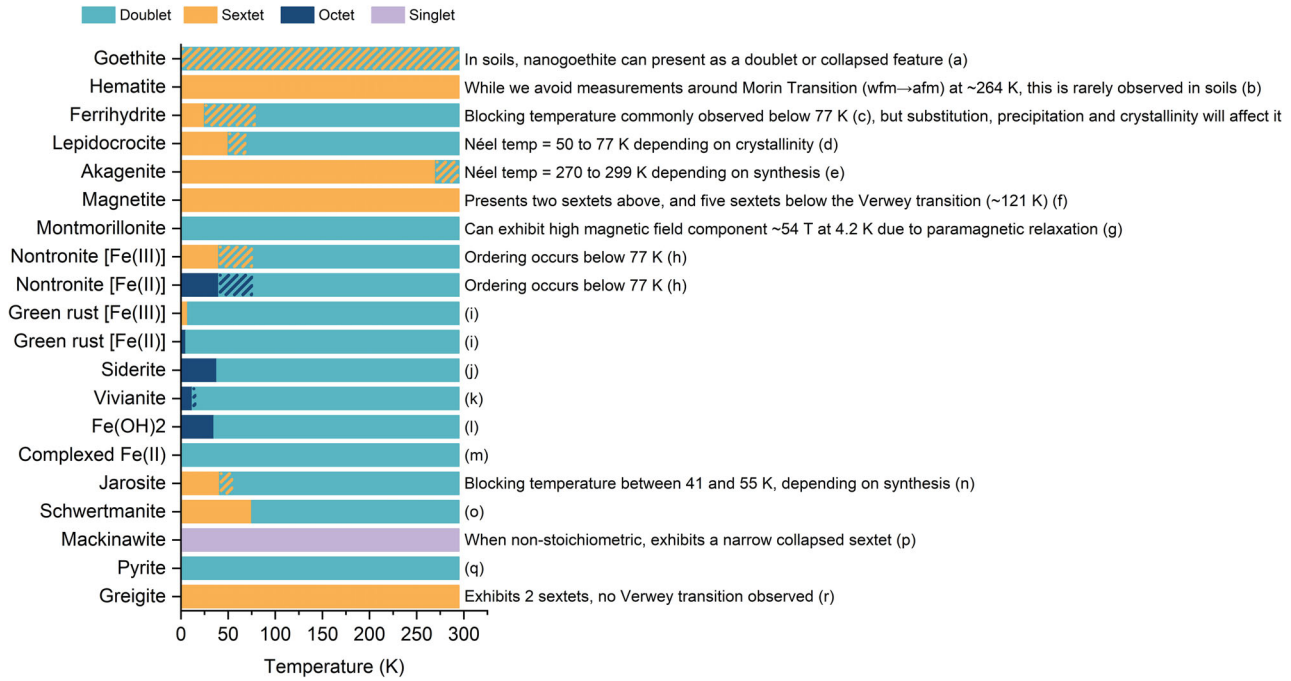

FIGURE 4 | Simplified representation of expected Mössbauer features (sextet, doublet, octet, or singlet) of various Fe phases at different temperatures. Hatched areas represent temperatures in which we expect a mixture of the features with those colors. Letters refer to references listed in the figure. (a) van der Zee et al. (2003), (b) Amin and Arajs (1987), (c) Byrne and Kappler (2019), (d) Murad and Schwertmann (1984), (e) Chambaere and De Grave (1984), (f) Doriguetto et al. (2003), (g) Murad et al. (2002), (h) Rothwell et al. (2023), (i) Rusch et al. (2008b), (j) Forester and Koon (1969), (k) Gonser and Grant (1967), (l) Miyamoto (1976), (m) Rancourt et al. (2005), (n) Grigg et al. (2024b), (o) Bigham et al. (1994), (p) Schröder et al. (2020), (q) Choi et al. (2021), (r) Wan et al. (2017).

measurement temperatures, it is important to note that most of these data are based on laboratory-synthesized samples. These transition temperatures can vary significantly with particle size, chemical substitutions, magnetic domain size, and crystallinity and should be evaluated accordingly.

3.3.2 | Calibration

Mössbauer spectrometers record a count rate that continually increases as the sample is run, typically for either 512 or 1024 channels. Analysis requires calibration—most often using a 7 μm thick α-Fe(0) foil—and conversion to velocity (mm/s). Most software packages have calibration routines, which also fold the spectra to combine the left and right-hand sides into a single spectrum.

3.3.3 | Software

Within the Earth science Mössbauer community, recoil is one of the most used software for fitting Mössbauer spectra (Lagarec and Rancourt 1998). Recoil was first published almost 30 years ago and, despite several limitations, performs robust fitting using many different models which can suit different applications. Nevertheless, commercial and free alternatives are available including MossA, WinNormos (Brand 2002), and MossWinn (Prescher et al. 2012). New approaches are, however, needed, for example those which include links to databases and potentially machine learning, for example including genetic algorithms (de Souza Jr. 1999). We discuss this in Section 5.

3.3.4 | Selection of Spectral Lineshape Model

In cases where single mineral phases are being evaluated and compared with references, it may be sufficient to apply the simplest of models, the Lorentzian lineshape, which follows a characteristic bell-shaped curve. Doublets are constructed from a superposition of two individual Lorentzian peaks, while sextets are constructed from six. Theoretically, all Mössbauer spectra should conform to a Lorentzian lineshape (Murad and Cashion 2004), but in most minerals—especially in complex soil and sediment samples—each Fe nucleus resides in one of a range of different atomic environments due to differences in particle size, the degree of ion substitution, magnetic domain size, and so on. Thus, even in a single natural mineral, these slight variations in nuclear environment create a distribution of slightly different Lorentzian MBS lineshapes (nonhomogenous line broadening; Rancourt and Ping 1991). For this reason, most Earth science Mössbauer spectroscopists use Voigt-based lineshape models, which are implemented in the recoil fitting software. The Voigt lineshape is mathematically complex and is formed by the convolution of Gaussian and Lorentzian lineshapes. There is no analytical solution to the Voigt line, however a simplistic approximation is often used (Rancourt 1989; Rancourt and Ping 1991). One of the advantages of using Voigt is that it effectively creates a sum of Lorentzian lines with a probability distribution (σ values in recoil) around the parameter values (see Table 1). Such an approach has clear advantages for soil and sediment samples where Fe is present in many different binding conditions leading to a distribution of parameter values around an average. This distribution can provide important information about the sample (see Section 4.2.1).

In high-spin Fe(II) phases, at temperatures below 40 K, forbidden nuclear energy transitions can occur and manifest as an octet, that is, eight peaks in the Mössbauer spectrum (example in Figure 1). As octets reflect complex interactions between the EFG and the hyperfine magnetic field (z), the fitting of octets is not trivial. A simple Lorentzian or combination of Lorentzian (i.e., Voigt) lineshapes can no longer be used to fit the data and instead the full Hamiltonian equation must be solved to fit the exact lineshape (see Kündig 1967). This requires the use of more parameters than just CS, QS, and H, that is, the asymmetry parameter for the EFG (η), and the angles describing the spatial relationship between the direction of EFG and z (φ, ϑ). This makes the fitting especially challenging, and it is often simply avoided in Earth science literature (Kupper et al. 2023). Despite the challenge of fitting octet phases, there are several recent examples where full Hamiltonian fitting was used to gain insights into the behavior of soils and sediments (e.g., Notini et al. 2023; Rothwell et al. 2023).

3.3.5 | Fitting Mössbauer Spectra

A Mössbauer spectrum may contain a mixture of singlets, doublets, sextets, and octets (Figure 1). Below, we lay out approaches for fitting spectral features (sub-spectra) with special emphasis on fitting octets as they are relatively less studied. The accuracy of the fit, and thereby of the interpretation of the results, depends on (1) the research question, (2) the model used, and (3) the quality (signal-to-noise) of the data. Determining the oxidation state is the most straightforward analysis (if no low-spin Fe(II) minerals such as pyrite (FeS_2) are present) and is less sensitive to the type of model or data quality. Higher quality data are needed for relative abundance information and extra care is needed in choosing a fitting model (and note, MBS only considers the relative number of Fe atoms, and not the individual minerals or phases).

Spectral analysis programs often provide a goodness-of-fit measure. In the case of recoil, this is the reduced χ^2 value that indicates the match between the model and the data (Lagarec and Rancourt 1998; Murad and Cashion 2004). From a purely mathematical point of view, the value of reduced χ^2 should ideally be equal to one. However, a good, realistic fit to Mössbauer spectra is not dependent only on the mathematical best fit but also on realistic hyperfine parameters of the modeled spectral sites and the environmental context. Lower quality data will return a better reduced χ^2, which all should agree is not the same as a better fit. We recommend the reduced χ^2 value be used as an indicator while fitting the spectrum along with inspection of the residual.

Fitting singlets: Singlets are relatively rare in Mössbauer spectra. A phase that exhibits a singlet is relatively straightforward to fit (allow the computer to iterate and optimize the value, often described as "floating") as it only has a CS and no QS. In a Voigt-based fitting (VBF) model, one would set the QS value to zero and then fit the CS and a σ value to account for any distribution of linewidth across Fe site population.

Fitting doublet and sextets: Doublets and sextets are commonly observed in Mössbauer spectra. Based on the (a)symmetry and the width of the peaks, it is useful to initially estimate how many doublets are present and then add that number of dia/paramagnetic sites (QSD site in the VBF model within recoil). Depending on whether the doublet appears wide or narrow, initial values for the parameters for Fe(II) or Fe(III) should be entered using those given in Figure 2 and then the fit optimized.

To model sextets, the approach is similar to fitting doublets; in the case of the VBF model, the quadrupole shift (ε) must be specified instead of QS, and the magnetic field strength (B_{hf}) must be specified along with its Gaussian width (σ). If the extended VBF (xVBF) model is used, the σ value for all parameters must be specified. Often it is challenging to decide which is most appropriate: (a) a single sextet with a broad σ value (see Section 2.3.1) or (b) a single sextet with multiple components or (c) multiple sextets. The interpretation of the first two are similar, reflecting a distribution of Fe across similar phases, whereas fitting with multiple sextets is most appropriate if assigning them to distinct Fe phases or known contributions of one phase (e.g., magnetite usually exhibits two sextets). Generally, if one can see distinct peaks, then multiple sextets should be included. Otherwise, it is up to the spectroscopist's interpretation. Generating multiple fits for a spectrum (reflecting different potential interpretations) is often a good approach (Thompson et al. 2006; Tishchenko et al. 2015).

In a scenario with both doublets and sextets, the positions of the peaks generally provide some guidance for fitting. The outermost peaks of the sextet can first be fit independent of the central doublets. Next, as the Fe(II) doublet has a higher QS (usually >2 mm/s), the peak on the right is clearly seen and can be used to constrain a doublet site with Fe(II) parameters. For example, the Fe–Ti mineral ilmenite is often easiest to identify by the unique position of its high line (right peak) near 1.4 mm/s (Thompson et al. 2011). If peaks remain around 0.4 mm/s that are unaccounted for, a doublet with parameters in the Fe(III) range should be added. After all peaks seen in the spectrum have been accounted for (irrespective of whether the spectral area is covered), the spectrum should be fit using the VBF or xVBF model.

Fitting collapsed sextets: It is challenging to fit phases transitioning between their paramagnetic and magnetic states (near T_B) at the collection temperature, but for natural soil and sediment samples this is an essential component of almost all spectra. These spectra may exhibit a shape that is wider than a doublet but does not show any distinct peaks (Latta, Bachman, et al. 2012; Notini et al. 2018), referred to sometimes as "collapsed sextet" or colloquially, a "potato." A collapsed feature should be fit by adding a magnetic site (HSD). The CS should be manually entered between 0.4 and 0.6 mm/s to match the expected full sextet CS, with the ε value and B_{hf} values fixed to zero and the σ value of the B_{hf} floated, or set to a fixed value between 18 and 30 T. We recommend including as few parameters as possible to decrease the likelihood of overfitting. Therefore, when using xVBF, set the σ of the quadrupole shift to zero (to match the settings of a VBF fit). We also recommend that the σ value be restricted to less than 30 T; at higher values, the fit may become meaningless as the collapsed feature approaches a flat line. It might be useful to fix the fit for the collapsed feature while tuning details in other phases; however, the fitting should be stable even when all (or most) parameters are floating. There

is always a fitting trade-off between the collapsed sextet and other sites used to fit the spectrum, as the collapsed sextet is an approximation.

3.3.6 | Interpreting Mössbauer Spectra

Once a fit appears to have been completed to a satisfactory level (i.e., reasonable χ^2 and the residual does not possess obvious signs of under fitting), a quick comparison of the hyperfine parameters of each site against correlation plots (CS vs. QS and B_{hf} vs. CS) will reveal whether the parameters are within acceptable limits. If a site is a doublet comparing CS and QS against a relevant correlation plot (e.g., Figure 2A) can indicate both the oxidation state of the doublet, and also whether the parameters are reasonable. For example, a doublet with CS = 0.0 mm/s and QS = 3.5 mm/s clearly falls outside of any of the accepted values for different Fe oxidation states or coordination environments and can therefore be considered incorrect. A similar approach can be made for sextets to identify reasonable fits.

Depending on the main research question, it may be of interest to the user to identify the mineral(s) present in their samples. This is best done through comparison of CS, QS, ε, and B_{hf} against publications, or reference databases. For Fe bearing minerals, tables in Dyar et al. (2006), Murad (2010) as well as Cornell and Schwertmann (2003), provide a useful starting point, though these lists are not exhaustive. The most comprehensive database for Mössbauer hyperfine parameters is maintained by the Mössbauer Effect Data Center (https://www.medc.dicp.ac.cn/index.htm), which was set up with the purpose of collecting Mössbauer parameters and can be accessed through a subscription fee. An older version of this database is available as the Mössbauer Mineral Handbook (Stevens et al. 2002). Alternatively, parameters indicated in Section 4 of this publication for specific minerals are also of use.

3.4 | When and How to Approach Fitting Ferrous Octets

Although fitting singlets, doublets, and sextets using the fitting models described in Section 3.3 is now well established, the fitting of octets, particularly in environmental samples, is less common. However, due to the increased availability of 4 – 5 K capable cryostats, octets are being recorded and interpreted more widely. In this section, we will outline a suggested workflow to identify and fit octets.

3.4.1 | Identifying Octets

When assessing spectra of pure mineral phases, octets can usually be identified based on the much smaller energy difference between the outer peaks (i.e., the "apparent magnetic hyperfine split") compared with Fe(III) sextets (Figure 2B). Octets may appear "collapsed," meaning that not all eight peaks are visible (Figure 1), and the spectra of pure minerals containing Fe(II) in more than one coordination environment may comprise more than eight peaks, which may vary in sharpness.

In samples containing mixtures that also include high-spin Fe(II) phases, the identification of an octet is more complex. For example, in spectra containing a mixture of ferrihydrite and octet-forming ferrous phases, the octet may appear as broadening in the spectra that cannot easily be distinguished from broad, collapsed sextets formed by Fe (oxyhydr)oxides near their blocking temperature. In this instance, it can be useful to measure the same sample at several temperatures. Measuring at a higher temperature (e.g., 77 K) as a starting point will be useful to determine the Fe(II)/Fe(III) ratio of a spectrum. It may also be useful to measure at intermediate cooler temperature steps, around the ordering temperature of minerals of interest. For example, if octet ordering appears below 38 K, then it is an indication that siderite is present, and the ordering is the emergence of the siderite octet (Figure 4). Finally, measuring at ≤5 K is useful to ensure that magnetic ordering is fully developed. If at this temperature it is still unclear if the broad, ordered area is due to collapsed Fe(III) or octet Fe(II), it may be a useful exercise to compare the Fe(II)/Fe(III) ratio of the higher temperature spectrum to the low temperature spectrum. To do this, fit the well resolved doublets and/or sextets in the spectrum (using VBF, see above) and do not fit the broadened area. If extra Fe(II) is required to match the higher temperature Fe(II)/Fe(III) fit, then this suggests that an octet is indeed present. Note, as pyrite or other Fe sulfides containing ferrihydrite Fe(II) are challenging to distinguish from paramagnetic Fe(III) (Figure 2A) and do not order magnetically, they can be included in the Fe(III) pool for the purpose of determining if an octet is present. Note also that this approach assumes that the recoilless fraction f of Fe(II) and Fe(III) components in the sample changes in the same pattern and magnitude with changes in temperature.

3.4.2 | Approach to Fitting Octets

Once the presence of an octet/octets in the spectrum has been established, the challenging task of fitting can begin. The first task here is to think about potential octet-forming ferrous minerals that are likely to be present in the sample. For example, if working in phosphate-rich conditions, vivianite could be a likely candidate. Again, a temperature profile of measurements can be useful to separate likely mineral phases by their ordering temperatures (Figure 4). Before attempting any fitting, it can also be useful to overlay spectra of pure reference minerals on spectra with unknown phases(s), to determine if any peaks align, suggesting that the reference phase may be present in the sample. Once potential minerals have been identified to include in the octet fit, the FSH (Full-Static Hamiltonian) fitting mode in recoil can be used to fit the spectra.

3.4.3 | Executing the Fit of Octets in Complex Environmental Samples

Due to the large number of parameters required to fit octets, care must be taken to avoid overfitting the spectra. When floating so many parameters, it can be easy to achieve a fit that visually appears good but with parameters that make little physical sense. A suggested workflow for identifying and fitting octets is provided in Figure 5.

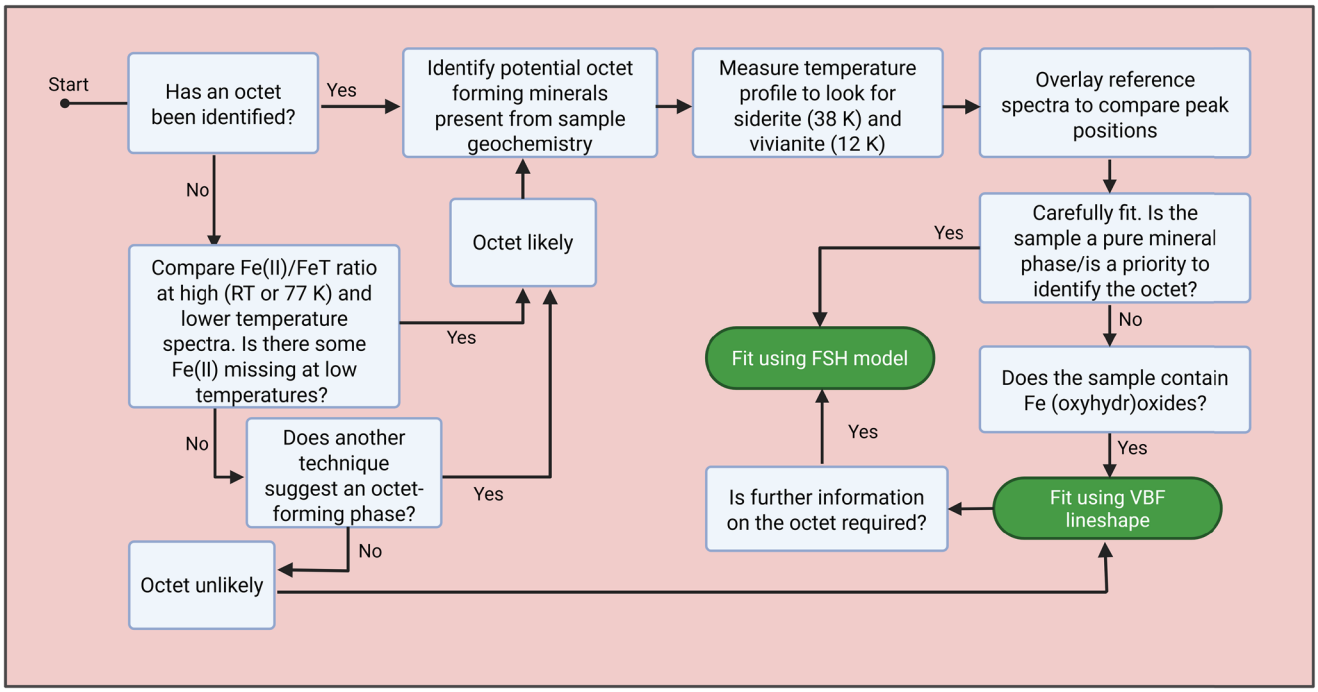

FIGURE 5 | Suggested workflow for identifying the presence of a high-spin Fe(II) octet in a sample and fitting the Mössbauer spectra. Created in BioRender. Notini de Andrade (2025); https://BioRender.com/s96s175.

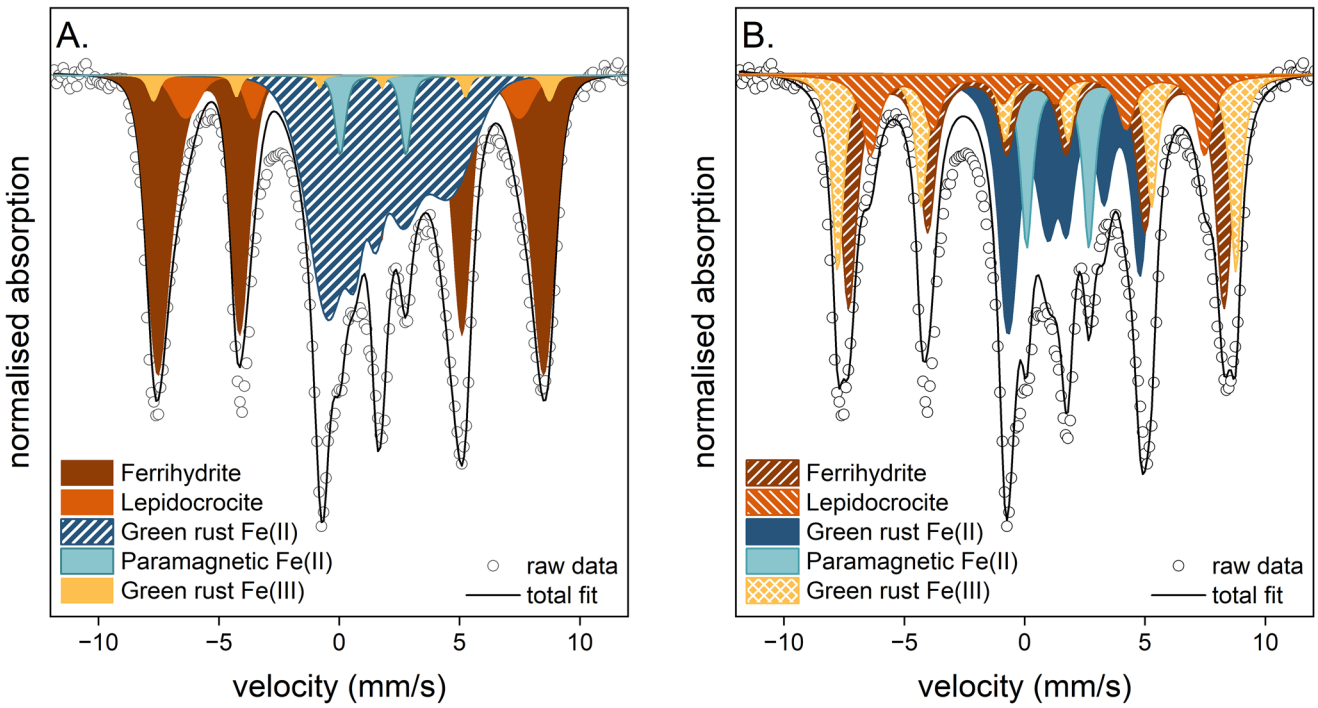

FIGURE 6 | Mössbauer spectra of a mixture of ferrihydrite and green rust fit using (a) the xVBF model allowing the ferrihydrite shape to be captured, and (b) the FSH mode allowing the green rust Fe(II) octet to be fit. Data reproduced with permission and re-analyzed with modified fitting from Notini et al. (2023).

Although octets can be fit using the FSH fitting model, this model does not capture the lineshapes of Fe(III) (oxyhydr)oxides well. For example, the broadening usually observed in ferrihydrite sextets that can be fit using a Voigt based lineshape is almost impossible to capture using the FSH mode (Figure 6B). Therefore, when faced with a complex sample containing both Fe(II) octet and Fe(III) (oxyhydr)oxide sextet phases, a user must decide which fitting protocol is best to use. If the priority is to fit the Fe (oxyhydr)oxide well, the shape of an octet can be approximated using the extended VBF fitting mode (Figure 6A). This is achieved

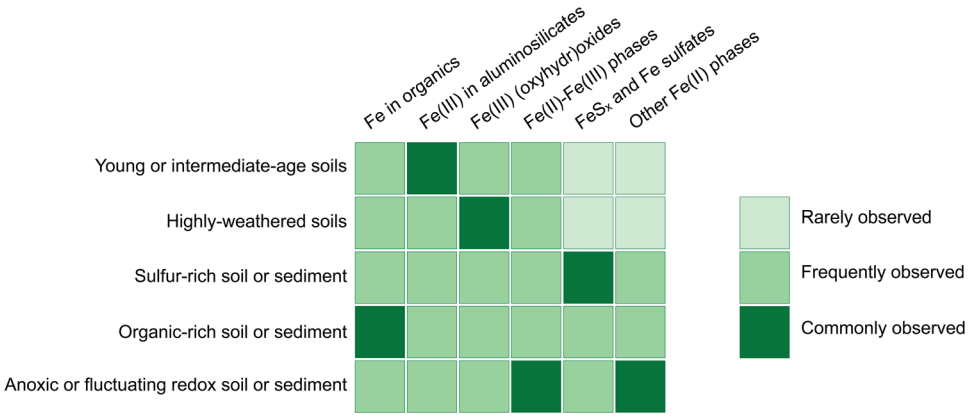

FIGURE 7 | Expected Fe phases as a function of soil conditions.

by adding a probability distribution (i.e., σ) to the QS, as explained in Section 3.3.5. Alternatively, if the priority is to quantify and identify the Fe(II) octet phase, then the FSH mode is preferable, which allows the octet phase to be well fitted (Figure 6B) at the expense of the Fe(III) sextets. Although the two fits are in good agreement for the Fe(II)/Fe(tot) ratio (40% for xVBF vs. 37% for FSH; Tables S2 and S3), the speciation of Fe(III) is quite different. As the xVBF fit for Fe(III) closely resembles the ferrihydrite starting material before the reduction of this sample, we propose that this is likely the best fit for the Fe(III) phases. However, to be certain, one could employ alternative characterization techniques such as Fe XAS to confirm. Often, fitting the spectrum using both modes, or in combination with another technique, can yield the most information (see data in Tables S2 and S3 for the example in Figure 6). However, literature values for parameters used in FSH fitting of octets are comparatively rarer than parameters to fit other Mössbauer spectral lineshapes.

4 | Fe Phases Commonly Explored by MBS in Soils and Sediments

Environmental conditions strongly influence Fe speciation in soils and sediments. For example, in young or intermediate aged soils, most of the Fe is likely in secondary aluminosilicates phases and other primary silicate minerals (Figure 7); whereas in more highly weathered soils, Fe (oyxhydr)oxide phases are more likely to dominate. As discussed above, contextual data (e.g., sample description, information from other analytical techniques or chemical assays) that helps constrain the likely Fe phases is often essential for interpreting Mössbauer spectra. For environmental samples, the parent material of the soil or sediment and the dominant conditions are a powerful first step. For this reason, we describe six broad groupings of Fe phases organized around the type of soil/sediment environment in which they are commonly found (Figure 7).

4.1 | Young or Intermediate-Aged Soils

Young/intermediate-aged soils, or sediments derived from them, typically have considerable fractions of their total Fe in primary minerals (those formed at high temperature and pressure), such as micas, pyroxenes, and olivines, and their initial weathering products. These include clay mineral phases such as 2:1 layer phyllosilicates, for example, illite or smectite, and 1:1 layer phyllosilicates such as kaolinite or serpentines. These soils are often strongly influenced by parent material type, so consideration of the underlying geology is often helpful.

4.1.1 | Aluminosilicates

The most abundant layered aluminosilicate phases (phyllosilicates) found in soils and sediments can contain Fe as isomorphic substitutions in both their tetrahedral and octahedral sheets. The octahedral binding environment is amenable to substantial incorporation of both Fe(III) and Fe(II), up to 40 wt%, although the majority of soil-forming phyllosilicates have low Fe content. In contrast, substitution of Fe(III) into the tetrahedral (silicate) sheet is limited to 10% of total mineral Fe (Kaufhold et al. 2017), and the existence of tetrahedral Fe(II) in phyllosilicates is still debated in the literature (Baron et al. 2016; Finck et al. 2019; Kaufhold et al. 2017).

The hyperfine parameters for Fe in phyllosilicates are generally very similar and cannot be used to identify or distinguish specific phyllosilicate minerals, as shown in Figure 8 (Coey 1980; Murad 2010). Phyllosilicate octahedral Fe(III) exhibits typical hyperfine parameters (Figure 2A), with larger QS values usually assigned to more distorted octahedral binding environments. These parameters also overlap with many other high-spin Fe(III) phases likely present in soils and sediments, making analyses of young and middle-aged soils using MBS alone particularly challenging (Murad 1998).

However, in phyllosilicates with low total Fe content or with Fe in its fully oxidized state, the high-spin Fe(III) remains present as one or more doublets even at low measurement temperatures (4.2 or 5 K) (Ballet and Coey 1982). This property has been used to identify the presence of Fe in phyllosilicates (and/or bound to organic material, see Section 4.3) in natural soils (Thompson et al. 2011). Structural Fe(II) in phyllosilicates largely presents as a doublet with a large QS value (2.5–3.0 mm/s) (Ballet et al. 1979; Dyar et al. 2006) indicative of high-spin Fe(II) (Figure 2A). The presence of this clay mineral Fe(II) is easy to identify and quantify, particularly based on the high energy peak at around 2.7 mm/s (Neumann et al. 2013; Schaefer et al. 2011). In most

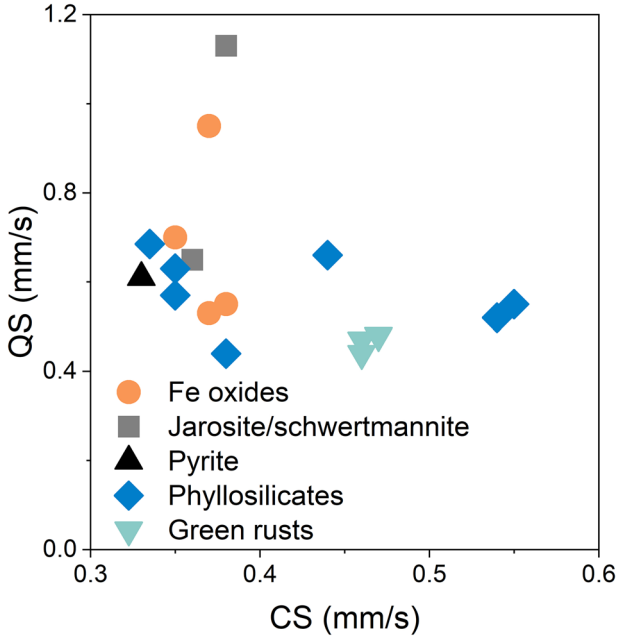

FIGURE 8 | Center shift (CS) versus quadrupole splitting (QS) for common paramagnetic Fe(III) in soils and sediments. Data are taken from Murad (1988) (ferrihydrite, lepidocrocite, akaganéite, jarosite, schwertmannite) and Morice et al. (1969) (pyrite). Green rust chloride, sulfate, and carbonate were synthesized and measured by A.N. (see Supporting Information).

phyllosilicates with low Fe content—which is the majority in soils and sediments—the Fe(II) doublet is also observed down to measurement temperatures of 4.2 K (Ballet and Coey 1982). Hence, measurements of phyllosilicate-rich soils at 4.2 K allow the determination of the reduction extent of phyllosilicate Fe. If phyllosilicates with very low Fe are physically separated from the soil, there is a potential for slow paramagnetic relaxation of the spectra to occur, resulting in an anomalously wide (>55 T) sextet feature (Murad and Cashion 2004; Stucki et al. 1988).

Fe(II)-rich (phyllo)silicates with high total Fe content: Very few low-Fe content phyllosilicates have been reported to show Fe(II) ordering due to slow paramagnetic relaxation at low temperatures (Murad et al. 2002). In contrast, the higher the Fe content in phyllosilicates, the higher the likelihood of interactions between neighboring Fe atoms and hence partial or complete ordering at low temperatures. In primary silicates, the formation of octets has been reported, for example, in the spectra of annite (Christie et al. 1992), fayalite (Lottermoser et al. 1995), and hedenbergite (Eeckhout and De Grave 2003) at low temperatures. In Fe(III)-rich smectite minerals such as nontronite, reduction to Fe(II) leads to more extensive ordering and/or the presence of Fe(II) results in ordering at lower total Fe contents (Rothwell et al. 2023)—a detailed discussion on how to analyze Mössbauer spectra with (partially) ordered Fe(II) components is given in Section 4.5.

4.2 | Highly Weathered Soils and Sediments

Highly weathered soils—which have an accumulation of Fe and Al relative to silicon (typically ultisols and oxisols in the Soil Taxonomy system)—or sediments derived from them, have Fe site populations typically dominated by Fe (oxyhydr)oxide phases. When aluminosilicate minerals are present, they are often 1:1 layer clay minerals, such as kaolinite, which do not incorporate much Fe into their structures. Well crystalline Fe (oxyhydr)oxide minerals (i.e., easily detectable by X-ray diffraction) are often quite straight forward to identify based on their distinct hyperfine parameters. In many cases even trace levels of crystalline Fe (oxyhydr)oxide phases can be detected and quantified in mineralogically complex systems. Hematite in particular is easily discernible owing to its large hyperfine field which is typically larger than any other Fe (oxyhydr)oxide (B_{hf} > 50 T at 295 K; $B_{hf} \approx 54$ T below 77 K; see Figure 2B), and relatively large negative quadrupole shift ($\varepsilon = -0.2$ mm/s). Similarly, stoichiometric magnetite is also quite distinctive owing to the presence of two overlapping sextets corresponding to octahedral and tetrahedrally coordinated mixed-valent Fe. Such phases are abundant in samples formed under geologic (high temperature and pressure) conditions. However, Fe oxides formed in soils or sediments (pedogenic) are generally of much lower crystallinity.

Pedogenic Fe oxides typically exist as small particles and commonly incorporate substitutions of elements such as Al and Si, or form in association with organic compounds. These features lower their crystallinity and influence their magnetic properties, requiring careful consideration during spectral interpretation (Murad 1998). The phenomena of superparamagnetism (discussed above) are particularly relevant for soil Fe (oxyhydr)oxides as nearly all soils have prominent SRO Fe phases present. For instance, while bulk hematite and goethite are magnetically ordered at 295 K, this ordering temperature will be suppressed below room temperature for small particles of hematite (<8 nm) and goethite (<20 nm), even without any substitution (Janot et al. 1973). With ion substitution, the crystallinity of these Fe (oxyhydr)oxide phases, particularly goethite, can decrease still further such that the ordering temperature of nano-crystalline goethite is suppressed below 13 K. As crystallinity decreases, the differences between the individual mineral phases become much harder to identify unambiguously and perhaps much less meaningful (Thompson et al. 2011).

In this section, we briefly describe some of the most common Fe minerals found in highly weathered soils and sediments, with particular attention focused on Fe (oxyhydr)oxides (ferrihydrite, goethite, lepidocrocite) and Fe oxides (hematite and magnetite).

4.2.1 | Fe(III) (Oxyhydr)Oxides

Ferrihydrite: Ferrihydrite is a SRO Fe(III) mineral with two recognized structures based on XRD analysis: 2-line and 6-line ferrihydrite (Figure 9). These two structures exhibit differences in their respective blocking temperatures (T_B) with 2-line ferrihydrite ordering between 5 – 77 K and 6-line ferrihydrite ordering between 77 and 295 K.

Well above T_B, the respective doublets of both types of ferrihydrite have CS values of ≈0.5 mm/s and QS values of ≈0.48 mm/s. Pure, magnetically ordered ferrihydrite is likely best fit with multiple sextets, with Byrne and Kappler (2019) suggesting two,

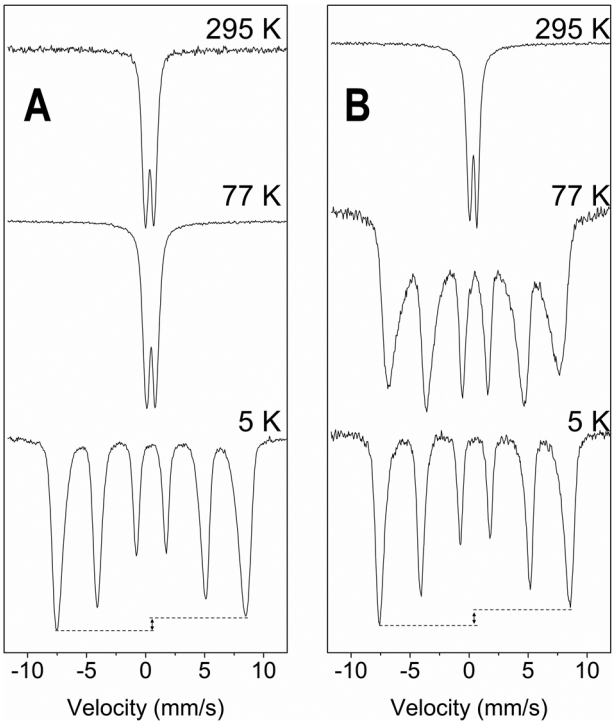

FIGURE 9 | Mössbauer spectra of 2-line ferrihydrite left (A) and 6-line ferrihydrite (B) at room temperature, 77 and 5 K reproduced from Byrne and Kappler (2019) with permission of American Mineralogist.

based on potential tetrahedral and octahedral Fe(III) sites, in agreement with (Maillot et al. 2011; Michel et al. 2007). In this case, 2-line ferrihydrite was fit with sextet A (CS = 0.49 mm/s; ε = 0.00 mm/s; H = 50.1 T) and sextet B (CS = 0.42 mm/s; ε = –0.01 mm/s; H = 46.8 T), while the 6-line ferrihydrite was fit with sextet A (CS = 0.50 mm/s; ε = –0.03 mm/s; H = 50.2 T) and B (CS = 0.40 mm/s; ε = –0.05 mm/s; H = 47.1 T). In soils or complex environmental samples, a single sextet is more often used (Sun et al. 2018) as several other (oxyhydr)oxide phases are often present and most phases (including ferrihydrite) are highly substituted by Al or coprecipitated with organic matter (Chen et al. 2018). In addition, discerning ferrihydrite from other oxyhydroxide phases when high degrees of substitution and low crystallinity are present can often be challenging (Thompson et al. 2011) and instead one can learn more by focusing on differences in crystallinity between samples (Chen et al. 2019). Thus, one might at best refer to similarities between reference 2-line or 6-line ferrihydrite and ferrihydrite in a natural soil sample.

Goethite: Goethite is the most common Fe(III) mineral in soils. The Mössbauer spectrum of goethite is highly dependent on its crystallinity. Well crystalline goethite has a T_N of ≈400 K (Forsyth et al. 1968; van der Woude and Dekker 1966) and appears as a magnetically ordered sextet from 5 K up to room temperature. At 77 K the spectra of well-ordered goethite are defined by a relatively low hyperfine field B_{hf} below 50.0 T and ε of about –0.25 mm/s (Vandenberghe et al. 2000). However, typically most goethite in soil is SRO, often termed micro-crystalline or nano-goethite, and is superparamagnetic (presenting a doublet) at 295 K (CS of ≈0.5 mm/s and QS of ≈0.4 mm/s). Goethite sextets often show wide and asymmetric features, which can be used in their identification (Murad 1982). At 5 K, laboratory prepared nano-goethite has similar CS (0.5 mm/s) and B_{hf} (≈50.0 T) values to well crystalline goethite, but can have ε values similar to bulk goethite (≈–0.22 mm/s; Larese-Casanova et al. 2010) or less negative (–0.12 mm/s; Joshi and Gorski 2016) and more similar to soil-borne phases suspected to be nano-goethite (Chen et al. 2018). Goethite can also be highly substituted by other cations. For example, up to 33 mol% of the Fe(III) in goethite can be substituted by aluminum, resulting in decreased T_N and magnetic ordering at lower temperatures (Fleisch et al. 1980; Fysh and Clark 1982; Golden et al. 1979; Goodman and Lewis 1981; Hogg et al. 1975; Janot et al. 1968).

Distinguishing nano-goethite from ferrihydrite in soils is quite challenging and often offers only marginal additional knowledge (Thompson et al. 2011). One approach is to note differences in the quadrupole shift (ε) for nano-goethite (–0.12 mm/s) and ferrihydrite (–0.03 mm/s) in sextets observed at low temperature (Figure 10). In most cases, SRO Fe (oxyhydr)oxides in soils are intermediate between published parameters for laboratory prepared goethite and ferrihydrite. Separating them can be helpful in some instances (Chen and Thompson 2021), but these differences are not likely indicative of distinctive environmental behavior. This is not surprising as these phases are often highly substituted, or coprecipitated with organic compounds.

Lepidocrocite: Lepidocrocite is commonly found in soils, for example, redoximorphic soils (Schwertmann 1988) and consists of octahedrally coordinated Fe (Ewing 1935). Lepidocrocite is paramagnetic at room temperature, exhibiting a single Fe(III) doublet (Hirt et al. 2002). Well-crystalline lepidocrocite typically magnetically orders into sextets between 73 and 77 K (T_N) (Johnson 1969; Murad and Schwertmann 1984), but this can be 50 K for nanocrystalline SRO lepidocrocite (Murad and Schwertmann 1984) or lower when coprecipitated with organic matter (Chen and Thompson 2018). At 5 K, lepidocrocite has been fitted by a sexted feature with a CS of ≈0.5 mm/s, an ε of 0.2 mm/s and a B_{hf} of ≈43 T (Cornell and Schwertmann 2003; Larese-Casanova et al. 2010; ThomasArrigo et al. 2017). The low hyperfine field normally provides a useful diagnostic to help distinguish lepidocrocite from other Fe(III) oxyhydroxides (see Figure 2B), but exceptions can occur for very low crystallinity phases (Whitaker et al. 2021).

4.2.2 | Fe Oxides

Hematite: Hematite occurs in warm climates and is the most common Fe oxide in soils and sediments (Vandenberghe et al. 2000)—note that goethite (an oxyhydroxide) is the most common Fe mineral—and is also prominent in banded Fe formations (Li et al. 2017). Well crystalline hematite has a T_N of 950 K (Ruskov et al. 1976) and typically exhibits a magnetically ordered sextet from 5 K to room temperature. Even in soils, most often hematite is fully ordered at 295 K, although lower crystalline hematite (sometimes termed microcrystalline) that orders below 295 K is also common (Thompson et al. 2011). At room temperature, the hematite sextet has a B_{hf} of ≈50 T (Vandenberghe et al. 2000), which increases above 50 T below 77 K (Cornell and Schwertmann 2003; Murad 1996; Ruecker et al. 2016). This high B_{hf} compared with other Fe (oxyhydr)oxides is thus a useful parameter for distinguishing hematite in samples from natural

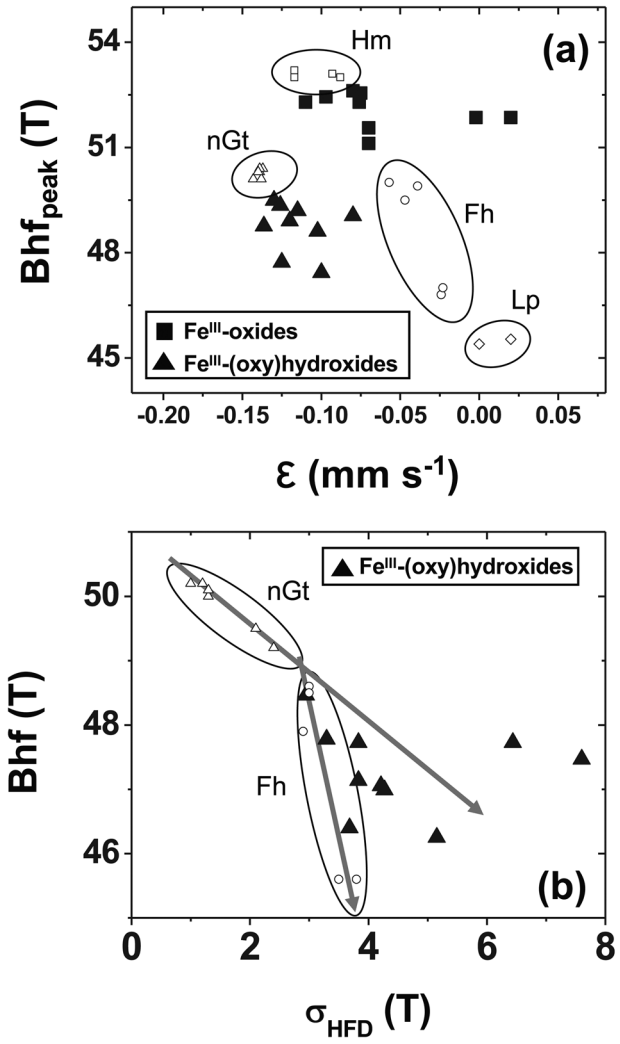

FIGURE 10 | Reproduced from Thompson et al. (2011) with permission from Elsevier for Fe-(oxyhydr)oxide sextets at 4.2 K from soils along the Maui Climate Gradient along with reference values from van der Zee et al. (2003). (a) Most probable hyperfine field, Hpeak, vs. average quadrupole shift, ε (Fh, ferrihydrites; Gt, goethites; Hm, hematites; Lp, lepidocrocites). (b) Average hyperfine field, B_{hf}, vs. the sigma-HFD, which is a measure of line width, for the soils and reference ferrihydrites and goethites. The arrows indicate the trend in the reference Fh's and Gt's from higher to lower crystallinity.

environments (see Figure 2B), while CS varies across typical values expected for Fe(III), between 0.4 and 0.5 mm/s (Byrne et al. 2014). Hematite can undergo the 'Morin Transition' in which the mineral will transition from being ferrimagnetic to fully antiferromagnetic as the temperature is lowered. In well crystalized hematite, the Morin transition is near 240 K and corresponds with a shift in ε values from ≈–0.2 mm/s above the transition to as high as 0.4 mm/s below the transition (Murad and Cashion 2004). However, as with goethite, Fe in hematite can also be substituted by other cations, with up to 16 mol% Fe(III) substituted by Al (Muan and Gee 1956; Schwertmann et al. 1979). With increasing Al content, the T_N decreases, and the Morin transition occurs over a larger temperature range (Srivastava and Sharma 1972). In soils, ion substitution, small particle size, or formation routes most often effectively suppress the Morin transition to below 4.2 K and thus ε values for soil-borne hematite are nearly always in the ≈–0.1 to –0.2 mm/s range (Chen et al. 2019).

Maghemite: Maghemite (γ-Fe_2O_3) is an Fe(III) oxide with a cubic spinel structure and T_N about 950 K (Murad 1996). Maghemite is a fully oxidized magnetite (see Section 4.5.1), with Fe(III) situated in both tetrahedral and octahedral sites. The Mössbauer spectra of maghemite are characterized by two sextets, which are, however, very similar to each other and do not show the distinct offset that the magnetite sextets show (Da Costa et al. 1994). In Murad (1996), typical hyperfine parameters of maghemite are presented: at room temperature, both hyperfine fields are close to 50 T, while the respective CSs are at 0.23 and 0.35 mm/s, increasing to near 0.5 mm/s at 5 K along with a B_{hf} value near 53 T (Cornell and Schwertmann 2003). In practice, this makes soil maghemite challenging to separate from hematite at low temperature as the B_{hf} values are both quite high. Distinguishing them is possible using the QS value, which is near zero or slightly positive for maghemite, assuming hematite has not passed through the Morin transition. Maghemite also has a much larger magnetic susceptibility (i.e., property describing magnetization in an applied magnetic field) than hematite (Torrent et al. 2006), and this has been effective in helping to separate these mineral phases in complex soil samples (Thompson et al. 2011).

4.3 | Organic-Rich Soil and Sediments

Soils and sediments rich in organic matter include most soil O-horizons, histic and spodic horizons, histosols (inclusive of peat-rich bogs and fens), some lake sediments, and near-shore marine sediments. Fe speciation in these environments is likely the only natural system where monomeric Fe-organic phases (consistent with a single Fe atom bonded through an oxygen atom to a carbon, nitrogen, or any atom other than Fe) are likely to be prevalent enough to contribute to bulk Mössbauer spectra. Conceptually, we can divide the types of association between Fe and organic matter into three categories (Kleber et al. 2021): (1) the sorption of organic matter to the surface of Fe minerals, (2) the complexation of Fe ions by organic matter, and (3) environmental transitions involving coprecipitation or coformation of a mixture of solid phase organic matter and Fe mineral phases. However, soils are not pure systems, and all of these types of interactions are intermingled; thus, soil spectra reflect combinations of each of these associations. We briefly mention these idealized categories below and their appearance in Mössbauer spectra followed by suggested interpretation in soil and sediment systems.

4.3.1 | Sorption of Organic Matter to Fe Minerals

Dissolved organic matter often sorbs to the surface of Fe minerals. As this association does not involve a significant portion of the mineral Fe forming Fe–OM bonds, it should theoretically not affect the Mössbauer spectrum of the Fe mineral (Schwertmann et al. 2005; Fritzsche et al. 2021; Voggenreiter et al. 2024). We are thus unlikely to detect differences due to organic matter adsorption in the Mössbauer spectra of any bulk crystalline mineral phases with particle sizes >30 nm. However, most of the Fe mineral surface area in soils is dominated by SRO Fe(III)

(oxyhydr)oxide phases because their small particle size confers a very high specific surface area (Cornell and Schwertmann 1996; Kleber et al. 2021). For these small particles, organic matter can significantly influence the aggregation process and suppress the degree of interparticle magnetic coupling, decreasing the blocking temperature for superparamagnetic phases, as shown in the model ferrihydrite system (Berquó et al. 2009).

4.3.2 | Complexation of Fe Ions with Organic Matter

In principle, monomeric organically complexed Fe(II) and Fe(III) should exhibit doublets at all measurement temperatures, consistent with the isolation of the Fe atoms from one another preventing the spin–spin coupling necessary for magnetic ordering. In the case of Fe(II), monomeric organic complexes may occur: organically complexed Fe(II) (using POM) has been shown to exhibit a doublet down to liquid helium temperatures with CS = 1.24 mm/s and QS = 2.72 mm/s (Joshi et al. 2024) and Fe(II) sorption to cell walls exhibited a doublet with higher QS values (CS = 1.15 to 1.30 mm/s, QS = 3.1 to 3.4 mm/s) (Rancourt et al. 2005).

However, in the case of Fe(III), monomeric complexes with organic matter are likely less common. Even in Fe(III)–citrate complexes—which are often used in XAS as a standard representing organically-complexed Fe(III)—Fe(III) is present in trimers when prepared at equal molar ratios with citrate (1:1 Fe:citrate) (Gautier-Luneau et al. 2005; Gracheva et al. 2024). Only when citrate is present in excess (1:20 Fe:citrate or 1:>20) do monomeric Fe–carboxylate complexes become dominant (Gracheva et al. 2024). The MBS spectrum of trimeric Fe(III) in complexation with citrate is not a doublet at 5 K, but rather a collapsed sextet indicative of nascent magnetic ordering (Gracheva et al. 2024). True monomeric Fe(III)–organic complexes (and likely even dimers; Zhu et al. 2013) would remain paramagnetic at 5 K and if sufficiently diluted and isolated from the soil, they would likely undergo slow paramagnetic relaxation, resulting in an anomalously wide sextet at 5 K consistent with a dilute paramagnet in relatively uniform distribution (Murad and Cashion 2004). Application of an external magnetic field can potentially help distinguish these paramagnetic components from superparamagnetic phases and this unique spectral relaxation is often used to identify monomeric Fe in laboratory solutions (Gracheva et al. 2024). However, slow paramagnetic relaxation of monomeric Fe organic complexes is highly unlikely to be observed in soils because the condition of uniform distributions of Fe throughout organic matter is often not satisfied. Schwertmann and Murad (1988) were able to use the presence of Fe(III) doublets and the development of slow paramagnetic relaxation to identify Fe(III) organic complexes in a peat soil, but only after treating the soil with pyrophosphate and removing the colloidal Fe phases via dialysis and analyzing the dialysate that leaked into the solution. When the whole peat was analyzed directly, Fe(III) sextets dominated the spectra, with only 14% of the spectral area present as a doublet at 4.2 K. For these reasons, identification of organic Fe(III) complexes via a low temperature doublet is challenging in soils and instead a significant portion of organically complexed Fe(III) is likely present in some polymeric form, which should exhibit a broad collapsed sextet at 5 K (Mikutta et al. 2024).

4.3.3 | Coprecipitation of Organic Compounds with Iron Phases

The majority of synthesis literature examining Fe organic matter associations with MBS focuses on coprecipitation, that is, when organic matter is present during Fe(III) hydrolysis or coupled Fe(II) oxidation and hydrolysis to form a solid phase. The source of organic matter may be DOM analogs such as those supplied by the International Humic Substances Society (IHSS) (MacCarthy 1976), organic matter extracted from soils or sediments (Eusterhues et al. 2008; Schwertmann et al. 2005; Voggenreiter et al. 2024), or specific classes of organic molecules such as polysaccharides (Mikutta et al. 2008). Collectively, Mössbauer studies of coprecipitated Fe (oxyhydr)oxides find that the mineral crystallinity—inclusive of particle size—decreases with increasing organic matter (Chen and Thompson 2018; Noor and Thompson 2022), resulting in a decrease in blocking temperature and often B_{hf} (Chen et al. 2015; Eusterhues et al. 2008; Schwertmann et al. 2005). The extent of this blocking temperature suppression also depends on the composition of the coprecipitated organic matter and the degree of other substitutions in the Fe phases (e.g., Al in goethite, see above).

4.3.4 | Interpretation of Fe Phases in Spectra of Organic-Rich Soils and Sediments

The interpretation of Fe phases in spectra in which association with organic matter is expected depends on the environmental conditions and the presence of Fe clays and sulfur-bearing minerals. In the case of Fe(II), complexation of aqueous Fe(II) by organic matter (dissolved and particulate) is likely the dominant pathway for association. Organically complexed Fe(II) may be identified as a doublet with parameters similar to other forms of Fe(II) when spectra are collected at liquid helium temperatures. However, if the sample contains Fe(II) in phyllosilicates or significant Fe(II) adsorbed to non-Fe mineral surfaces, the distinction between organically complexed Fe(II) and clay or mineral-adsorbed Fe(II) is difficult. Therefore, assessing if clay Fe(II) or other Fe(II) phases are likely major components in the sample is essential.

In the case of Fe(III), unambiguous identification of Fe association with organic matter is more complicated. Often, organic matter coprecipitates with Fe(III) oxyhydroxides which are often superparamagnetic and thus have low blocking temperatures. Depression of blocking temperature could occur due to sorption and/or coprecipitation with organic matter and likely co-occurs with Al or other ion substitution that also depresses blocking temperature. This distinction is likely immaterial to the interpretation of an environmental sample spectrum. If an Fe(III) doublet is observed to persist down to 5 K, the standard interpretation in a system without sulfur-bearing phases (see Section 4.4) is that it can be assigned to either adsorbed Fe(III) or Fe(III) in silicates or organic complexes (Thompson et al. 2011; Wilmoth et al. 2018).

We suggest that organically complexed Fe(III) is not evidenced by a doublet at 5 K alone but rather a mix of doublet and broad sextet (Joshi et al. 2024; Mikutta et al. 2024). In addition, nanoparticulate Fe is widespread in soils and sediments, leading

to similar spectral patterns. Even within biological materials, such as plant, microbial, and fungal cells, most of the Fe is present as clusters of very SRO nanoparticles (Bauminger et al. 1980; Kadir et al. 1991; Spartalian et al. 1975) rather than in monomeric complexes. All organisms use some type of ferritin protein to tightly manage Fe inside nearly all their cells, as spurious oxidation of Fe(II) can generate dangerous free radicals via Fenton chemistry. Fe is stored in ferritin as nanoparticles resembling ferrihydrite, typically between 50 and 4000 Fe atoms depending on the Fe nutrition status of the organism. These structures will manifest as a sextet at low temperature—although often cooling below 4.2 K is required to see magnetic ordering that would likely go undetected in some analyses. This is supported by several studies that have combined Fe K-edge XAS with MBS to evaluate Fe in soils or sediments. In all known cases (Giannetta et al. 2022; Ginn et al. 2017; Joshi et al. 2024; Mikutta et al. 2024; Whitaker et al. 2021), the quantitative assignments of monomeric Fe(III) complexed to organics is larger in XAS (typically assigned based on linear combination fitting using a Fe(III)–citrate or catechol standard) than in MBS (represented as a doublet at 5 K or lower). This likely reflects differences in the length scales of the two analytical techniques and also suggests Fe(III) organic complexes are more likely polynuclear than monomeric (Mikutta et al. 2024). We thus suggest that most of the Fe in organic-rich (or any) soils is contained in some form of Fe cluster or nanoparticle, or in larger minerals. For many earth scientists, this observation comes as a surprise because of the strong influence and early prevalence and application of pyrophosphate extractions to approximate organically complexed Fe in soils and sediments (McKeague 1967). Yet nearly 40 years ago (Parfitt and Childs 1988) illustrated that pyrophosphate also extracts SRO and colloidal mineral phases.

4.4 | Sulfur Bearing Environments

In environmental systems that are abundant in sulfur (S), the (trans)formation of Fe–S minerals strongly influences the biogeochemistry of the system. Marine environments have a high proportion of reduced sulfur bearing minerals, particularly pyrite (FeS_2) and mackinawite (FeS). Indeed, the global sedimentary pyrite pool is 10^{21} g (Schlesinger and Bernhardt 2013). These Fe(II)–S_x minerals are formed due to microbial respiration in the sediment where oxygen may only penetrate a few centimeters deep (Canfield et al. 2005), resulting in sulfate (SO_4^{2-}) reduction. Sulfide (HS^-), produced by sulfate reduction, reacts with Fe(II) present in the porewater to form mackinawite (FeS). In addition, HS^- may also reduce Fe(III) in Fe (oxyhydr)oxides and form polysulfides (Rickard and Luther 2007; Wan et al. 2014) that further results in the formation of pyrite. These reactions have been extensively studied in marine systems but the formation of mackinawite also occurs in many terrestrial wetlands and floodplain sediments (Hansel et al. 2015; Kwon et al. 2014; ThomasArrigo et al. 2016). In addition to mackinawite and pyrite, a mixed Fe(II)–Fe(III) phase, greigite (Fe_3S_4), can also form by the reaction of Fe and HS^- (Rickard and Luther 2007).

Sulfide-bearing Fe minerals in sedimentary or geological deposits can become exposed to Earth's atmosphere and oxidize when wetlands are drained or during mining excavations. The oxidation of reduced S produces large amounts of acidity, and, therefore, environments that are strongly impacted by sulfur oxidation are identified as acid sulfate soils, acid mine drainage environments, or acid rock drainage environments, depending on the source of reduced S (Karimian et al. 2018; Simate and Ndlovu 2014). Usually, these environments are defined as having pH values below 4, although a pH below 2 is possible in extreme cases. Under acidic conditions, in the presence of elevated concentrations of S and Fe, a suite of hydroxysulfate minerals may be formed. Among the most thermodynamically stable and commonly observed mineral products are jarosite-type minerals including K-, Na-, or H_3O-jarosite ($AFe_3(SO_4)_2(OH)_6$, where A is mostly K, Na, or H_3O, respectively). Less thermodynamically stable Fe hydroxysulfate minerals are also commonly observed, including schwertmannite ($Fe_8O_8(OH)_{8-2x}(SO_4)x{\cdot}nH_2O$) (Schoepfer and Burton 2021), an SRO mineral first described in the 1990s (Bigham et al. 1994), as well as efflorescent Fe sulfate minerals such as copiapite ($(Fe(II)Fe(III)_4(SO_4)_6(OH)_2{\cdot}20H_2O$) and rozenite ($FeSO_4{\cdot}4H_2O$) (Basallote et al. 2019; Fanning et al. 1993).

Sulfur-bearing Fe minerals have received relatively little attention from the environmental MBS community compared with other Fe minerals such as Fe (oxyhydr)oxides. Below, we briefly describe the spectral parameters for the most common sulfur-bearing Fe minerals, followed by the challenges of analyzing samples containing these minerals.

4.4.1 | Minerals Containing Reduced Sulfur and Fe

Mackinawite (FeS) is the first formation product of the reaction between Fe(II) and HS^-. Due to its symmetrical, undistorted tetrahedral coordination, mackinawite that is purely stoichiometric, that is, the molar ratio of Fe to S is 1:1, is unique in appearing as a singlet at 77 and 5 K. At 5 K, the CS is ≈0.5 mm/s and QS is 0 mm/s (Schröder et al. 2020; Vaughan and Ridout 1971).

Although mackinawite synthesized in the laboratory may exhibit this characteristic singlet, Mössbauer spectra of soil/sediment samples rarely show this property, likely due to nonstoichiometry. The Mössbauer spectrum of nonstoichiometric mackinawite (sometimes referred to as "FeS_x") does not have the same symmetry and exhibits a collapsed sextet. In laboratory studies, the B_{hf} has been reported as ≈27 T (Schröder et al. 2020; Wan et al. 2017). However, it is unknown how the deviation from stoichiometry affects this collapsed sextet feature. In light of this knowledge gap, a few studies have assigned collapsed sextets to FeS_x under sulfidic conditions, irrespective of the strength of the hyperfine field (Bronner et al. 2023; Kubeneck et al. 2024; Morice et al. 1969). Further, differentiation between FeS_x and other phases that might result in collapsed sextets (e.g., very poorly crystalline Fe(III) (oxyhydr)oxides; Chen et al. 2015) is difficult, resulting in nonunique fits. While analyzing samples that may contain FeS, we recommend first ascertaining its presence qualitatively based on color and smell upon the addition of weak acid. It is also helpful to quantify the mass of FeS based on the acid volatile sulfide (AVS) method (Rickard and Morse 2005); however, note that the quantification of Fe based on AVS depends on the assumption of stoichiometry.

Greigite (Fe_3S_4) is the thio-spinel form of Fe, analogous to magnetite. The spectrum contains two sextets that represent tetrahedral sites (CS ≈ 0.37 mm/s, $\varepsilon \approx 0$ mm/s, $B_{hf} \approx 30$ T) and octahedral sites (CS ≈ 0.7 mm/s, $\varepsilon \approx -0.015$ mm/s, $B_{hf} \approx 32$ T) (Wan et al. 2017). As the hyperfine fields of greigite are weaker than that of Fe (oxyhydr)oxides, greigite is relatively straightforward to distinguish from well-ordered Fe (oxyhydr)oxides and magnetite (Figure 2B), especially if magnetic properties are confirmed.

Pyrite (FeS_2) is a low-spin Fe(II) mineral that exhibits a doublet at all temperatures owing to its diamagnetism. Typical parameters are CS ≈ 0.4 mm/s and QS ≈ 0.6 mm/s (Morice et al. 1969; Wan et al. 2017). While the perpetual doublet distinguishes pyrite from other minerals that may magnetically order at low temperatures in laboratory studies, the parameters of pyrite are similar to those of Fe(III) in phyllosilicates (Figure 8). Thus, pyrite and phyllosilicate Fe(III) cannot be reliably distinguished in Mössbauer spectra. Similarly, a pyrite doublet may also be obscured by an Fe(III) phase that is partially ordered even at 5 K, for example, very poorly crystalline Fe(III) (oxyhydr)oxides (Chen et al. 2015). Therefore, we recommend complementing Mössbauer analysis with XRD, where possible, to determine if pyrite exists in the sample. In addition, Fe K-edge XAS may be useful to distinguish between pyrite, Fe(III) in phyllosilicates, and partially ordered Fe(III) (oxyhydr)oxides. It may also be advisable to quantify the pyrite Fe using a sequential HCl and HNO_3 extraction and constrain the pyrite doublet based on this value (Huerta-Diaz and Morse 1990). The application of an external magnetic field may also help to distinguish between pyrite and clay Fe(III), as Fe(III) would be expected to order under the influence of a magnetic field while the pyrite doublet is expected to be unaffected as it is diamagnetic. We know of no studies so far that have attempted this.

4.4.2 | Minerals Containing Oxidized Sulfur and Iron

Jarosite ($KFe_3(SO_4)_2(OH)_6$) and related minerals are often identified by their yellow color and may form as large mottles in acid sulfate soils (Grigg et al. 2024a; Trueman et al. 2020). Jarosite exhibits a doublet (CS ≈ 0.38 mm/s and a wide QS ≈ 1 mm/s) at room temperature (Ruecker et al. 2016) and a sextet (CS ≈ 0.48 mm/s, $\varepsilon \approx -0.08$ mm/s, $H \approx 47$ T) at 5 K (Grigg, Notini, et al. 2024b). The ordering temperature occurs between 35 and 60 K, with substitutions for Fe reducing the ordering of the mineral (Grigg, Notini, et al. 2024b). Substitutions for potassium and sulfur are known to alter the QS of doublets and increase the number of Fe sites with unique parameters.

Schwertmannite ($Fe_8O_8(OH)_{8-2x}(SO_4)_x$) is a poorly crystalline mineral with a high surface area. At room temperature, schwertmannite exhibits an asymmetric doublet (fit with two doublets: (1) CS ≈ 0.39 mm/s, QS ≈ 0.89 mm/s, (2) CS ≈ 0.37 mm/s, QS ≈ 0.62 mm/s) (As et al. 2024; Cashion and Murad 2012). At 5 K, schwertmannite exhibits a sextet, with the ordering temperature reported to be between 120 and 60 K (Bigham et al. 1994; Cashion and Murad 2012; Eneroth and Bender Koch 2004).

The spectra of jarosite and schwertmannite are not identical but may be difficult to effectively distinguish from one another when both are above or below the blocking temperatures. The distinction between the spectra of the two hydroxysulfate minerals may be clarified by comparing the mineral blocking temperatures within the range of 120 – 60 K. However, in the sulfur oxidizing environments mentioned previously, Fe (oxyhydr)oxides may also be present in addition to schwertmannite and jarosite, which complicates an unambiguous fit (Grigg et al. 2024a). For example, nanoparticulate goethite has been reported to order between 225 and 77 K, and by some reports, 4 K (Bhattacharyya et al. 2022; van der Zee et al. 2003), indicating that spectra collected between 120 and 60 K may contain collapsed sextets that represent both schwertmannite and nano-goethite. A similar problem may arise at temperatures <60 K, depending on the ordering temperature of jarosite (Grigg, Notini, et al. 2024b) and ferrihydrite (Eusterhues et al. 2008). In cases where these minerals may be present, complementary techniques such as XRD should be used to detect the presence of jarosite, schwertmannite, and goethite (ferrihydrite does not create distinct reflections in XRD patterns). Further, SEM analyses may indicate the presence of ferrihydrite, although only as aggregates. We also recommend doing temperature profiles of the sample: for example, spectra collected at (1) >120 K, (2) 77 K, (3) 30 K, and (4) 5 K can constrain different (oxy)hydroxide and hydroxysulfate phases present in the sample.

4.5 | Low Oxygen and Reducing Environments

Freshwater-influenced environments, that is, those lacking dissolved S species, can also experience fluctuating oxidizing and reducing conditions, and examples include wetlands and rice paddy soils. These environments are particular hotspots for redox-driven element cycling, and MBS can be useful to characterize the Fe mineralogy of these environments (Borch et al. 2010). In the absence of sulfide or sulfide-producing conditions, nonsulfidic Fe(II)-bearing or mixed-valence (Fe(II)/Fe(III)-containing) minerals may form upon reduction of Fe (oxyhydr)oxides. In contrast to Fe sulfides that contain Fe(II) in the low-spin state, most other ferrous minerals tend to contain high-spin Fe(II), with the important exception of the mixed-valent Fe oxide magnetite.

4.5.1 | Magnetite

Magnetite is a magnetic Fe(II)/Fe(III) oxide with the chemical formula $[Fe(II)Fe(III)_2O_4]$, which appears as a black, cubic, ferrimagnetic mineral. Identification of magnetite in a complex environmental sample through MBS can prove difficult when done without additional information. Best practice is to confirm the presence of magnetic minerals using magnetic susceptibility measurements coupled with X-ray diffraction or another complimentary technique. Magnetite exists in the environment as a result of both abiotic and biotic processes, in addition to its nature as an accessory mineral in rocks. For example, Fe(III)-reducing bacteria such as *Geobacter sulfurreducens* reduce SRO phases such as ferrihydrite to magnetite under anoxic conditions (Lovley et al. 2011). It can also occur in various sediments, soils and rocks, including riverbeds (Sphar 1962), semiarid wetland soils (Auerswald et al. 2001), in banded Fe formations (Li et al. 2017), and due to anthropogenic activities (Usman et al. 2018).

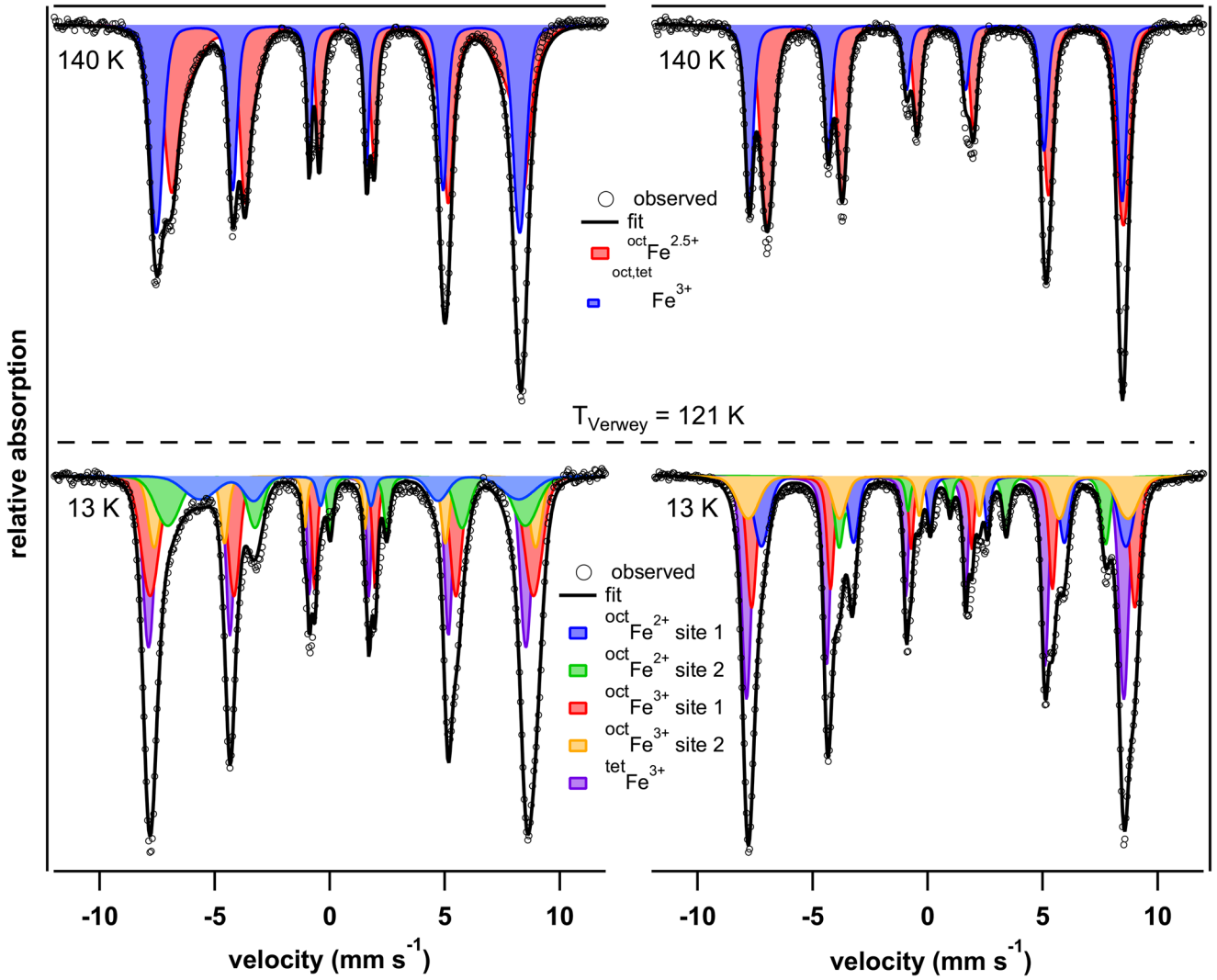

FIGURE 11 | Mössbauer spectra of nanomagnetite (left) and powdered single-crystal magnetite (right) at 140 K with two sextets characteristic of octahedral $Fe^{2.5+}$ and tetrahedral Fe^{3+}. Below the Verwey transition, the 13 K spectrum is made up of multiple sub-spectra; here it is fit with five sextets according to Berry et al. (1998). The figure is reproduced with permission from American Minerologist and fit from data in Gorski and Scherer (2010).

The unit cell of stoichiometric magnetite contains eight Fe(II) atoms in octahedral coordination, eight Fe(III) atoms in octahedral coordination, and eight Fe(III) atoms in tetrahedral coordination. An unpaired electron on octahedral Fe(II) rapidly exchanges between octahedral Fe(II) and Fe(III) and gives rise to magnetite's unique magnetic properties and also gives rise to its characteristic Mössbauer spectra. Typically, when measured above the Verwey temperature (see below) the magnetite spectrum is characterized by two sextets corresponding to octahedrally bound Fe(II) and Fe(III) that give rise to an "$Fe^{2.5+}$ sextet," and tetrahedral bound Fe(III) respectively (Figure 11).

The hyperfine parameters of magnetite depend upon temperature; however, for a spectrum collected at 140 K (Figure 11) the octahedral site is defined by: CS = 0.72 mm/s, ε = −0.04 mm/s, B_{hf} = 47.4 T. The corresponding tetrahedral site has: CS = 0.38 mm/s, ε = 0.00 mm/s, B_{hf} = 50.2 T. The relative areas of each sextet in the magnetite Mössbauer spectrum equal 66% for the octahedral site, and 33% for the tetrahedral site (Gorski and Scherer 2010).

The stoichiometry (x = Fe(II)/Fe(III) ratio) of magnetite can be determined by comparison of the relative areas of each sextet (Gorski and Scherer 2010), though this cannot distinguish between the effects of cation substitution and oxidation.

Magnetite has a specific temperature transition, the Verwey temperature (T_v), which usually occurs at ≈121 K. Below T_v, magnetite undergoes a transition from cubic to monoclinic structure, which causes a relatively steep step change in the magnetization of magnetite and a strong decrease in conductivity (García and Subías 2004; Walz 2002). Below T_v, the Mössbauer spectra of magnetite are much more complicated. Proposed fits of low-temperature magnetite spectra range from four (Řezníček et al. 2017), to five (Hargrove and Kündig 1970), or even to up to nine sextets (de la Figuera and Marco 2019) (Figure 11). Furthermore, T_v is dependent on the stoichiometry of the magnetite particles which can further compound the complexities of interpreting low temperature Mössbauer spectra (Özdemir et al. 1993). Fitting and interpretation of low temperature magnetite spectra require more research, but at the current state of knowledge, we suggest

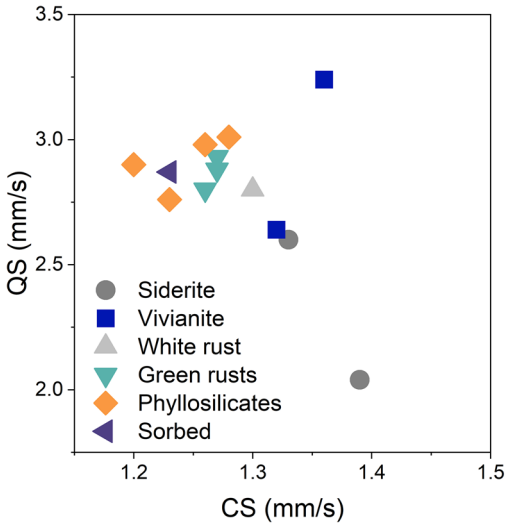

FIGURE 12 | Common high-spin ferrous phases in soils and sediments exhibit doublets with high values of center shift (CS) and quadrupole split (QS) in Mössbauer spectra measured at 77 K. The parameters for white rust, green rusts, reduced smectites, and sorbed Fe(II) cluster together and are almost impossible to distinguish. Vivianite and siderite can be identified based on the CS/QS values of one of their Fe(II) doublets. Data are taken from Rothwell et al. (2024) (siderite), Kubeneck et al. (2025) (vivianite), this manuscript measured by Neumann (white rust and green rust), Vasilopanagos et al. (2022) (illite IMt–2), Rothwell et al. (2023) (nontronite NAu–1), Latta et al. (2017) (montmorillonite SWy–2), Schaefer et al. (2011) (nontronite NAu–2), and Neumann et al. (2013) (sorbed Fe(II)). Green and white rust, and vivianite measured by A. N. (Table S4). All samples were measured at 77 K with the exception of the SWy–2 and NAu–2 samples, which were measured at 13 K.

measurement at 140 K, especially if determination of oxidation state is a priority. If considerable quantities of magnetite are present in a sample, the complex nature of the low-temperature magnetite spectrum will overlap other SRO Fe (oxyhydr)oxide components.

Finally, the magnetite Mössbauer spectrum is also dependent upon purity. For example, transition metal dopants such as cobalt or zinc can result in changes to the octahedral and tetrahedral sites depending upon the preference of the substituting cation (Byrne et al. 2014; Byrne et al. 2013). The consequence is stoichiometry and the presence of impurities can alter the sample similarly.

4.5.2 | High-Spin Fe(II)-Containing Phases Forming Octets

At most measurement temperatures, high-spin Fe(II) is paramagnetic and forms doublets with high CS and QS values relative to paramagnetic Fe(III), making it easy to identify the presence of Fe(II) in the sample (Figure 2A). Although simple to fit, these doublets are often not unique and may be challenging to interpret. For example, sorbed Fe(II), phyllosilicate Fe(II), and Fe(II) in green rust are generally impossible to distinguish (Figure 12). Due to the uniquely narrow (siderite) or wide (vivianite) QS of one of their doublets, siderite and vivianite can, with care, be identified in their paramagnetic state. However, due to the nonuniqueness of the second doublets, it can still be difficult to quantify these phases in samples containing complex mixtures of Fe(II)-bearing phases.

At low temperatures, these high-spin Fe(II) phases order magnetically into octets (see Section 2.1). While this may, at first sight, not simplify the interpretation of the spectra as it does for Fe (oxyhydr)oxides, octets can be identified and fit, which can add valuable insights for sample characterization that cannot be gained from other techniques.

White rust (ferrous hydroxide, $Fe(OH)_2$) precipitates in very reducing conditions and pH values greater than 7.5, depending on the aqueous Fe(II) concentration (Culpepper et al. 2018). In natural environments, this mineral is rare as other anions such as carbonate will outcompete OH^- and form siderite (see below), and its oxidation to magnetite is rapid. White rust prepared in the laboratory has been investigated and provides the easiest case of a magnetically ordered Fe(II) octet phase. When measured at 77 K, its Fe(II) shows typical high-spin Fe(II) hyperfine parameters (CS ≈ 1.2–1.3 mm/s, QS ≈ 3.0 mm/s; Figure 2A) (Entwistle et al. 2019). At low temperatures (<34 K; Miyamoto 1976), the Fe(II) in white rust becomes magnetically ordered and usually presents 4 distinct peaks (Figure 13A). The FSH fit parameters include the CS (1.48 mm/s); the electrical quadrupole interaction $e^2qQ/2$, which usually is of similar magnitude as QS but of a negative value (–3.1 mm/s); and the hyperfine magnetic field B_{hf} with a value of around 20 T. To correctly describe the measured spectrum, the relative orientation between the hyperfine field and the electrical field gradient need to be input. For white rust, this is done by setting the polar angle (ϑ) to 90° (Miyamoto 1976).

Siderite: The ferrous carbonate mineral siderite ($FeCO_3$), occurs commonly in anoxic, nonsulfidic environments, often forming as a result of microbial Fe reduction producing both aqueous Fe(II) and alkalinity (Suess 1979). In its paramagnetic state, the Mössbauer spectrum comprises a doublet with parameters CS ≈ 1.2 mm/s and a characteristically narrow QS ≈ 2.0 mm/s (Figure 12). However, a second doublet is also commonly observed, with more typical Fe(II) parameters of CS ≈ 1.2 mm/s and QS ≈ 2.6 mm/s. The origin of this second doublet is unclear and is suggested to be a result of either the presence of chukanovite $Fe_2(CO_3)(OH)_2$, or due to SRO ferrous carbonate at the mineral surface (Rothwell et al. 2025). The T_N of siderite is reported as 37 K (Frederichs et al. 2003), and the Mössbauer spectrum of siderite below this temperature forms an octet. This octet is challenging to fit and to our knowledge only one published study has done so with parameters CS = 1.35 mm/s, B_{hf} = 18.4 T, $e^2qQ/2$ = 2.02 mm/s, η = 0, φ = 0°, and ϑ = 0° (Ok 1969). However, we found for our data that similarly to the presence of a second doublet to fit the paramagnetic spectrum, a second octet is required for a satisfactory fit of the magnetically ordered spectra (Figure 13B). We present this fit here for the first time for the siderite spectra presented in (Rothwell et al. 2025) with the second octet comprising approximately 20% of the spectral area and fit parameters listed in Table S4.

Vivianite: Vivianite is a ferrous phosphate mineral ($Fe_3(PO_4)_2{\times}8H_2O$) that may play an important role in the

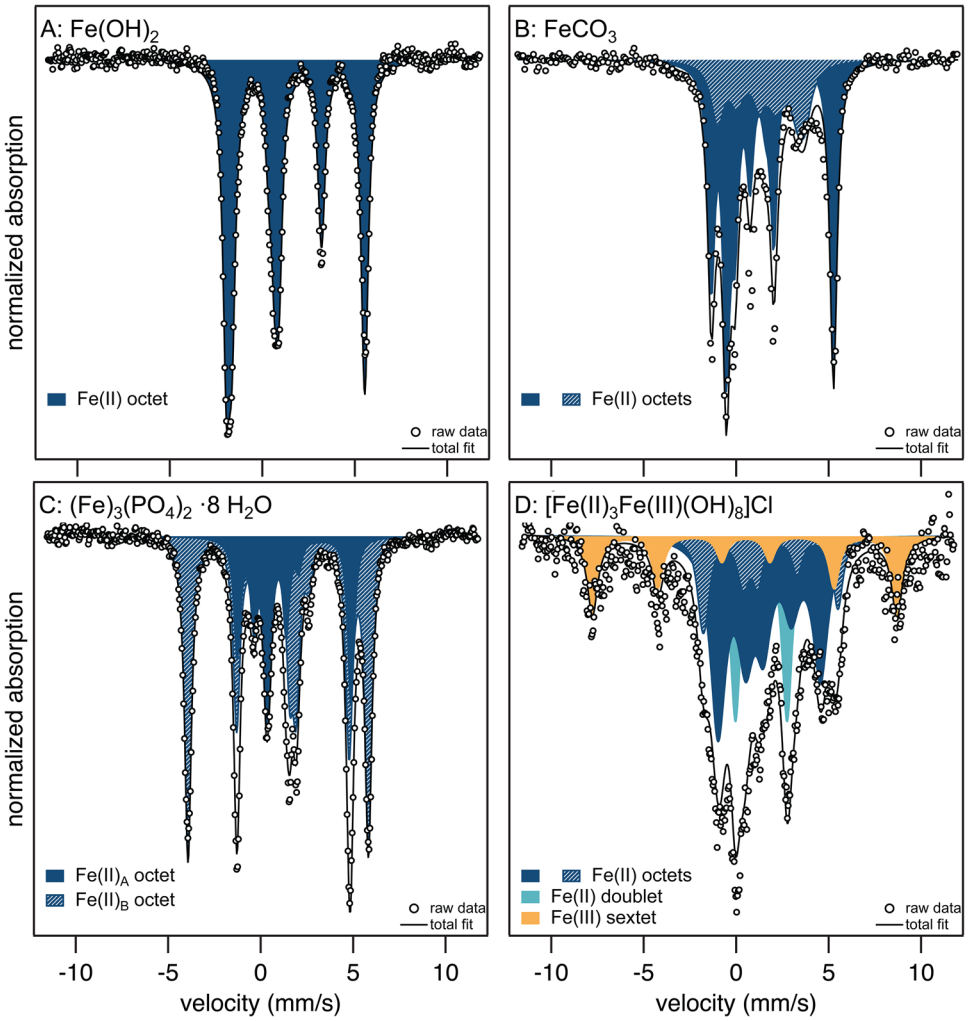

FIGURE 13 | Example spectra of (A) white rust ($Fe(OH)_2$); sample from Entwistle et al. (2019), (B) siderite ($FeCO_3$). Reproduced from Rothwell et al. (2024) with permission from the Royal Society of Chemistry, (C) vivianite ($Fe_3(PO_4)_2 \cdot 8H_2O$, sample from Paskin et al. (2023), and (D) green rust chloride ($[Fe(II)_3Fe(III)(OH)_8]Cl$) collected at 4 K and fit using the FSH approach. Mössbauer parameters resulting from the fits are listed in Table S4.

global phosphorous cycle, acting as a sink for phosphate under anoxic conditions and a phosphate source upon oxidation (Rothe et al. 2016). Vivianite contains Fe(II) in two octahedral sites with one Fe atom occupying an isolated octahedral position (Fe_A), while the other two Fe atoms are located in a double octahedral position (Fe_B) (Mori and Ito 1950). At a measurement temperature of 77 K, the Fe_A and Fe_B sites can be distinguished in samples of pure vivianite with fit parameters CS ≈ 1.3 mm/s and QS ≈ 2.6 mm/s (Fe_A) and CS ≈ 1.3 mm/s and characteristically wide QS ≈ 3.2 mm/s (Fe_B), respectively (Dyar et al. 2014). This allows, for example, the location of isomorphic substitution (Kubeneck et al. 2023) to be identified and for vivianite to be quantified in samples containing mixed Fe phases (Kubeneck et al. 2025). At measurement temperatures below 12 K, both Fe(II) sites in vivianite form octets. As for siderite, fits of the vivianite octets are rare in literature and to our knowledge only two published fits exist (Gonser and Grant 1967). However, we did not find these parameters provided a satisfactory fit for our data (of a sample from Paskin et al. 2023), and we present here an optimized fit based on the hyperfine field gradients proposed by Forsyth et al. (1970) and Gonser and Grant (1967). The Mössbauer parameters for the fit in Figure 13C are given in Table S4.

Green rusts: Green rusts are Fe(II)-rich minerals with the molar fraction x of trivalent cations (i.e., Fe(III)), typically ranging from 0.25 to 0.33. The general formula of these layered double hydroxide minerals $[Fe(II)_{1-x}Fe(III)_x(OH)_2]^x \times [(x/n)A^{n-}, mH_2O]^{x-}$ also indicates the presence of structural water and intercalated anions (A^{n-}). The most common associated anions are sulfate, carbonate, and chloride (Usman et al. 2018). Although green rust can be an important material as a redox-active sorbent for contaminants, it is thought to be metastable in soils and sediments. However, various recent studies have found green rust forms as a result of Fe (oxyhydr)oxide transformation in soils and may be more widespread than previously anticipated (Lefebvre et al. 2024; Notini et al. 2023). Its unambiguous identification in complex samples containing a combination of mineral phases is challenging though, because in its paramagnetic state, green rust Fe exhibits typical hyperfine values found for high-spin Fe(II) and Fe(III) (Figures 12 and 8, respectively) that are independent of the type of intercalating anion and nondistinct from other phases.

Hyperfine parameters obtained from fitting the Mössbauer spectra of synthetic samples obtained at 4 K can aid the identification of green rusts in natural samples. Ordering of Fe(II) and Fe(III)

occurs only at very low temperatures, below 10 K (Rusch et al. 2008a), which in itself might be used as an indicator for the presence of green rusts. As an example, the spectrum of green rust chloride is shown in Figure 13D, demonstrating the presence of Fe(II) octets and Fe(III) sextet with an additional nonordered Fe(II) component present as a doublet. From our FSH fits, values of CS, $e^2qQ/2$, and B_{hf} were obtained and, again, do not differ for the different intercalating anions (Table S4). Similar to white rust, the polar angle (ϑ) between the hyperfine field and the electrical field gradient was set to 90°. The characteristic combination of hyperfine field value and polar angle could be used to identify green rusts. The Fe(III) sextet instead has hyperfine parameters that are similar to many Fe (oxyhydr)oxides, with CS = 0.49 – 0.58 mm/s, $e^2qQ/2 = -0.35$ to -0.06 mm/s, and $B_{hf} = 49 - 51$ T and is thus not relevant for unambiguously identifying green rust. Its absence, however, indicates the presence of a different high-spin Fe(II) phase.

5 | Calls to the Scientific Community

The application of MBS to environmental samples continues to expand and there are several growing needs for our community. Many Earth scientists come to MBS without the deep fundamental training in physics necessary to develop theory related to the unique spectral features we see in environmental samples. Future expansion of Mössbauer techniques to environmental samples can benefit greatly from more collaborations between condensed matter physicists and Earth scientists. Potentially such collaborations could be used in automating Mössbauer analysis that may further encourage its uptake (de Souza Jr. 1999). We also need to work as a community to establish protocols and conventions for data reporting and sharing of Mössbauer spectra in the environmental science literature.

5.1 | Development of the Technique in Environmental Samples

Several common phases found in environmental samples remain difficult to identify and fit in Mössbauer spectra, and many have been identified in this review. In particular, octets formed by high-spin ferrous compounds remain challenging to fit. Current best practice relies on the application of a full static Hamiltonian model as implemented in recoil (Lagarec and Rancourt 1998); however, this cannot also effectively model the Voigt line shape that is often most appropriate to model other phases in the sample. Increasingly, research into reducing soil environments is demonstrating that these compounds are common in the environment. Further theoretical support is required to improve the interpretation of low-temperature spectra containing high-spin ferrous compounds.

There is also a need to further investigate Fe compounds containing sulfur. Currently, there is no consensus regarding the structure and formation processes of the FeS_x minerals that are identified in some natural samples. FeS_x minerals have been identified as sextets at 5 K with a wide range of values for B_{hf} (Thiel et al. 2019; Wan et al. 2017). It also remains unclear why FeS_x minerals may form in the environment rather than stoichiometric mackinawite, which produces a distinctive singlet in Mössbauer spectra. By improving our understanding of FeS_x phases, it should be possible to increase the amount of environmentally relevant information that can be extracted from the Mössbauer fits of these phases.

5.2 | Reporting of Mössbauer Data in Environmental Science Literature

The fitting of Mössbauer spectra of environmental samples is often performed to identify the hyperfine parameters of the phases contained in the sample, including the CS, QS or ε, and B_{hf}. However, the modeling of the spectra is based on several other fundamental parameters that should also be reported to ensure comparability of the results in the literature. Some guidelines for reporting of parameters have been established previously (Grandjean and Long 2021), and many of these recommendations are particularly important for the comparison of environmental samples. The line broadening is essential to producing a reliable fit and can provide useful information about a phase in its geochemical context. In a Voigt-based model, the width of the lines is based on both the Γ (associated with the width of the Lorentzian component of the Voigt model and normally associated with instrumental broadening) and the σ of the QS or B_{hf} (associated with the width of the Gaussian component of the Voigt model and normally associated with the distribution of Fe sites within the fitted phase). The distribution of other parameters in an extended Voigt-based fit should also be reported. Furthermore, asymmetry of spectra is often modeled with the addition of several components with identical CS and ε but different B_{hf} and σ of B_{hf}. The fitting error associated with all parameters is important information to help assess the Mössbauer parameters. The reduced χ^2 value should be reported for the fit along with the hyperfine parameters; however, we strongly recommend against comparing values between sample sets as this value is dependent on the data quality, the extent of absorption, and the model used.

When Mössbauer spectra or fitting parameters are published, the data of the unfitted (but folded) spectrum is of great value to other researchers who wish to check alternative fitting models or compare previous measurements with new experimental data. These objectives can only be achieved if the spectral data are available, but currently a large amount of published data are not available in a format that can be accessed by other researchers. Plotted data or fitting parameters are not sufficient for this purpose. We call on the community to consider always making spectral data available along with the publication of new work that is based on MBS by uploading folded spectral data to appropriate repositories or databases.

Acknowledgments

We thank the attendees of the "Iron Moessbauer applied to environmental systems" workshop, Bristol 2024 (funded through UKRI FLF MR/V023918/1) for their contributions to the overall discussion of this manuscript. A.T. acknowledges funding from US National Science Foundation projects 2307254 and 2241390. A.N. acknowledges funding from the Alexander von Humboldt Foundation through a Humboldt Research Fellowship for Experienced Researchers. D.L. was supported by the U.S.

Department of Energy, Office of Science, Office of Basic Energy Sciences, Chemical Sciences, Geosciences, and Biosciences Division, through its Geosciences program at Pacific Northwest National Laboratory (PNNL). J.M.B is funded by a UKRI Future Leaders Fellowship (MR/V023918/1).

We thank *C.A. Gorski* for providing the magnetite spectral data used in this paper and *Alice Paskin* for providing the vivianite sample that was analyzed for this paper. A.N. is indebted to *Liane G. Benning* for hosting A.N. at GFZ Potsdam during the fellowship and to *Jeffrey Paulo Perez* for help and expert insights related to the synthesis of green rusts. *Phil Larese-Casanova* is thanked for introducing A.N. to FSH fitting of octets and *Catherine McCammon* for resolving the riddle of vivianite octet fitting. *Phil Larese-Casanova* is thanked for preparing the figure that has inspired Figure 4.

Conflicts of Interest

The authors declare no conflicts of interest.

Data Availability Statement

The data that support the findings of this study are from previously published or referenced materials except those in parts of Figure 13. Those data have been uploaded and stored in a Zenodo repository at https://doi.org/10.5281/zenodo.15722488. Any additional information is available from the corresponding author upon reasonable request.

References

Amarasiriwardena, D. D., E. DeGrave, L. H. Bowen, and S. B. Weed. 1986. "Quantitative Determination of Aluminum-Substituted Goethite-Hematite Mixtures by Mössbauer Spectroscopy." *Clays and Clay Minerals* 34, no. 3: 250–256. https://doi.org/10.1346/CCMN.1986.0340304.

Amin, N., and S. Arajs. 1987. "Morin Temperature of Annealed Submicronic A-F_2O_3 Particles." *Physical Review B* 35, no. 10: 4810. https://doi.org/10.1103/PhysRevB.35.4810.

As, K., S. Peiffer, P. O. Uhuegbue, et al. 2024. "Sulfate Affinity Controls Phosphate Sorption and the Proto-Transformation of Schwertmannite." *Chemical Geology* 653: 122043. https://doi.org/10.1016/j.chemgeo.2024.122043.

Auerswald, K., J. Friedl, I. Litaor, and H. Stanjek. 2001. "Iron Oxide Mineralogy of a Semi-Arid Wetland." *Mitteilung Deutsche Bodenkundliche Gesellschaft* 96: 677–678.

Ballet, O., and J. M. D. Coey. 1982. "Magnetic Properties of Sheet Silicates; 2: 1 Layer Minerals." *Physics and Chemistry of Minerals* 8, no. 5: 218–229. https://doi.org/10.1007/BF00309481.

Ballet, O., J. M. D. Coey, and O. Massenet. 1979. "Electric Field Gradient at Fe^{2+} Sites in Trioctahedral Layer Silicates." *Le Journal De Physique Colloques* 40, no. C2. C2-283–C2-285. https://doi.org/10.1051/jphyscol:19792100.

Baron, F., S. Petit, E. Tertre, and A. Decarreau. 2016. "Influence of Aqueous Si and Fe Speciation on Tetrahedral Fe (III) Substitutions in Nontronites: A Clay Synthesis Approach." *Clays and Clay Minerals* 64, no. 3: 230–244. https://doi.org/10.1346/CCMN.2016.0640309.

Barrero, C. A., K. E. García, A. L. Morales, S. Kodjikian, and J. M. Greneche. 2006. "New Analysis of the Mössbauer Spectra of Akaganeite." *Journal of Physics: Condensed Matter* 18, no. 29: 6827.

Basallote, M. D., C. R. Cánovas, M. Olias, et al. 2019. "Mineralogically-Induced Metal Partitioning During the Evaporative Precipitation of Efflorescent Sulfate Salts From Acid Mine Drainage." *Chemical Geology* 530: 119339. https://doi.org/10.1016/j.chemgeo.2019.119339.

Bauminger, E. R., S. G. Cohen, D. P. E. Dickson, A. Levy, S. Ofer, and J. Yariv. 1980. "Mössbauer Spectroscopy of Escherichia Coli and its Iron-Storage Protein." *Biochimica Et Biophysica Acta (BBA)-Protein Structure* 623, no. 2: 237–242. https://doi.org/10.1016/0005-2795(80)90252-4.

Berquó, T. S., S. K. Banerjee, R. G. Ford, R. L. Penn, and T. Pichler. 2007. "High Crystallinity Si-ferrihydrite: An Insight Into its Néel Temperature and Size Dependence of Magnetic Properties." *Journal of Geophysical Research: Solid Earth* 112, no. B2. https://doi.org/10.1029/2006JB004583.

Berquó, T. S., J. J. Erbs, A. Lindquist, R. L. Penn, and S. K. Banerjee. 2009. "Effects of Magnetic Interactions in Antiferromagnetic Ferrihydrite Particles." *Journal of Physics: Condensed Matter* 21, no. 17: 176005. https://doi.org/10.1088/0953-8984/21/17/176005.

Berry, F. J., S. Skinner, and M. F. Thomas. 1998. "Mössbauer Spectroscopic Examination of a Single Crystal of." *Journal of Physics: Condensed Matter* 10, no. 1: 215. https://doi.org/10.1088/0953-8984/10/1/024.

Bhattacharyya, A., R. K. Kukkadapu, M. Bowden, J. Pett-Ridge, and P. S. Nico. 2022. "Fast Redox Switches Lead to Rapid Transformation of Goethite in Humid Tropical Soils: A Mössbauer Spectroscopy Study." *Soil Science Society of America Journal* 86, no. 2: 264–274. https://doi.org/10.1002/saj2.20382.

Bigham, J. M., L. Carlson, and E. J. A. A. Murad. 1994. "Schwertmannite, a New Iron Oxyhydroxysulphate From Pyhäsalmi, Finland, and Other Localities." *Mineralogical Magazine* 58, no. 393: 641–648. https://doi.org/10.1180/minmag.1994.058.393.14.

Bigham, J. M., D. C. Golden, L. H. Bowen, S. W. Buol, and S. B. Weed. 1978. "Mössbauer and X-Ray Evidence for the Pedogenic Transformation of Hematite to Goethite." *Soil Science Society of America Journal* 42, no. 6: 979–981. https://doi.org/10.2136/sssaj1978.03615995004200060032x.

Bødker, F., M. F. Hansen, C. B. Koch, K. Lefmann, and S. Mørup. 2000. "Magnetic Properties of Hematite Nanoparticles." *Physical Review B* 61, no. 10: 6826. https://doi.org/10.1103/PhysRevB.61.6826.

Borch, T., R. Kretzschmar, A. Kappler, et al. 2010. "Biogeochemical Redox Processes and their Impact on Contaminant Dynamics." *Environmental Science & Technology* 44, no. 1: 15–23. https://doi.org/10.1021/es9026248.

Bowen, L. H., S. B. Weed, and J. G. Stevens. 1969. "Mossbauer Study of Micas and Their Potassium-Depleted Products." *American Mineralogist: Journal of Earth and Planetary Materials* 54, no. 1–2: 72–84.

Brand, R. A. 2002. *Normos Mössbauer Fitting Program*. University Duisburg.

Bronner, R., K. Thompson, C. Dreher, et al. 2023. "Co-Reduction of Fe (III) and S0 Drives Fe-S Biomineral Formation and Phosphate Mobilisation." *Geochemical Perspectives Letters* 24: 27–32.

Byrne, J. M., V. S. Coker, E. Cespedes, et al. 2014. "Biosynthesis of Zinc Substituted Magnetite Nanoparticles With Enhanced Magnetic Properties." *Advanced Functional Materials* 24, no. 17: 2518–2529. https://doi.org/10.1002/adfm.201303230.

Byrne, J. M., V. S. Coker, S. Moise, et al. 2013. "Controlled Cobalt Doping in Biogenic Magnetite Nanoparticles." *Journal of The Royal Society Interface* 10, no. 83: 20130134. https://doi.org/10.1098/rsif.2013.0134.

Byrne, J. M., and A. Kappler. 2019. "Mössbauer Spectroscopy." In J. Kenney H. Veeramani, and A. S. Alessi (Eds.), *Analytical geomicrobiology: A handbook of instrumental techniques* (314–338). Cambridge: Cambridge University Press.

Canfield, D. E., E. Kristensen, and B. Thamdrup. 2005. "Aquatic Geomicrobiology." *Advances in Marine Biology* 48: 1–599.

Cashion, J. D., and E. Murad. 2012. Mössbauer Spectra of the Acid Mine Drainage Mineral Schwertmannite from the Sokolov Basin, Czech Republic. Proceedings of the 36th Annual Condensed Matter and Materials Meeting, Australia, 103.

Chambaere, D., and E. De Grave. 1984. "On the Néel Temperature of βFeOOH: Structural Dependence and its Implications." *Journal of Magnetism and Magnetic Materials* 42, no. 3: 263–268. https://doi.org/10.1016/0304-8853(84)90107-0.

Chen, C., D. Barcellos, D. D. Richter, P. A. Schroeder, and A. Thompson. 2019. "Redoximorphic Bt Horizons of the Calhoun CZO Soils Exhibit Depth-Dependent Iron-Oxide Crystallinity." *Journal of Soils and Sediments* 19: 785–797. https://doi.org/10.1007/s11368-018-2068-2.

Chen, C., Y. Dong, and A. Thompson. 2023. "Electron Transfer, Atom Exchange, and Transformation of Iron Minerals in Soils: the Influence of Soil Organic Matter." *Environmental Science & Technology* 57, no. 29: 10696–10707. https://doi.org/10.1021/acs.est.3c01876.

Chen, C., S. J. Hall, E. Coward, and A. Thompson. 2020. "Iron-Mediated Organic Matter Decomposition in Humid Soils can Counteract Protection." *Nature Communications* 11, no. 1: 2255. https://doi.org/10.1038/s41467-020-16071-5.

Chen, C., R. Kukkadapu, and D. L. Sparks. 2015. "Influence of Coprecipitated Organic Matter on Fe^{2+} (aq)-catalyzed Transformation of Ferrihydrite: Implications for Carbon Dynamics." *Environmental Science & Technology* 49, no. 18: 10927–10936. https://doi.org/10.1021/acs.est.5b02448.

Chen, C., C. Meile, J. Wilmoth, D. Barcellos, and A. Thompson. 2018. "Influence of pO_2 on Iron Redox Cycling and Anaerobic Organic Carbon Mineralization in a Humid Tropical Forest Soil." *Environmental Science & Technology* 52, no. 14: 7709–7719. https://doi.org/10.1021/acs.est.8b01368.

Chen, C., and A. Thompson. 2018. "Ferrous Iron Oxidation Under Varying pO_2 Levels: the Effect of Fe (III)/Al (III) Oxide Minerals and Organic Matter." *Environmental Science & Technology* 52, no. 2: 597–606. https://doi.org/10.1021/acs.est.7b05102.

Chen, C., and A. Thompson. 2021. "The Influence of Native Soil Organic Matter and Minerals on Ferrous Iron Oxidation." *Geochimica Et Cosmochimica Acta* 292: 254–270. https://doi.org/10.1016/j.gca.2020.10.002.

Choi, H., J. Y. Seo, Y. R. Uhm, G. M. Sun, and C. S. Kim. 2021. "Crystalline Structure and Magnetic Properties of Pyrite FeS_2." *AIP Advances* 11, no. 1. https://doi.org/10.1063/9.0000110.

Christie, I. A. D., D. G. Rancourt, G. Lamarche, M. Royer, H. Kodama, and J. L. Robert. 1992. "Low Temperature Mössbauer Spectroscopy and Magnetism of Synthetic Annite Mica." *Hyperfine Interactions* 68: 315–318. https://doi.org/10.1007/BF02396499.

Coey, J. M. D. 1980. "Clay Minerals and Their Transformations Studied With Nuclear Techniques: the Contribution of Mössbauer Spectroscopy." *Atomic Energy Review* 18, no. 1: 73–124.

Concas, G., F. Congiu, G. Muscas, and D. Peddis. 2017. "Determination of Blocking Temperature in Magnetization and Mossbauer Time Scale: a Functional Form Approach." *The Journal of Physical Chemistry C* 121, no. 30: 16541–16548. https://doi.org/10.1021/acs.jpcc.7b01748.

Cornell, R. M., and U. Schwertmann. 1996. *The Iron Oxides: Soils*. New York: Wiley-VCH.

Cornell, R. M., and U. Schwertmann. 2003. *The Iron Oxides: Structure, Properties, Reactions, Occurrences, and Uses*, (Vol. 664). Weinheim: Wiley-VCH.

Coward, E. K., A. Thompson, and A. F. Plante. 2018. "Contrasting Fe Speciation in Two Humid Forest Soils: Insight Into Organomineral Associations in Redox-Active Environments." *Geochimica Et Cosmochimica Acta* 238: 68–84. https://doi.org/10.1016/j.gca.2018.07.007.

Culpepper, J. D., M. M. Scherer, T. C. Robinson, A. Neumann, D. Cwiertny, and D. E. Latta. 2018. "Reduction of PCE and TCE by Magnetite Revisited." *Environmental Science: Processes & Impacts* 20, no. 10: 1340–1349.

Da Costa, G. M., E. De Grave, L. H. Bowen, R. E. Vandenberghe, and P. M. A. De Bakker. 1994. "The Center Shift in Mössbauer Spectra of Maghemite and Aluminum Maghemites." *Clays and Clay Minerals* 42, no. 5: 628–633. https://doi.org/10.1346/CCMN.1994.0420515.

De Grave, E., L. H. Bowen, and S. B. Weed. 1982. "Mössbauer Study of Aluminum-Substituted Hematites." *Journal of Magnetism and Magnetic Materials* 27, no. 1: 98–108. https://doi.org/10.1016/0304-8853(82)90288-8.

De Grave, E., G. M. Da Costa, L. H. Bowen, U. Schwertmann, and R. E. Vandenberghe. 1996. "57Fe Mössbauer Effect Study of Al-substituted Lepidocrocites." *Clays and Clay Minerals* 44, no. 2: 214–219. https://doi.org/10.1346/CCMN.1996.0440206.

De Grave, E., and A. Van Alboom. 1991. "Evaluation of Ferrous and Ferric Mössbauer Fractions." *Physics and Chemistry of Minerals* 18: 337–342. https://doi.org/10.1007/BF00200191.

de la Figuera, J., and J. F. Marco. 2019. "Magnetite and The Verwey Transition, From γ-rays to Low-Energy Electrons." *Hyperfine Interactions* 240: 1–15. https://doi.org/10.1007/s10751-019-1577-8.

de Souza Jr, P. A. 1999. "Automation in Mössbauer Spectroscopy Data Analysis." *Laboratory Robotics and Automation* 11, no. 1: 3–23. https://doi.org/10.1002/(SICI)1098-2728(1999)11:1⟨3::AID-LRA2⟩3.0.CO;2-F.

Diamant, A., M. Pasternak, and A. Banin. 1982. "Characterization of Adsorbed Iron in Montmorillonite by Mössbauer Spectroscopy." *Clays and Clay Minerals* 30, no. 1: 63–66. https://doi.org/10.1346/CCMN.1982.0300108.

Doriguetto, A. C., N. G. Fernandes, A. I. C. Persiano, E. N. Filho, J. M. Greneche, and J. D. Fabris. 2003. "Characterization of a Natural Magnetite." *Physics and Chemistry of Minerals* 30, no. 5: 249–255. https://doi.org/10.1007/s00269-003-0310-x.

Dyar, M. D., D. G. Agresti, M. W. Schaefer, C. A. Grant, and E. C. Sklute. 2006. "Mossbauer Spectroscopy of Earth and Planetary Materials." *Annual Review of Earth and Planetary Sciences* 34: 83–125.

Dyar, M. D., E. R. Jawin, E. Breves, et al. 2014. "Mössbauer Parameters of Iron in Phosphate Minerals: Implications for Interpretation of Martian Data." *American Mineralogist* 99, no. 5–6: 914–942. http://doi.org/10.2138/am.2014.4701.

Eeckhout, S. G., and E. De Grave. 2003. "^{57}Fe Mössbauer-Effect Studies of Ca-rich, Fe-Bearing Clinopyroxenes: Part I. Paramagnetic Spectra of Magnesian Hedenbergite." *American Mineralogist* 88, no. 7: 1129–1137. https://doi.org/10.2138/am-2003-0721.

Eneroth, E., and C. Bender Koch. 2004. "Fe-Hydroxysulphates From Bacterial Fe^{2+} Oxidation." *Hyperfine Interactions* 156, no. 1: 423–429.

Entwistle, J., D. E. Latta, M. M. Scherer, and A. Neumann. 2019. "Abiotic Degradation of Chlorinated Solvents by Clay Minerals and Fe (II): Evidence for Reactive Mineral Intermediates." *Environmental Science & Technology* 53, no. 24: 14308–14318. https://doi.org/10.1021/acs.est.9b04665.

Eusterhues, K., F. E. Wagner, W. Häusler, et al. 2008. "Characterization of Ferrihydrite-Soil Organic Matter Coprecipitates by X-ray Diffraction and Mössbauer Spectroscopy." *Environmental Science & Technology* 42, no. 21: 7891–7897. https://doi.org/10.1021/es800881w.

Ewing, F. J. 1935. "The Crystal Structure of Diaspore." *Journal of Chemical Physics* 3, no. 4: 203–207. https://doi.org/10.1063/1.1749634.

Fanning, D. S., M. C. Rabenhorst, and J. M. Bigham. 1993. "Colors of Acid Sulfate Soils." *Soil Color* 31: 91–108. https://doi.org/10.2136/sssaspecpub31.c6.

Finck, N., M. L. Schlegel, K. Dardenne, et al. 2019. "Structural Iron in Smectites With Different Charge Locations." *Physics and Chemistry of Minerals* 46: 639–661. https://doi.org/10.1007/s00269-019-01028-y.

Fleisch, J., R. Grimm, J. Grübler, and P. Gütlich. 1980. "Determination of The Aluminum Content of Natural and Synthetic Alumogoethites Using Mössbauer Spectroscopy." *Le Journal De Physique Colloques* 41, no. C1: C1–169. https://doi.org/10.1051/jphyscol:1980146.

Forester, D. W., and N. C. Koon. 1969. "Mössbauer Investigation of Metamagnetic $FeCO_3$." *Journal of Applied Physics* 40, no. 3: 1316–1317. https://doi.org/10.1063/1.1657649.

Forsyth, J. B., I. G. Hedley, and C. E. Johnson. 1968. "The Magnetic Structure and Hyperfine Field of Goethite (α-FeOOH)." *Journal of Physics C: Solid State Physics* 1, no. 1: 179–188. https://doi.org/10.1088/0022-3719/1/1/321.

Forsyth, J. B., C. E. Johnson, and C. Wilkinson. 1970. "The Magnetic Structure of Vivianite, $Fe_3(PO_4)_2$•8 H_2O." *Journal of Physics C: Solid State Physics* 3, no. 5: 1127. https://doi.org/10.1088/0022-3719/3/5/026.

Frederichs, T., T. von Dobeneck, U. Bleil, and M. J. Dekkers. 2003. "Towards the Identification of Siderite, Rhodochrosite, and Vivianite in Sediments by Their Low-Temperature Magnetic Properties." *Physics and Chemistry of the Earth, Parts A/B/C* 28, no. 16–19: 669–679. https://doi.org/10.1016/S1474-7065(03)00121-9.

Fritzsche, A., J. Bosch, M. Sander, et al. 2021. "Organic Matter from Redoximorphic Soils Accelerates and Sustains Microbial Fe(III) Reduction." *Environmental Science & Technology*, 55, no. 15: 10821–10831. https://doi.org/10.1021/acs.est.1c01183.

Fysh, S. A., and P. E. Clark. 1982. "Aluminous Goethite: A Mössbauer study." *Physics and Chemistry of Minerals* 8: 180–187. https://doi.org/10.1007/BF00308241.

García, J., and G. Subías. 2004. "The Verwey Transition—A New Perspective." *Journal of Physics: Condensed Matter* 16, no. 7: R145. https://doi.org/10.1088/0953-8984/16/7/R01.

Gautier-Luneau, I., C. Merle, D. Phanon, et al. 2005. "New Trends in The Chemistry of Iron (III) Citrate Complexes: Correlations Between X-ray structures and Solution Species Probed by Electrospray Mass Spectrometry and Kinetics of Iron Uptake From Citrate by Iron Chelators." *Chemistry–A European Journal* 11, no. 7: 2207–2219. https://doi.org/10.1002/chem.200401087.

Giannetta, B., C. Plaza, A. Thompson, A. F. Plante, and C. Zaccone. 2022. "Iron Speciation In Soil Size Fractions Under Different Land Uses." *Geoderma* 418: 115842. https://doi.org/10.1016/j.geoderma.2022.115842.

Ginn, B., C. Meile, J. Wilmoth, Y. Tang, and A. Thompson. 2017. "Rapid Iron Reduction Rates Are Stimulated by High-Amplitude Redox Fluctuations in a Tropical Forest SSoil." *Environmental Science & Technology* 51, no. 6: 3250–3259. https://doi.org/10.1021/acs.est.6b05709.

Golden, D. C., L. H. Bowen, S. B. Weed, and J. M. Bigham. 1979. "Mössbauer Studies of Synthetic and Soil-Occurring Aluminum-Substituted Goethites." *Soil Science Society of America Journal* 43, no. 4: 802–808. https://doi.org/10.2136/sssaj1979.03615995004300040038x.

Gonser, U., and R. W. Grant. 1967. "Determination of Spin Directions and Electric Fields Gradient Axes in Vivianite by Polarized Recoil Freefly-Rays." *Physica Status Solidi* 21: 331. https://doi.org/10.1515/9783112494929-035.

Goodman, B. A., M. V. Cheshire, and J. Chadwick. 1991. "Characterization of The Fe (III)—Fulvic Acid Reaction by Mössbauer Spectroscopy." *Journal of Soil Science* 42, no. 1: 25–38. https://doi.org/10.1111/j.1365-2389.1991.tb00088.x.

Goodman, B. A., and D. G. Lewis. 1981. "Mössbauer Spectra of Aluminous Goethites (α-FeOOH)." *Journal of Soil Science* 32, no. 3: 351–364. https://doi.org/10.1111/j.1365-2389.1981.tb01711.x.

Gorski, C. A., and M. M. Scherer. 2010. "Determination of Nanoparticulate Magnetite Stoichiometry by Mössbauer Spectroscopy, Acidic Dissolution, and Powder X-Ray Diffraction: A Critical Review." *American Mineralogist* 95, no. 7: 1017–1026. https://doi.org/10.2138/am.2010.3435.

Gracheva, M., Z. Klencsár, Z. Homonnay, et al. 2024. "Revealing the Nuclearity of Iron Citrate Complexes at Biologically Relevant Conditions." *Biometals* 37, no. 2: 461–475. https://doi.org/10.1007/s10534-023-00562-1.

Grandjean, F., and G. J. Long. 2021. "Best Practices and Protocols in Mössbauer Spectroscopy." *Chemistry of Materials* 33, no. 11: 3878–3904. https://doi.org/10.1021/acs.chemmater.1c00326.

Grigg, A. R., L. Notini, R. Kaegi, L. K. ThomasArrigo, and R. Kretzschmar. 2024a. "Aluminium Substitution Affects Jarosite Transformation to Iron Oxyhydroxides in The Presence of Aqueous Fe (II)." *Geochimica Et Cosmochimica Acta* 374: 72–84. https://doi.org/10.1016/j.gca.2024.04.008.

Grigg, A. R., L. Notini, R. Kaegi, L. K. ThomasArrigo, and R. Kretzschmar. 2024b. "Structural Effects of Aluminum and Iron Occupancy in Minerals of The Jarosite-Alunite Solid Solution." *ACS Earth and Space Chemistry* 8, no. 2: 194–206. https://doi.org/10.1021/acsearthspacechem.3c00174.

Grigg, A. R., W. Wisawapipat, K. Barmettler, et al. 2024c. "Stability and Transformation of Jarosite and Al-Substituted Jarosite in An Acid Sulfate Paddy Soil Under Laboratory and Field Conditions." *Geochimica Et Cosmochimica Acta* 382: 128–141. https://doi.org/10.1016/j.gca.2024.07.026.

Gütlich, P., C. Schröder, and V. Schünemann. 2012. "Mössbauer Spectroscopy—An Indispensable Tool In Solid State Research." *Spectroscopy Europe* 24, no. 4: 21.

Häggström, L., R. Wäppling, and H. Annersten. 1969. "Mössbauer Study of Iron-Rich Biotites." *Chemical Physics Letters* 4, no. 3: 107–108. https://doi.org/10.1016/0009-2614(69)80067-9.

Handler, R. M., B. L. Beard, C. M. Johnson, and M. M. Scherer. 2009. "Atom Exchange Between Aqueous Fe (II) and Goethite: An Fe Isotope Tracer Study." *Environmental Science & Technology* 43, no. 4: 1102–1107. https://doi.org/10.1021/es802402m.

Hansel, C. M., C. J. Lentini, Y. Tang, D. T. Johnston, S. D. Wankel, and P. M. Jardine. 2015. "Dominance of Sulfur-Fueled Iron Oxide Reduction in Low-Sulfate Freshwater ediments." *The ISME Journal* 9, no. 11: 2400–2412. https://doi.org/10.1038/ismej.2015.50.

Hargrove, R. S., and W. Kündig. 1970. "Mössbauer Measurements of Magnetite Below The Verwey Transition." *Solid State Communications* 8, no. 5: 303–308. https://doi.org/10.1016/0038-1098(70)90455-2.

Hirt, A. M., L. Lanci, J. Dobson, P. Weidler, and A. U. Gehring. 2002. "Low-Temperature Magnetic Properties of Lepidocrocite." *Journal of Geophysical Research: Solid Earth* 107, no. B1: EPM 5–1–EPM 5–9. https://doi.org/10.1029/2001JB000242.

Hogg, C. S., P. J. Malden, and R. E. Meads. 1975. "Identification of Iron-Containing Impurities in Natural Kaolinites Using The Mössbauer Effect." *Mineralogical Magazine* 40, no. 309: 89–96. https://doi.org/10.1180/minmag.1975.040.309.12.

Hohmann, C., E. Winkler, G. Morin, and A. Kappler. 2010. "Anaerobic Fe (II)-Oxidizing Bacteria Show As Resistance and Immobilize As During Fe (III) Mineral recipitation." *Environmental Science & Technology* 44, no. 1: 94–101. https://doi.org/10.1021/es900708s.

Huerta-Diaz, M. A., and J. W. Morse. 1990. "A Quantitative Method For Determination of Trace Metal Concentrations in Sedimentary Pyrite." *Marine Chemistry* 29: 119–144. https://doi.org/10.1016/0304-4203(90)90009-2.

Jackson, M. J., and B. Moskowitz. 2021. "On The Distribution of Verwey Transition Temperatures in Natural Magnetites." *Geophysical Journal International* 224, no. 2: 1314–1325. https://doi.org/10.1093/gji/ggaa516.

Janot, C., M. Chabanel, and E. Herzog. 1968. "Étude d'une Limonite par Effet Mössbauer." *Bulletin De Minéralogie* 91, no. 2: 166–171.

Janot, C., H. Gibert, and C. Tobias. 1973. "Caractérisation de Kaolinites Ferrifères par Spectrométrie Mössbauer." *Bulletin De Minéralogie* 96, no. 4: 281–291.

Johnson, C. E. 1969. "Antiferromagnetism of γ FeOOH: A Mossbauer Effect Study." *Journal of Physics C: Solid State Physics* 2, no. 11: 1996. https://doi.org/10.1088/0022-3719/2/11/314.

Joshi, P., and C. A. Gorski. 2016. "Anisotropic Morphological Changes in Goethite During Fe^{2+}-Catalyzed Recrystallization." *Environmental Science & Technology* 50, no. 14: 7315–7324. https://doi.org/10.1021/acs.est.6b00702.

Joshi, P., L. K. ThomasArrigo, D. Sawwa, L. Sauter, and A. Kappler. 2024. "Complexation by Particulate Organic Matter Alters Iron Redox Behavior." *ACS Earth and Space Chemistry* 8, no. 2: 310–322. https://doi.org/10.1021/acsearthspacechem.3c00288.

Kadir, F. H., G. R. Moore, C. Greenwood, A. Thompson, N. M. Read, and D. P. Dickson. 1991. "Mössbauer Spectroscopic Studies of Iron in Pseudomonas aeruginosa." *Journal of Inorganic Biochemistry* 43, no. 4: 753–758. https://doi.org/10.1016/0162-0134(91)80046-K.

Karimian, N., S. G. Johnston, and E. D. Burton. 2018. "Iron and Sulfur Cycling in Acid Sulfate Soil Wetlands Under Dynamic Redox Conditions: A review." *Chemosphere* 197: 803–816. https://doi.org/10.1016/j.chemosphere.2018.01.096.

Kaufhold, S., J. W. Stucki, N. Finck, et al. 2017. "Tetrahedral Charge and Fe Content in Dioctahedral Smectites." *Clay Minerals* 52, no. 1: 51–65. https://doi.org/10.1180/claymin.2017.052.1.03.

Kleber, M., I. C. Bourg, E. K. Coward, C. M. Hansel, S. C. Myneni, and N. Nunan. 2021. "Dynamic Interactions At the Mineral–Organic Matter Interface." *Nature Reviews Earth & Environment* 2, no. 6: 402–421. https://doi.org/10.1038/s43017-021-00162-y.

Kodama, H., M. Schnitzer, and E. Murad. 1988. "An Investigation of Iron (III)-Fulvic Acid Complexes by Mössbauer Spectroscopy and Chemical Methods." *Soil Science Society of America Journal* 52, no. 4: 994–998. https://doi.org/10.2136/sssaj1988.03615995005200040017x.

Koeksoy, E., M. Halama, N. Hagemann, et al. 2018. "A Case Study For Late Archean and Proterozoic Biogeochemical Iron-and Sulphur Cycling In A Modern Habitat—the Arvadi Spring." *Geobiology* 16, no. 4: 353–368. https://doi.org/10.1111/gbi.12293.

Kubeneck, L. J., L. Notini, K. A. Rothwell, et al. 2024. "Transformation of Vivianite in Intertidal Sediments With Contrasting Sulfide Conditions." *Geochimica Et Cosmochimica Acta* 370: 173–187. https://doi.org/10.1016/j.gca.2024.01.020.

Kubeneck, L. J., K. A. Rothwell, L. Notini, et al. 2025. "In Situ Vivianite Formation in Intertidal Sediments: Ferrihydrite-Adsorbed P Triggers Vivianite Formation." *Environmental Science & Technology* 59, no. 1: 523–532. https://doi.org/10.1021/acs.est.4c10710.

Kubeneck, L. J., L. K. ThomasArrigo, K. A. Rothwell, R. Kaegi, and R. Kretzschmar. 2023. "Competitive Incorporation of Mn and Mg in VivianiteAt Varying Salinity and Effects on Crystal Structure and Morphology." *Geochimica Et Cosmochimica Acta* 346: 231–244. https://doi.org/10.1016/j.gca.2023.01.029.

Kündig, W. 1967. "Evaluation of Mössbauer Spectra For ^{57}Fe." *Nuclear Instruments and Methods* 48, no. 2: 219–228. https://doi.org/10.1016/0029-554X(67)90320-5.

Kupper, R. J., N. Zhou, C. S. Chan, A. Thompson, and J. G. Catalano. 2023. "Oxidation Rates and Redox Stabilization of Ferrous Iron in Trioctahedral Smectites." *Geochimica Et Cosmochimica Acta* 355: 282–300. https://doi.org/10.1016/j.gca.2023.06.029.

Kwon, M. J., M. I. Boyanov, D. A. Antonopoulos, et al. 2014. "Effects of Dissimilatory Sulfate Reduction on FeIII (hydr) oxide Reduction and Microbial Community Development." *Geochimica Et Cosmochimica Acta* 129: 177–190. https://doi.org/10.1016/j.gca.2013.09.037.

Lagarec, K., and D. G. Rancourt. 1998. *Recoil-Mössbauer Spectral Analysis Software For Windows*. Ottawa: University of Ottawa.

Lalonde, A. E., D. G. Rancourt, and J. Y. Ping. 1998. "Accuracy of ferric/ferrous determinations in micas: A comparison of Mössbauer spectroscopy and the Pratt and Wilson wet-chemical methods." *Hyperfine Interact* 117: 175–204.

Larese-Casanova, P., S. B. Haderlein, and A. Kappler. 2010. "Biomineralization of Lepidocrocite and Goethite by Nitrate-Reducing Fe (II)-Oxidizing Bacteria: Effect of pH, Bicarbonate, Phosphate, and Humic Acids." *Geochimica Et Cosmochimica Acta* 74, no. 13: 3721–3734. https://doi.org/10.1016/j.gca.2010.03.037.

Latta, D. E., J. E. Bachman, and M. M. Scherer. 2012. "Fe Electron Transfer and Atom Exchange in Goethite: Influence of Al-substitution and Anion Sorption." *Environmental Science & Technology* 46, no. 19: 10614–10623. https://doi.org/10.1021/es302094a.

Latta, D. E., M. I. Boyanov, K. M. Kemner, E. J. O'Loughlin, and M. M. Scherer. 2012. "Abiotic Reduction of Uranium by Fe (II) in Soil." *Applied Geochemistry* 27, no. 8: 1512–1524. https://doi.org/10.1016/j.apgeochem.2012.03.003.

Latta, D. E., A. Neumann, W. A. P. J. Premaratne, and M. M. Scherer. 2017. "Fe (II)–Fe (III) Electron Transfer in A Clay Mineral With Low Fe Content." *ACS Earth and Space Chemistry* 1, no. 4: 197–208. https://doi.org/10.1021/acsearthspacechem.7b00013.

Lefebvre, P., A. R. Grigg, and R. Kretzschmar. 2024. "Geochemical Decoupling of Iron and Zinc During Transformation of Zn-Bearing Ferrihydrite in Reducing Sediments." *Environmental Science & Technology* 58, no. 45: 20224–20234. https://doi.org/10.1021/acs.est.4c09261.

Li, Y. L., K. O. Konhauser, and M. Zhai. 2017. "The Formation of Magnetite in the Early Archean Oceans." *Earth and Planetary Science Letters* 466: 103–114. https://doi.org/10.1016/j.epsl.2017.03.013.

Liao, S., X. Wang, H. Yin, et al. 2020. "Effects of Al Substitution on Local Structure and Morphology of Lepidocrocite and its Phosphate Adsorption Kinetics." *Geochimica Et Cosmochimica Acta* 276: 109–121. https://doi.org/10.1016/j.gca.2020.02.027.

Lottermoser, W., K. Forcher, G. Amthauer, and H. Fuess. 1995. "Powder- and Single Crystal Mössbauer Spectroscopy on Synthetic ayalite." *Physics and Chemistry of Minerals* 22: 259–267. https://doi.org/10.1007/BF00202259.

Lovley, D. R., T. Ueki, T. Zhang, et al. 2011. "*Geobacter:* The Microbe Electric's Physiology, Ecology, and Practical Applications." In K. P. Robert (Ed.), *Advances in Microbial Physiology*, (1–100). Cambridge: Academic Press.

MacCarthy, P. 1976. "A proposal to establish a reference collection of humic materials for interlaboratory comparisons." *Geoderma*, 16, no. 2: 179–181.

MacKenzie, K. J. D., and M. E. Bowden. 1983. "Thermal and Mössbauer Studies of Iron-Containing Hydrous Silicates. IV. Amesite." *Thermochimica Acta* 64, no. 1–2: 83–106. https://doi.org/10.1016/0040-6031(83)80132-4.

Maillot, F., G. Morin, Y. Wang, et al. 2011. "New Insight Into the Structure of Nanocrystalline Ferrihydrite: EXAFS Evidence for Tetrahedrally Coordinated Iron (III)." *Geochimica Et Cosmochimica Acta* 75, no. 10: 2708–2720. https://doi.org/10.1016/j.gca.2011.03.011.

McKeague, J. A. 1967. "An Evaluation of 0.1 M Pyrophosphate and Pyrophosphate-dithionite in Comparison With Oxalate as Extractants of The Accumulation Products in Podzols and Some Other Soils." *Canadian Journal of Soil Science* 47, no. 2: 95–99. https://doi.org/10.4141/cjss67-017.

Michel, F. M., L. Ehm, S. M. Antao, et al. 2007. "The Structure of Ferrihydrite, A Nanocrystalline Material." *Science* 316, no. 5832: 1726–1729. https://doi.org/10.1126/science.1142525.

Mikutta, C., R. Mikutta, S. Bonneville, et al. 2008. "Synthetic Coprecipitates of Exopolysaccharides and Ferrihydrite. Part I: Characterization." *Geochimica Et Cosmochimica Acta* 72, no. 4: 1111–1127. https://doi.org/10.1016/j.gca.2007.11.035.

Mikutta, C., M. Niegisch, A. Thompson, et al. 2024. "Redox Cycling of Straw-Amended Soil Simultaneously Increases Iron Oxide Crystallinity and the Content of Highly Disordered Organo-Iron (III) Solids." *Geochimica Et Cosmochimica Acta* 371: 126–143. https://doi.org/10.1016/j.gca.2024.02.009.

Mikutta, C., J. G. Wiederhold, O. A. Cirpka, T. B. Hofstetter, B. Bourdon, and U. Von Gunten. 2009. "Iron Isotope Fractionation and Atom Exchange During Sorption of Ferrous Iron To Mineral Surfaces." *Geochimica Et Cosmochimica Acta* 73, no. 7: 1795–1812. https://doi.org/10.1016/j.gca.2009.01.014.

Miyamoto, H. 1976. "The Magnetic Properties of Fe(OH)2." *Materials Research Bulletin* 11, no. 3: 329–335. https://doi.org/10.1016/0025-5408(76)90199-9.

Mori, H., and T. Ito. 1950. "The Structure of Vivianite and Symplesite." *Acta Crystallographica* 3, no. 1: 1–6. https://doi.org/10.1107/S0365110x5000001X.

Morice, J. A., L. V. C. Rees, and D. T. Rickard. 1969. "Mössbauer Studies of Iron Sulphides." *Journal of Inorganic and Nuclear Chemistry* 31, no. 12: 3797–3802. https://doi.org/10.1016/0022-1902(69)80299-X.

Mössbauer, R. L. 1962. "Recoilless Nuclear Resonance Absorption of Gamma Radiation: A New Principle Yields Gamma Lines of Extreme Narrowness for Measurements of Unprecedented Accuracy." *Science* 137, no. 3532: 731–738. https://doi.org/10.1126/science.137.3532.731.

Muan, A., and C. L. Gee. 1956. "Phase Equilibrium Studies in the System Iron Oxide-A12O3 in AIR and at 1 Atm. O2 pressure." *Journal of the American Ceramic Society* 39, no. 6: 207–214. https://doi.org/10.1111/j.1151-2916.1956.tb15647.x.

Murad, E. 1982. "The Characterization of Goethite by Mössbauer Spectroscopy." *American Mineralogist* 67, no. 9–10: 1007–1011.

Murad, E. 1996. "Magnetic Properties of Microcrystalline Iron (III) Oxides and Related Materials As Reflected in Their Mössbauer Spectra." *Physics and Chemistry of Minerals* 23, no. 4: 248–262. https://doi.org/10.1007/BF00207766.

Murad, E. 1998. "Clays and Clay Minerals: What Can Mössbauer Spectroscopy Do To Help Understand Them?." *Hyperfine Interactions* 117, no. 1: 39–70. https://doi.org/10.1023/A:1012635124874.

Murad, E. 2010. "Mossbauer Spectroscopy of Clays, Soils and Their Mineral Constituents." *Clay Minerals* 45, no. 4: 413–430. https://doi.org/10.1180/claymin.2010.045.4.413.

Murad, E., and J. Cashion. 2004. *Mössbauer Spectroscopy of Environmental Materials and Their Industrial Utilization*. Springer Science & Business Media.

Murad, E., and U. Schwertmann. 1980. "The Möessbauer Spectrum of Ferrihydrite and its Relations to Those of Other Iron Oxides." *American Mineralogist* 65, no. 9–10: 1044–1049.

Murad, E., and U. Schwertmann. 1982. "Influence of Foreign Element Substitution on the Mossbauer-Spectra of Iron-Oxides." In H. U. Bambauer (Ed.), *Fortschritte der Mineralogie*, (150–151). Stuttgart: Schweizbart Science Publisher.

Murad, E., and U. Schwertmann. 1983a. "The Influence of Aluminium Substitution and Crystallinity on the Mössbauer Spectra of Goethite." *Clay Minerals* 18, no. 3: 301–312. https://doi.org/10.1180/claymin.1983.018.3.07.

Murad, E., and U. Schwertmann. 1983b. "The Influence of Aluminium Substitution and Crystallinity on the Mössbauer Spectra of Goethite." *Clay Minerals* 18, no. 3: 301–312. https://doi.org/10.1180/claymin.1983.018.3.07.

Murad, E., and U. Schwertmann. 1984. "The Influence of Crystallinity on the Mössbauer Spectrum of Lepidocrocite." *Mineralogical Magazine* 48, no. 349: 507–511. https://doi.org/10.1180/minmag.1984.048.349.04.

Murad, E., and U. Schwertmann. 1988. "The Characterization of Poorly Chrystalline Si-Containing Natural Iron Oxides by Mössbauer Spectroscopy." *Hyperfine Interactions* 41: 835–838. https://doi.org/10.1007/BF02400520.

Murad, E., U. Wagner, F. E. Wagner, and W. Häusler. 2002. "The Thermal Reactions of Montmorillonite: A Mössbauer Study." *Clay Minerals* 37, no. 4: 583–590. https://doi.org/10.1180/0009855023740061.

Neiser, S., D. Rentsch, U. Dippon, et al. 2015. "Physico-Chemical Properties of the New Generation IV Iron Preparations Ferumoxytol, Iron Isomaltoside 1000 and Ferric Carboxymaltose." *Biometals* 28: 615–635. https://doi.org/10.1007/s10534-015-9845-9.

Neumann, A., T. L. Olson, and M. M. Scherer. 2013. "Spectroscopic Evidence for Fe (II)–Fe (III) Electron Transfer at Clay Mineral Edge and Basal Sites." *Environmental Science & Technology* 47, no. 13: 6969–6977. https://doi.org/10.1021/es304744v.

Noor, N., and A. Thompson. 2022. "Localized Alteration of Ferrihydrite Natural Organic Matter Coprecipitates Following Reaction With Fe (II)." *Soil Science Society of America Journal* 86, no. 2: 253–263. https://doi.org/10.1002/saj2.20366.

Notini, L., D. E. Latta, A. Neumann, et al. 2018. "The Role of Defects in Fe (II)–Goethite Electron Transfer." *Environmental Science & Technology* 52, no. 5: 2751–2759. https://doi.org/10.1021/acs.est.7b05772.

Notini, L., D. E. Latta, A. Neumann, et al. 2019. "A Closer Look at Fe (II) Passivation of Goethite." *ACS Earth and Space Chemistry* 3, no. 12: 2717–2725. https://doi.org/10.1021/acsearthspacechem.9b00224.

Notini, L., K. Schulz, L. J. Kubeneck, et al. 2023. "A New Approach for Investigating Iron Mineral Transformations in Soils and Sediments Using 57Fe-Labeled Minerals and 57Fe Mossbauer Spectroscopy." *Environmental Science & Technology* 57, no. 27: 10008–10018. https://doi.org/10.1021/acs.est.3c00434.

Ok, H. N. 1969. "Relaxation Effects in Antiferromagnetic Ferrous Carbonate." *Physical Review* 185, no. 2: 472–476. https://doi.org/10.1103/PhysRev.185.472.

Ôno, K., and A. Ito. 1964. "Mössbauer Study of Magnetic Properties in Ferrous Compounds." *Journal of the Physical Society of Japan* 19, no. 6: 899–907. https://doi.org/10.1143/JPSJ.19.899.

Özdemir, Ö., D. J. Dunlop, and B. M. Moskowitz. 1993. "The Effect of Oxidation on the Verwey Transition in Magnetite." *Geophysical Research Letters* 20, no. 16: 1671–1674. https://doi.org/10.1029/93GL01483.

Parfitt, R. L., and C. W. Childs. 1988. "Estimation of Forms of Fe and Al-a Review, and Analysis of Contrasting Soils by Dissolution and Mossbauer Methods." *Soil Research* 26, no. 1: 121–144. https://doi.org/10.1071/SR9880121.

Paskin, A., T. Couasnon, J. P. H. Perez, et al. 2023. "Nucleation and Crystallization of Ferrous Phosphate Hydrate via An Amorphous Intermediate." *Journal of the American Chemical Society* 145, no. 28: 15137–15151. https://doi.org/10.1021/jacs.3c01494.

Prescher, C., C. McCammon, and L. Dubrovinsky. 2012. "MossA: A Program for Analyzing Energy-Domain Mössbauer Spectra From Conventional and Synchrotron Sources." *Applied Crystallography* 45, no. 2: 329–331. https://doi.org/10.1107/S0021889812004979.

Rancourt, D. G. 1989. "Accurate site populations From Mössbauer spectroscopy." *Nuclear Instruments and Methods in Physics Research Section B: Beam Interactions With Materials and Atoms* 44, no. 2: 199–210. https://doi.org/10.1016/0168-583X(89)90428-X.

Rancourt, D. G. 1998. "Mössbauer spectroscopy in clay science." *Hyperfine Interactions* 117, no. 1: 3–38. https://doi.org/10.1023/A:1012651628508.

Rancourt, D. G., and J. Y. Ping. 1991. "Voigt-Based Methods for Arbitrary-Shape Static Hyperfine Parameter Distributions in Mössbauer Spectroscopy. Nuclear Instruments and Methods in YYY." *Physics Research Section B: Beam Interactions with Materials and Atoms* 58, no. 1: 85–97. https://doi.org/10.1016/0168-583X(91)95681-3.

Rancourt, D. G., P. J. Thibault, D. Mavrocordatos, and G. Lamarche. 2005. "Hydrous Ferric Oxide Precipitation in the Presence of Nonmetabolizing Bacteria: Constraints on the Mechanism of a Biotic Effect." *Geochimica Et Cosmochimica Acta* 69, no. 3: 553–577. https://doi.org/10.1016/j.gca.2004.07.018.

Rea, B. A., J. A. Davis, and G. A. Waychunas. 1994. "Studies of the Reactivity of the Ferrihydrite Surface by Iron Isotopic Exchange and Mössbauer Spectroscopy." *Clays and Clay Minerals* 42: 23–34. https://doi.org/10.1346/CCMN.1994.0420104.

Řezníček, R., V. Chlan, H. Štěpánková, et al. 2017. "Understanding the Mössbauer Spectrum of Magnetite Below the Verwey Transition: Ab Initio Calculations, Simulation, and Experiment." *Physical Review B* 96, no. 19: 195124. https://doi.org/10.1103/PhysRevB.96.195124.

Rickard, D., and G. W. Luther. 2007. "Chemistry of Iron Sulfides." *Chemical Reviews* 107, no. 2: 514–562. https://doi.org/10.1021/cr0503658.

Rickard, D., and J. W. Morse. 2005. "Acid Volatile Sulfide (AVS)." *Marine Chemistry* 97, no. 3–4: 141–197. https://doi.org/10.1016/j.marchem.2005.08.004.

Roca, A. G., J. F. Marco, M. D. P. Morales, and C. J. Serna. 2007. "Effect of Nature and Particle Size on Properties of Uniform Magnetite and

Maghemite Nanoparticles." *The Journal of Physical Chemistry C* 111, no. 50: 18577–18584. https://doi.org/10.1021/jp075133m.

Rothe, M., A. Kleeberg, and M. Hupfer. 2016. "The Occurrence, Identification and Environmental Relevance of Vivianite in Waterlogged Soils and Aquatic Sediments." *Earth-Science Reviews* 158: 51–64. https://doi.org/10.1016/j.earscirev.2016.04.008.

Rothwell, K. A., M. P. Pentrak, L. A. Pentrak, J. W. Stucki, and A. Neumann. 2023. "Reduction Pathway-Dependent Formation of Reactive Fe (II) Sites in Clay Minerals." *Environmental Science & Technology* 57, no. 28: 10231–10241. https://doi.org/10.1021/acs.est.3c01655.

Rothwell, K. A., L. K. ThomasArrigo, R. Kaegi, and R. Kretzschmar. 2025. "Low Molecular Weight Organic Acids Stabilise Siderite Against Oxidation and Influence the Composition of Iron (oxyhydr) oxide Oxidation Products." *Environmental Science: Processes & Impacts* 27, no. 1: 133–145. https://doi.org/10.1039/D4EM00363B.

Ruecker, A., C. Schröder, J. Byrne, P. Weigold, S. Behrens, and A. Kappler. 2016. "Geochemistry and Mineralogy of Western Australian Salt Lake Sediments: Implications for Meridiani Planum on Mars." *Astrobiology* 16, no. 7: 525–538. https://doi.org/10.1089/ast.2015.1429.

Rusch, B., J. M. Génin, C. Ruby, M. Abdelmoula, and P. Bonville. 2008b. "Mössbauer Study of Magnetism in FeII– III (oxy-) hydroxycarbonate Green Rusts; Ferrimagnetism of FeII– III Hydroxycarbonate." *Hyperfine Interactions* 187, no. 1: 7–12. https://doi.org/10.1007/s10751-008-9862-y.

Rusch, B., J. M. R. Génin, C. Ruby, M. Abdelmoula, and P. Bonville. 2008a. "Ferrimagnetic Properties in FeII–III (oxy) Hydroxycarbonate Green Rusts." *Solid State Sciences* 10, no. 1: 40–49. https://doi.org/10.1016/j.solidstatesciences.2007.07.007.

Ruskov, T., T. Tomov, and S. Georgiev. 1976. "Mössbauer Investigation of the Morin Transition in Hematite." *Physica Status Solidi (a)* 37, no. 1: 295–302. https://doi.org/10.1002/pssa.2210370137.

Schaefer, M. V., C. A. Gorski, and M. M. Scherer. 2011. "Spectroscopic Evidence for Interfacial Fe (II)– Fe (III) Electron Transfer in a Clay Mineral." *Environmental Science & Technology* 45, no. 2: 540–545. https://doi.org/10.1021/es102560m.

Schlesinger, W. H., and E. S. Bernhardt. 2013. *Biogeochemistry: An analysis of global change*. New York: Academic Press.

Schoepfer, V. A., and E. D. Burton. 2021. "Schwertmannite: A review of its Occurrence, Formation, Structure, Stability and Interactions With Oxyanions." *Earth-Science Reviews* 221: 103811. https://doi.org/10.1016/j.earscirev.2021.103811.

Schröder, C., M. Wan, I. B. Butler, A. Tait, S. Peiffer, and C. A. McCammon. 2020. "Identification of Mackinawite and Constraints on its Electronic Configuration Using Mössbauer Spectroscopy." *Minerals* 10, no. 12: 1090. https://doi.org/10.3390/min10121090.

Schulz, K., L. Notini, A. R. Grigg, et al. 2023. "Contact With Soil Impacts Ferrihydrite and Lepidocrocite Transformations During Redox Cycling in a Paddy Soil." *Environmental Science: Processes & Impacts* 25, no. 12: 1945–1961. https://doi.org/10.1039/D3EM00314K.

Schulz, K., W. Wisawapipat, K. Barmettler, et al. 2024. "Iron Oxyhydroxide Transformation in a Flooded Rice Paddy Field and the Effect of Adsorbed Phosphate." *Environmental Science & Technology* 58, no. 24: 10601–10610. https://doi.org/10.1021/acs.est.4c01519.

Schulze, D. G., and U. Schwertmann. 1984. "The Influence of Aluminium on Iron Oxides: X. Properties of Al-substituted Goethites." *Clay Minerals* 19, no. 4: 521–539. https://doi.org/10.1180/claymin.1984.019.4.02.

Schwertmann, U. 1988. "Occurrence and Formation of Iron Oxides in Various Pedoenvironments." In J. W. Stucki, B. A. Goodman, and U. Schwertmann, (Eds.), *Iron in Soils and Clay Minerals* (267–308). Dordrecht: Springer Netherlands.

Schwertmann, U., R. W. Fitzpatrick, R. M. Taylor, and D. G. Lewis. 1979. "The Influence of Aluminum on Iron Oxides. Part II. Preparation and Properties of Al-ubstituted Hematites." *Clays and Clay Minerals* 27, no. 2: 105–112. https://doi.org/10.1346/CCMN.1979.0270205.

Schwertmann, U., and E. Murad. 1988. "The Nature of An Iron Oxide—Organic Iron Association in a Peaty Environment." *Clay Minerals* 23, no. 3: 291–299. https://doi.org/10.1180/claymin.1988.023.3.06.

Schwertmann, U., F. Wagner, and H. Knicker. 2005. "Ferrihydrite–Humic Associations: Magnetic Hyperfine Interactions." *Soil Science Society of America Journal* 69, no. 4: 1009–1015. https://doi.org/10.2136/sssaj2004.0274.

Simate, G. S., and S. Ndlovu. 2014. "Acid Mine Drainage: Challenges and Opportunities." *Journal of Environmental Chemical Engineering* 2, no. 3: 1785–1803. https://doi.org/10.1016/j.jece.2014.07.021.

Spartalian, K., W. T. Oosterhuis, and N. Smarra. 1975. "Mössbauer Effect Studies in the Fungus Phycomyces." *Biochimica Et Biophysica Acta (BBA)-General Subjects* 399, no. 1: 203–212. https://doi.org/10.1016/0304-4165(75)90226-3.

Sphar, J. 1962. "Occurrence of Magnetite in the Arkansas River Bed Between Ford and Arkansas City." *Transactions of the Kansas Academy of Science (1903-)* 65, no. 3: 257–262. https://doi.org/10.2307/3626425.

Srivastava, J. K., and R. P. Sharma. 1972. "Magnetic Dilution Effects on Morin Phase Transition in Hematite." *Physica Status Solidi (B)* 49, no. 1: 135–146. https://doi.org/10.1002/pssb.2220490112.

Stanfield, C. H., Q. R. Miller, A. K. Battu, et al. 2024. "Carbon Mineralization and Critical Mineral Resource Evaluation Pathways for Mafic–Ultramafic Assets." *ACS Earth and Space Chemistry* 8, no. 6: 1204–1213. https://doi.org/10.1021/acsearthspacechem.4c00005.

Stevens, J. G., A. M. Khasanov, H. Pollak, and L. Zhe. 2002. *Mössbauer Mineral Handbook*. Asheville: Mössbauer Effect Data Center.

Stucki, J. W., K. Su, L. Pentráková, and M. Pentrák. 2014. "Methods for Handling Redox-Sensitive Smectite Dispersions." *Clay Minerals* 49, no. 3: 359–377. https://doi.org/10.1180/claymin.2014.049.3.02.

Suess, E. 1979. "Mineral Phases Formed in Anoxic Sediments by Microbial Decomposition of Organic Matter." *Geochimica Et Cosmochimica Acta* 43, no. 3: 339–352. https://doi.org/10.1016/0016-7037(79)90199-6.

Sun, J., B. J. Mailloux, S. N. Chillrud, A. van Geen, A. Thompson, and B. C. Bostick. 2018. "Simultaneously Quantifying Ferrihydrite and Goethite in Natural Sediments Using the Method of Standard Additions With X-ray Absorption Spectroscopy." *Chemical Geology* 476: 248–259. https://doi.org/10.1016/j.chemgeo.2017.11.021.

Taylor, P. D. P., R. Maeck, and P. De Bièvre. 1992. "Determination of the Absolute Isotopic Composition and Atomic Weight of a Reference Sample of Natural Iron." *International Journal of Mass Spectrometry and Ion Processes* 121, no. 1–2: 111–125. https://doi.org/10.1016/0168-1176(92)80075-C.

Tennakoon, D. T., J. M. Thomas, and M. J. Tricker. 1974. "Surface and Intercalate Chemistry of Layered Silicates. Part II. An iron–57 Mössbauer Study of the Role of Lattice-Substituted Iron in the Benzidine Blue Reaction of Montmorillonite." *Journal of the Chemical Society, Dalton Transactions*, no. 20: 2211–2215. https://doi.org/10.1039/DT9740002211.

Thiel, J., J. M. Byrne, A. Kappler, B. Schink, and M. Pester. 2019. "Pyrite Formation From FeS and H2S is Mediated Through Microbial Redox Activity." *Proceedings of the National Academy of Sciences of the United States of America* 116, no. 14: 6897–6902. https://doi.org/10.1073/pnas.1814412116.

ThomasArrigo, L. K., C. Mikutta, J. Byrne, A. Kappler, and R. Kretzschmar. 2017. "Iron (II)-Catalyzed Iron Atom Exchange and Mineralogical Changes in Iron-Rich Organic Freshwater Flocs: An Iron Isotope Tracer Study." *Environmental Science & Technology* 51, no. 12: 6897–6907. https://doi.org/10.1021/acs.est.7b01495.

ThomasArrigo, L. K., C. Mikutta, R. Lohmayer, B. Planer-Friedrich, and R. Kretzschmar. 2016. "Sulfidization of Organic Freshwater Flocs From A Minerotrophic Peatland: Speciation Changes of Iron, Sulfur, and Arsenic." *Environmental Science & Technology* 50, no. 7: 3607–3616. https://doi.org/10.1021/acs.est.5b05791.

ThomasArrigo, L. K., L. Notini, S. Vontobel, S. Bouchet, T. Nydegger, and R. Kretzschmar. 2024. "Emerging Investigator Series: Coprecipitation With Glucuronic Acid Limits Reductive Dissolution and Transformation of Ferrihydrite in An Anoxic Soil." *Environmental Science: Processes & Impacts* 26, no. 9: 1489–1502. https://doi.org/10.1039/D4EM00238E.

Thompson, A., O. A. Chadwick, D. G. Rancourt, and J. Chorover. 2006. "Iron-Oxide Crystallinity Increases During Soil Redox Oscillations." *Geochimica Et Cosmochimica Acta* 70, no. 7: 1710–1727. https://doi.org/10.1016/j.gca.2005.12.005.

Thompson, A., D. G. Rancourt, O. A. Chadwick, and J. Chorover. 2011. "Iron Solid-Phase Differentiation Along A Redox Gradient in Basaltic Soils." *Geochimica Et Cosmochimica Acta* 75, no. 1: 119–133. https://doi.org/10.1016/j.gca.2010.10.005.

Tishchenko, V., C. Meile, M. M. Scherer, T. S. Pasakarnis, and A. Thompson. 2015. "Fe^{2+} Catalyzed Iron Atom Exchange and Re-Crystallization in A Tropical Soil." *Geochimica Et Cosmochimica Acta* 148: 191–202. https://doi.org/10.1016/j.gca.2014.09.018.

Torrent, J., V. Barrón, and Q. Liu. 2006. "Magnetic Enhancement Is Linked to and Precedes Hematite Formation in Aerobic Soil." *Geophysical Research Letters* 33, no. 2. https://doi.org/10.1029/2005GL024818.

Trueman, A. M., M. J. McLaughlin, L. M. Mosley, and R. W. Fitzpatrick. 2020. "Composition and Dissolution Kinetics of Jarosite-Rich Segregations Extracted From An Acid Sulfate Soil With Sulfuric Material." *Chemical Geology* 543: 119606. https://doi.org/10.1016/j.chemgeo.2020.119606.

Usman, M., J. M. Byrne, A. Chaudhary, et al. 2018. "Magnetite and Green Rust: Synthesis, Properties, and Environmental Applications of Mixed-Valent Iron Minerals." *Chemical Reviews* 118, no. 7: 3251–3304. https://doi.org/10.1021/acs.chemrev.7b00224.

Vandenberghe, R. E., C. A. Barrero, G. M. Da Costa, E. Van San, and E. De Grave. 2000. "Mössbauer Characterization of Iron Oxides and (oxy) hydroxides: The Present State of the Art." *Hyperfine Interactions* 126: 247–259. https://doi.org/10.1023/A:1012603603203.

Vandenberghe, R. E., and E. De Grave. 2013. "Application of Mössbauer Spectroscopy in Earth Sciences." In Y., Yoshida and G., Langouche (Eds.), *Mössbauer Spectroscopy: Tutorial Book*, (91–185). Berlin, Heidelberg: Springer.

van der Woude, F., and A. J. Dekker. 1966. "Mössbauer ffect in α-FeOOH." *Physica Status Solidi (B)* 13, no. 1: 181–193. https://doi.org/10.1002/pssb.19660130117.

van der Zee, C., D. R. Roberts, D. G. Rancourt, and C. P. Slomp. 2003. "Nanogoethite is the Dominant Reactive Oxyhydroxide Phase in Lake and Marine Sediments." *Geology* 31, no. 11: 993–996. https://doi.org/10.1130/G19924.1.

Vasilopanagos, C., C. Carteret, S. Hillier, A. Neumann, H. J. Brooksbank, and H. C. Greenwell. 2022. "Effect of Structural Fe Reduction on Water Sorption by Swelling and Non-Swelling Clay Minerals." *Minerals* 12, no. 4: 453. https://doi.org/10.3390/min12040453.

Vaughan, D. J., and M. S. Ridout. 1971. "Mössbauer Studies of Some Sulphide Minerals." *Journal of Inorganic and Nuclear Chemistry* 33, no. 3: 741–746. https://doi.org/10.1016/0022-1902(71)80472-4.

Voggenreiter, E., P. Schmitt-Kopplin, L. ThomasArrigo, C. Bryce, A. Kappler, and P. Joshi. 2024. "Emerging Investigator Series: Preferential Adsorption and Coprecipitation of Permafrost Organic Matter With Poorly Crystalline Iron Minerals." *Environmental Science: Processes & Impacts* 26, no. 8: 1322–1335. https://doi.org/10.1039/D4EM00241E.

Voggenreiter, E., L. ThomasArrigo, M. Bottaro, et al. 2025. "Suppression of Methanogenesis by Microbial Reduction of Iron-Organic Carbon Associations in Fully Thawed Permafrost Soil." *Journal of Geophysical Research: Biogeosciences* 130, no. 3: e2024JG008650. https://doi.org/10.1029/2024JG008650.

Wagner, U., W. Knorr, A. Forster, E. Murad, R. Salazar, and F. E. Wagner. 1988. "Mössbauer Study of Illite Associated With Iron Oxi-hydroxides." *Hyperfine Interactions* 41: 855–858. https://doi.org/10.1007/BF02400525.

Wagner, U., E. Murad, W. Knorr, and F. E. Wagner. 1990. "Mössbauer Study of Illitic Clays Containing Iron-Rich Impurities." *Hyperfine Interactions* 57: 2313–2317. https://doi.org/10.1007/BF02405805.

Walz, F. 2002. "The Verwey Transition-A Topical Review." *Journal of Physics: Condensed Matter* 14, no. 12: R285. https://doi.org/10.1088/0953-8984/14/12/203.

Wan, M., C. Schröder, and S. Peiffer. 2017. "Fe (III): S (-II) Concentration Ratio Controls the Pathway and the Kinetics of Pyrite Formation During Sulfidation of Ferric Hydroxides." *Geochimica Et Cosmochimica Acta* 217: 334–348. https://doi.org/10.1016/j.gca.2017.08.036.

Wan, M., A. Shchukarev, R. Lohmayer, B. Planer-Friedrich, and S. Peiffer. 2014. "Occurrence of Surface Polysulfides During the Interaction Between Ferric (hydr) oxides and Aqueous Sulfide." *Environmental Science & Technology* 48, no. 9: 5076–5084. https://doi.org/10.1021/es405612f.

Whitaker, A. H., R. E. Austin, K. L. Holden, et al. 2021. "The Structure of Natural Biogenic Iron (oxyhydr) oxides Formed in Circumneutral pH Environments." *Geochimica Et Cosmochimica Acta* 308: 237–255. https://doi.org/10.1016/j.gca.2021.05.059.

Williams, A. G., and M. M. Scherer. 2004. "Spectroscopic Evidence for Fe (II)– Fe (III) Electron Transfer at the Iron Oxide– Water Interface." *Environmental Science & Technology* 38, no. 18: 4782–4790. https://doi.org/10.1021/es049373g.

Wilmoth, J. L., M. A. Moran, and A. Thompson. 2018. "Transient O_2 Pulses Direct Fe Crystallinity and Fe (III)-Reducer Gene Expression Within A Soil Microbiome." *Microbiome* 6: 1–14. https://doi.org/10.1186/s40168-018-0574-5.

Winkler, P., K. Kaiser, A. Thompson, K. Kalbitz, S. Fiedler, and R. Jahn. 2018. "Contrasting Evolution of Iron Phase Composition in Soils Exposed to Redox Fluctuations." *Geochimica Et Cosmochimica Acta* 235: 89–102. https://doi.org/10.1016/j.gca.2018.05.019.

Yoshida, Y., and G. Langouche. 2013. *Mössbauer Spectroscopy*. Berlin Heidelberg: Springer.

Zhou, N., R. J. Kupper, J. G. Catalano, A. Thompson, and C. S. Chan. 2022. "Biological Oxidation of Fe (II)-Bearing Smectite by Microaerophilic Iron Oxidizer Sideroxydans lithotrophicus Using Dual Mto and Cyc2 Iron Oxidation Pathways." *Environmental Science & Technology* 56, no. 23: 17443–17453. https://doi.org/10.1021/acs.est.2c05142.

Zhu, M., B. W. Puls, C. Frandsen, J. D. Kubicki, H. Zhang, and G. A. Waychunas. 2013. "In Situ Structural Characterization of Ferric Iron Dimers in Aqueous Solutions: Identification of μ-oxo Species." *Inorganic Chemistry* 52, no. 12: 6788–6797. https://doi.org/10.1021/ic302053w.

Ziganshin, A. M., E. E. Ziganshina, J. Byrne, et al. 2015. "Fe (III) Mineral Reduction Followed by Partial Dissolution and Reactive Oxygen Species Generation During 2,4,6-trinitrotoluene Transformation by The Aerobic Yeast Yarrowia lipolytica." *AMB Express* 5: 1–12. https://doi.org/10.1186/s13568-014-0094-z.

Supporting Information

Additional supporting information can be found online in the Supporting Information section.

Supporting File 1: jpln12024-sup-0001-SuppMat.pdf.